INFORMATION TO USERS

This reproduction was made from a copy of a document sent to us for microfilming. While the most advanced technology has been used to photograph and reproduce this document, the quality of the reproduction is heavily dependent upon the quality of the material submitted.

The following explanation of techniques is provided to help clarify markings or notations which may appear on this reproduction.

1. The sign or "target" for pages apparently lacking from the document photographed is "Missing Page(s)". If it was possible to obtain the missing page(s) or section, they are spliced into the film along with adjacent pages. This may have necessitated cutting through an image and duplicating adjacent pages to assure complete continuity.

2. When an image on the film is obliterated with a round black mark, it is an indication of either blurred copy because of movement during exposure, duplicate copy, or copyrighted materials that should not have been filmed. For blurred pages, a good image of the page can be found in the adjacent frame. If copyrighted materials were deleted, a target note will appear listing the pages in the adjacent frame.

3. When a map, drawing or chart, etc., is part of the material being photographed, a definite method of "sectioning" the material has been followed. It is customary to begin filming at the upper left hand corner of a large sheet and to continue from left to right in equal sections with small overlaps. If necessary, sectioning is continued again—beginning below the first row and continuing on until complete.

4. For illustrations that cannot be satisfactorily reproduced by xerographic means, photographic prints can be purchased at additional cost and inserted into your xerographic copy. These prints are available upon request from the Dissertations Customer Services Department.

5. Some pages in any document may have indistinct print. In all cases the best available copy has been filmed.

University Microfilms International
300 N. Zeeb Road
Ann Arbor, MI 48106

Downloaded from SHAREOK. Persistent Handle URL: https://hdl.handle.net/11244/257

1323800

DUTTA, SUBIJOY

AN EXPERIMENTAL INVESTIGATION OF DISPERSIVITY AND ITS ROLE AS AN OIL RESERVOIR ROCK PROPERTY

THE UNIVERSITY OF OKLAHOMA M.S. 1984

University
Microfilms
International 300 N. Zeeb Road, Ann Arbor, MI 48106

Copyright 1984

by

DUTTA, SUBIJOY

All Rights Reserved

THE UNIVERSITY OF OKLAHOMA

GRADUATE COLLEGE

AN EXPERIMENTAL INVESTIGATION OF DISPERSIVITY AND ITS ROLE AS AN OIL RESERVOIR ROCK PROPERTY

A THESIS

SUBMITTED TO THE GRADUATE FACULTY

in partial fulfillment of the requirements for the

degree of

MASTER OF SCIENCE

BY

SUBIJOY DUTTA

Norman, Oklahoma

1984

AN EXPERIMENTAL INVESTIGATION OF DISPERSIVITY
AND ITS ROLE AS AN OIL RESERVOIR ROCK PROPERTY

A THESIS

APPROVED FOR THE SCHOOL OF PETROLEUM AND
GEOLOGICAL ENGINEERING

APPROVED BY

D. E. Menzie

Charles J. Mankin

Brian H. Samaroo

© 1984

SUBIJOY DUTTA

ALL RIGHTS RESERVED

ACKNOWLEDGEMENT

At the very onset I would like to express my appreciation and thanks to Dr. Donald E. Menzie for his invaluable guidance from the very beginning of this study. His continuous guidance during the experimental runs was of enormous help in completing this investigation.

The author wishes to extend his sincere appreciation to Dr. Charles J. Mankins for his interest and cooperation in completing this study.

My special appreciation goes to Dr. Carlos F. Alcocer, who has been working in the Enhanced Oil Recovery project by Nitrogen injection using the same reservoir model. Most of the physical parameters of Experimental Setup #1 was determined jointly by the author and Dr. Alcocer.

I would like to express my special gratitude to Dr. Kris K. Agrawal, Director, General Mining Corporation, for his great coordination and help towards completion of this report by allowing me to use his computer system for complete processing of this thesis report.

I would also like to thank my friends who encouraged me all through this study.

Most of all I would like to thank my parents, Mr. and Mrs. Subinoy Kr. Dutta who have contributed the most towards my graduate work by providing me a strong encouragement and assistance all along.

ABSTRACT

" AN EXPERIMENTAL INVESTIGATION OF DISPERSIVITY AND ITS ROLE AS AN OIL RESERVOIR ROCK PROPERTY "

A few studies have been conducted in the past to investigate the effect of dispersivity on mobile and immobile fluids and its variation with the wetting phase saturation in a flooding process. This study is directed towards investigating the role of dispersivity in a miscible flooding process. The purpose of this investigation is to establish dispersivity as an oil reservoir rock property. Three setups of equipment were used to inject naptha and displace crude oil by miscible flooding process in three different reservoir models. Theoretical correlation of this experimental investigation and the observed results and their significance is discussed in this report. Summarized experimental results and and the pertinent figures are included in the result section of this report. Further investigation on correlation of dispersivity with pore size distribution of a reservoir rock and the corresponding changes in the behavioral pattern of several rocks with different physical properties is underway.

TABLE OF CONTENTS

Page

ACKNOWLEDGEMENTS iii

LIST OF TABLES vii

LIST OF FIGURES viii

Chapter

1.0 INTRODUCTION 1

2.0 EXPERIMENTAL SETUP AND DESCRIPTION OF EQUIPMENT 9

1. High Pressure Variable Volumetric Rate Positive Displacement Pump 11

2. Simulated Reservoir Model 12

3. Temperature Control System 13

4. Refractometer 14

5. Inflow and Outflow System 17
(a) PVT Cell 17
(b) Mercury Pump 18
(c) Gas Compressor 19
(d) Vacuum Pump 19
(e) Back Pressure Regulator 19
(f) Sampling Tubes 20
(g) Production Equipment 20

TABLE OF CONTENT(Continued..)

6. Additional Equipment 21

(A) Epoxy Coated Core 32

(B) Core Holder 34

(C) High Pressure Mini Pump 34

(D) Graduated Epoxy Container 34

(E) Pressure Gauge 34

(F) Refractometer 35

3.0 THEORETICAL CORRELATION 37

3.1 Statistical Approach 41

3.2 Continuum Approaches 51

(A) Convective Dispersion Model 56
(B) Dispersion-Capacitance Model 65

4.0 EXPERIMENTAL RESULTS 77

Run #1 81
Run #2 86
Run #3 91
Run #4 96
Run #5 101
Run #6 106
Run #7 111
Run #8 116

TABLE OF CONTENT(Continued..)

5.0 DISCUSSION 121

6.0 CONCLUSIONS AND RECOMMENDATIONS 140

NOMENCLATURE 143

BIBLIOGRAPHY 144

APPENDICES 146

APPENDIX A
Calibration of the LDG Mini Pump A-1

APPENDIX B
Calibration of the Refractometer B-1

APPENDIX C
Determination of the Absolute
Permeabilities of The Reservoir Models C-1

APPENDIX D
Listing of the Computer Program 'DISCAL' D-1
Oil Concentration Profiles used for
Volume computations D-8

LIST OF TABLES

TABLE		PAGE
1.	Physical Properties and PVT Characteristics of Crude Oil from South Elm Unit	23
2.	Calculated Values of Dispersion Coefficient Corresponding to Beta Distribiution Parameters	49
3.	Calculation of Slug Size using the Dispersion Model	67
4.	Experimental Observation #1	83
5.	Experimental Observation #2	88
6.	Experimental Observation #3	93
7.	Experimental Observation #4	98
8.	Experimental Observation #5	103
9.	Experimental Observation #6	108
10.	Experimental Observation #7	113
11.	Experimental Observation #8	118
12.	Grouping of Experimental Runs based upon their Similarity	126

LIST OF FIGURES

FIGURE		PAGE
1.	Schematic Diagram of Experimental Setup #1	10
2.	Details of Temperature Control System	15
3.	Sample Calibration Curve for Naptha-1 and Crude Oil	16
4.	Details of Recombination System	25
5.	Saturation Pressure Curve for South Lone Elm Crude Oil Recombined With Natural Gas (GOR - 575 scf/stb)	29
6.	Saturation Pressure Curve for South Lone Elm Crude Oil Recombined With Natural Gas (GOR - 400 scf/stb)	30
7.	Schematic Diagram of Experimental Setup #2	33
8a	Mixing Due to Obstruction	39
8b	Incomplete Connectivity of the Medium	39
8c	Recirculation Caused by Local Regions of Reduced Pressure	39
9.	Elemental Pore for Statistical Model	45
10.	Solvent Concentration Profile in an Idealized Linear Displacement	58

LIST OF FIGURES (Continued...)

FIGURE		PAGE
11.	Mixing Zones in a Miscible Slug Process	63
12.	Effluent Concentration Profiles Showing Capacitance Effects	66
13.	Displacement of Solvent in a Dual Porosity System	70
14.	Flowchart for the Computer Program 'DISCAL' ...	80
15.	Calculated Lamda Vs Effluent Concentration for Run #1	84
16.	Effluent Concentration vs Time for Run #1	85
17.	Calculated Lamda Vs Effluent Concentration for Run #2	89
18.	Effluent Concentration vs Time for Run #2	90
19.	Calculated Lamda Vs Effluent Concentration for Run #3	94
20.	Effluent Concentration vs Time for Run #3	95
21.	Calculated Lamda Vs Effluent Concentration for Run #4	99
22.	Effluent Concentration vs Time for Run #4	100

LIST OF FIGURES (Continued...)

FIGURE		PAGE
23.	Calculated Lamda Vs Effluent Concentration for Run #5	104
24.	Effluent Concentration vs Time for Run #5	105
25.	Calculated Lamda Vs Effluent Concentration for Run #6	109
26.	Effluent Concentration vs Time for Run #6	110
27.	Calculated Lamda Vs Effluent Concentration for Run #7	114
28.	Effluent Concentration vs Time for Run #7	115
29.	Calculated Lamda Vs Effluent Concentration for Run #8	119
30.	Effluent Concentration vs Time for Run #8	120
31.	Typical Effluent-Composition Curve	122
32.	Different Effluent Concentration vs Time	128
33.	Crude Oil Recovery Vs Dispersion Coefficient	130
34.	Dispersion Coefficient vs Velocity	131
35.	Dispersivity vs Velocity	133
36.	Dispersion Coefficient and Dispersivity vs Velocity	134
37.	Dispersivity Vs Dispersion Coefficient	136
38.	Floodfront Positions as a Function of Dimensionless Time	138

AN EXPERIMENTAL INVESTIGATION OF DISPERSIVITY AND ITS ROLE AS AN OIL RESERVOIR ROCK PROPERTY

1.0 INTRODUCTION

At the present time approximately 2.05×10^8 MMBTU of energy is being used on the average per day in the United States. Different sources of energy such as coal, oil and gas, nuclear fuel, and solar power contribute towards this total consumption[18]. Major portion of this energy demand is met by oil and gas. Coal, nuclear fuel, and solar power are the subsequent sources of energy listed in the decreasing order of their usage.

Oil and Gas reserves identified in the United States or elsewhere exist in a limited quantity. Since the hydrocarbon deposition took place over a period of one million year or more, replacement or replenishment of the hydrocarbon deposit is not considered feasible for the purpose of evaluation of total resources. The oil and gas reserves are thus a non-renewable form of energy for all practical purposes. The best and most efficient method of recovering this non-renewable energy is of paramount

importance in the petroleum industry.

In most of the enhanced recovery processes such as miscible drives, carbon dioxide flooding, as well as other recovery methods, mixing of two miscible fluids in a porous medium plays a very important role. Many studies have been devoted to mechanics of miscible displacement, focusing on the longitudinal and transverse dispersion.

The performance of an oil recovery process can be greatly influenced by the presence of an immobile phase of oil, water, or gas. Furthermore, the flood velocity exerts an additional effect on the role of the immiscible phase. Various ways of expressing the respective dispersion coefficient in terms of diffusion, grain diameter, and pore velocity have been studied by different researchers as succinctly covered in the following paragraphs.

Perkins and Johnston[20] were one of the first few researchers to focus on the dispersion and diffusion phenomena in a miscible displacement process. They reported in their study that in a fluid flow through porous media dispersion may be greater than that due to diffusion alone. They also noted that at moderate flow rates, the porous medium will create a slightly asymmetrical mixed zone with the convective dispersion coefficient approximately proportional to the first power of the average fluid

velocity. Factors affecting the dispersion coefficient were identified by them as (1) edge effect in packed tubes, (2) particle size distribution, (3) particle shape (4) packing or permeability heterogeneities, (5) viscosity ratios, (6) gravity forces, (7) amount of turbulence, and (8) effect of an immobile phase.

Mahnaz Kasraie et al.[15] studied the effect of an immobile phase on dispersion in a porous media. Solvent flooding was specifically examined in their study in the context of immobile oil, water, and gas phases. The phase saturations were reduced below the critical values to study an extended saturation range. The effect of entrained polymer on dispersive mixing was also covered in their study. Dispersion in a porous medium was found to decrease in the case of wetting immobile phase, and increase in the case of nonwetting immobile phase (oil or gas).

Miscible displacement studies in the presence of an immobile water phase in Berea sandstone cores have been conducted by Raimondi, Torcaso, and Henderson[21]. They found that the effective mixing coefficient increased when the water saturation was increased above the irreducible value. Longer mixing zones were also observed when the water saturation was increased.

The effect of an immobile water phase on mixing characteristics were also investigated by Thomas et al.[26]. In their study they noted that the presence of the immobile phase significantly altered the pore size distribution. The effect of an immobile gas phase on mixing was studied by Orlob et al.[19] They reported that entrapment of a small volume of gas in the pore space may trap some of the liquid, and keep it from the flow stream. The residual gas phase, if localized in the larger pore spaces, led to greater uniformity in the pore size distribution, and hence a reduction in the mixing coefficient. It was also observed that a small amount of trapped gas, below 5% of the pore space, had very little effect on dispersion.

S. M. Chen et al.[9] reviewed the assumptions and limitations of a dispersion model, which is conventionally used to calculate the slug size requirements. Their study suggested possible modifications to the dispersion-capacitance model, as it is applied to the carbonate reservoirs, which commonly exhibits dual porosity. It was identified that the relative contributions of mass transfer and interflow between the dual porosity systems of the carbonate reservoirs are of significant importance to the dispersion- capacitance model developed by Coats and Smith[10] earlier. The mass transfer coefficient in the

mathematical model of Coats and Smith was modified for the dual porosity system by Chen et al.

A few other factors affecting the slug size, such as multiple contact miscible displacement process, water blocking of solvent at high water saturations, and residual solvent within and behind the solvent bank were also examined by Chen et al.[9]. Two distinct mechanisms which contribute to the growth of the mixing zone were identified by them as molecular diffusion and convective dispersion. Even in the absence of gross fluid movement, a mixing zone was found to develop due to the random thermal motion of the molecules. This random motion of the molecules are commonly referred to as molecular diffusion. Additional mixing of the fluid is attributed to convective dispersion mechanism resulting from uneven flow paths brought about by microscopic heterogeneities.

Effect of water saturation on the dispersion coefficient was immaculately studied by Stalkup[24]while investigating the miscible displacement phenomena in reservoir rocks. He reported that the observed values of dispersion coefficient increased greatly with increasing water saturation for tests carried out in strongly water-wet sandstone cores. It was suggested that the presence of

water may alter the pore size distribution available for miscible displacement, and that this is one factor contributing to the increase in mixing zone length.

The mechanism whereby solvent is blocked by water is a result of two separate effects, one due to the density difference between the solvent and water, and the other due to viscosity differences. Blocking of solvent by mobile water was studied first by Blackwell et al.[5]. Their experiments involved the displacement of solvent banks by a solvent/water mixture. It was observed that because the solvent water mixture tended to segregate, with water underriding the solvent, the solvent bank could not be completely displaced and a substantial volume of solvent was trapped by water and remained at the bottom of the core.

An investigation of the microscopic dispersion phenomena was carried out by R. J. Blackwell[6]. The microscopic mixing process was separated into longitudinal and transverse dispersion corresponding to the flow in the direction of mean flow and perpendicular to the direction of mean flow respectively.

In both longitudinal and transverse mixing, the dispersion was found to result from an interplay between convection and diffusion.

Effect of dispersivity in two-phase systems

with miscible flooding was investigated by R. M. Giordano et al.[13]. They observed that with increasing dispersivity the oil bank breaks through earlier and the transition zone length increases. Studying the effect of dispersion in various core length and different injection rate they reported that variation of core length from one to eight feet and variation of injection rate from 2 ft/day to 20 ft/day had no discernable effect on the experimental effluent results.

All of these aforementioned studies were directed towards investigating the effect of dispersivity on mobile and immobile fluids and its variation with the wetting phase saturation in a flooding process.

The present study was originated by distinct observation of the variation in efficiency of a tertiary recovery process due to a change in dispersion coefficient of the reservoir rock during a miscible displacement. The object of this study is to establish the dispersion coefficient as a reservoir rock property and use this reservoir rock characteristic to predict the performance of a miscible flood. Several experiments using miscible displacement technique were conducted and the resulting dispersion coefficient and the dispersivity of the experimental reservoir rock were correlated with the total

recovery of the displaced fluid and the flood efficiency of the system. An investigation into the effect of dispersion coefficient on the areal coverage of a miscible flooding process and its interrelationship is also an objective of this study. The dispersivity of a reservoir rock and its effect on the effective sweep area of a miscible flooding process is also investigated in this study.

Details of this experimental study and the observations therefrom are reported in separate sections of this report. Each of these sections such as the Experimental setup, Theoretical correlation, Experimental Results, Discussion, and Conclusions and Recommendations provide relevant information pertaining to the specified subject.

2.0 EXPERIMENTAL SETUP AND DESCRIPTION OF EQUIPMENT

Three different experimental setups to represent different physical characteristics of oil reservoirs were made available by the University of Oklahoma for conducting this study. This experimental study was initiated by the findings of tertiary flooding with naptha during the cleaning process of the enhanced oil recovery project by Nitrogen injection. Miscible displacement of oil from the reservoir by flooding with naptha was aimed at recovering all or part of the crude left in the reservoir after the secondary recovery process by Nitrogen injection. The naptha flood was initially used to clean the reservoir after completion of one run and to make the reservoir ready for the next run. The existing experimental setup for Nitrogen injection was slightly modified to cater to the need of this study. A schematic diagram of the experimental equipment setup used in the first part of this study, referred to as Setup #1 hereinafter, is shown in Figure 1.
This experimental equipment consisted of a consolidated sandpack. The dispersion coefficient of this

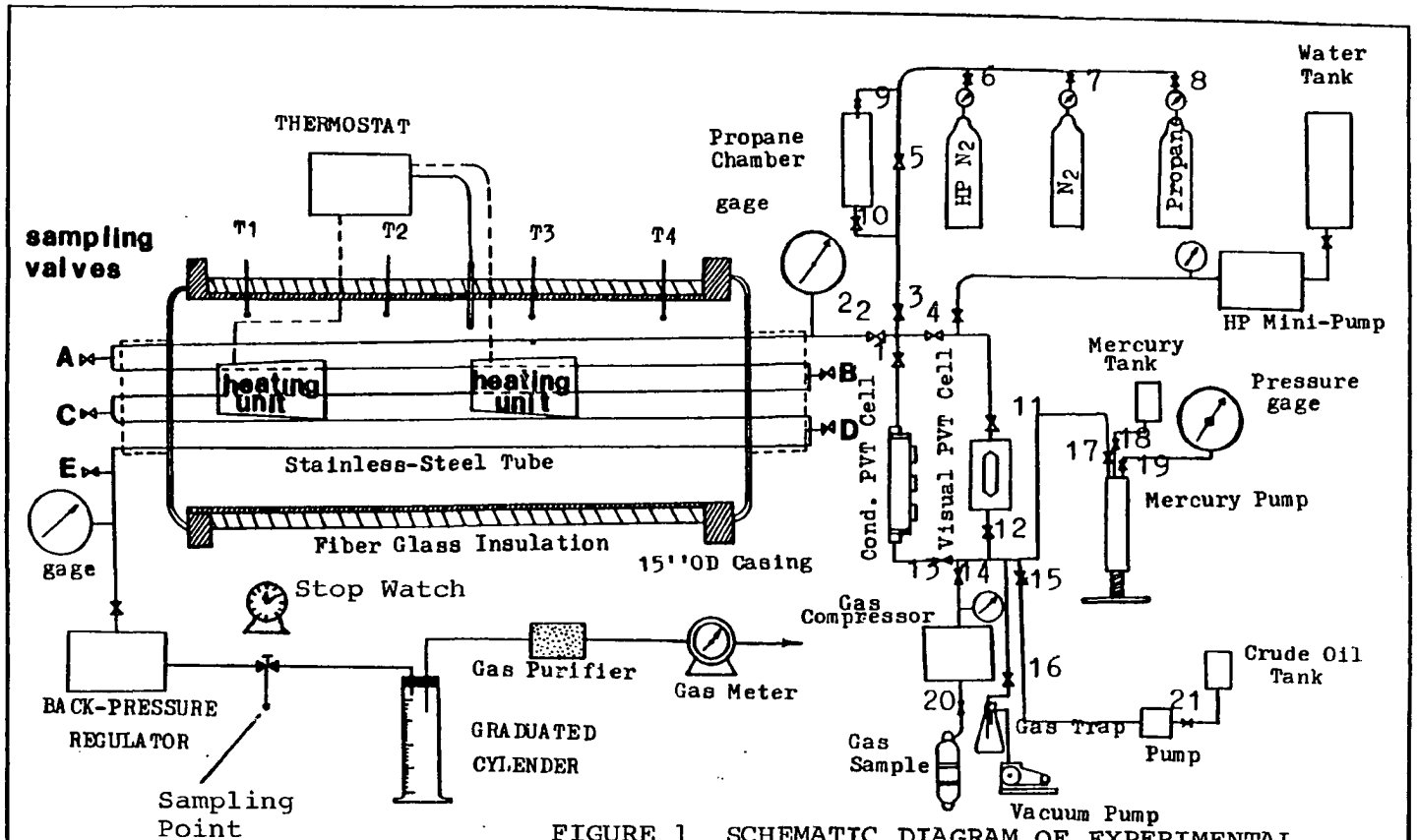

FIGURE 1 SCHEMATIC DIAGRAM OF EXPERIMENTAL SETUP #1

NOTE: This experimental Setup was used in conjunction with the N_2 project[1].

sandpack under several different conditions of flooding were determined. This experimental setup is divided into the folowing components:

1. High Pressure (HP) mini pump
2. Simulated reservoir model
3. Temperature control system
4. Refractometer
5. Inflow and outflow system
6. Additional Equipment

Each of these components are detailed below:

1. High Pressure Variable Volumetric Rate Positive Displacement Pump -

This pump is a "LDG" minipump duplex model 2396-57 with a maximum capacity of 580 ml/hr. The capacity is proportional to motor speed. The pump's working pressure is 6,000 psi. The weight of this duplex pump is 24 lbs. net and its dimensions are: 10-1/8" W, 8-3/4" D., and 7-3/8" H. The maximum working temperature is 122° F. This LDG minipump requires protection from liquid contact and is not recommended to be operated in a potentially explosive environment. The pump is equipped with compression type of tube fittings built into suction and discharge cartridges of the pump. The suction side accepts only 1/8" outside

diameter tube; the discharge only accepts 1/16" outside diameter tube. Calibration of the pump is shown in Appendix A.

2. Simulated Reservoir Model -

The reservoir model used in this experiment is represented by a linear artificial core constructed by filling five stainless steel tubes, 25 feet long and 0.435 inches Internal Diameter, with consolidated sand packs. The model is provided with five sampling valves along the length of the tube to facilitate sampling from the intermediate points during the displacement test.

The properties of the reservoir model were experimentally determined in a joint effort with C. A. Alarcon[1], who was investigating the effect of high pressure Nitrogen injection on enhanced oil recovery. The average porosity was found to be 32% and the absolute permeability was found to be 910 mD. Several displacements of Nitrogen at different rates were done and a computer program was written to calculate the absolute liquid permeability. The program and graphical calculations of absolute permeability are shown in Appendix A to this report.

3. Temperature Control System -

One of the primary objectives of this flooding process was to simulate an actual reservoir condition by raising the pressure and temperature of the reservoir to represent the actual field condition. A computer program having a subroutine 'SSUPLI' was developed to simulate the heat transfer in the reservoir model. The specifications of the heating system and the heater size for the reservoir model for the desired temperatures were determined from the results of this computer model.

The temperature control system included in this experiment consisted of: Heating units, Thermostats, R-13 insulation blankets, and thermometers.

Two commercial heating units manufactured by Arvin Industries, Inc., model 29H60-3, were used in this experiment. Each heating unit has a heating capacity of 1500 BTU/hr. The two heaters were used to supply heat independently to the annulus between the stainless steel tube containing the consolidated sandpack and the 15" diameter pipe. A chromalox Industrial Thermostat - AR-2524 was used to control the heat requirements in the annulus.

The operating range for chromalox thermostat is 50° - 250° F. The operating current and voltage is 25 Amps and 120 Volts respectively. The source temperature is read by means of a sensitive bulb with 0.250" diameter and 5.5" length. Thermostats are tested and calibrated at the factory to the temperature of the sensing bulb. However, they should be calibrated to the actual working temperature. The temperature control system is conspicuously depicted in Figure 2.

Four regular thermometers were installed in the 15" diameter pipe to sense the temperature of the reservoir model.

4. Refractometer -

An Abbe refractometer was made available by the University of Oklahoma for this experimental study. Determination of the effluent concentrations of the miscible fluids was made possible with the help of the refractometer, which played a key role in this investigation. From the effluent mixture of oil and naptha, optical analyses of the samples at different points of the flood were performed with the refractometer and the naptha and oil concentrations were determined. It was necessary to calibrate the instrument before use and a calibration curve for the two given miscible fluids was prepared. A sample calibration curve for Naptha-1 and oil used in first six runs are shown in Figure 3. Details of operation of the refractometer and the

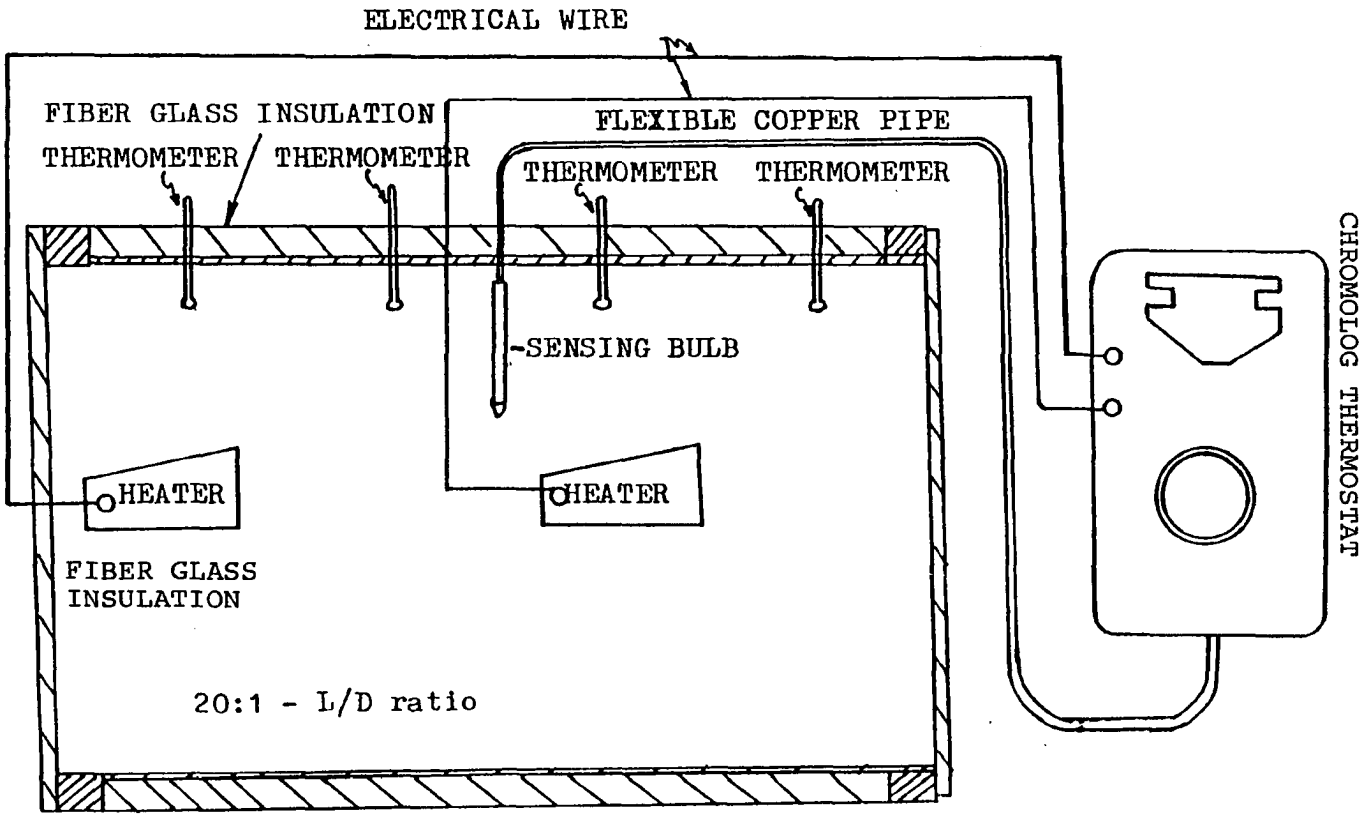

FIGURE 2 DETAILS OF THE TEMPERATURE CONTROL SYSTEM

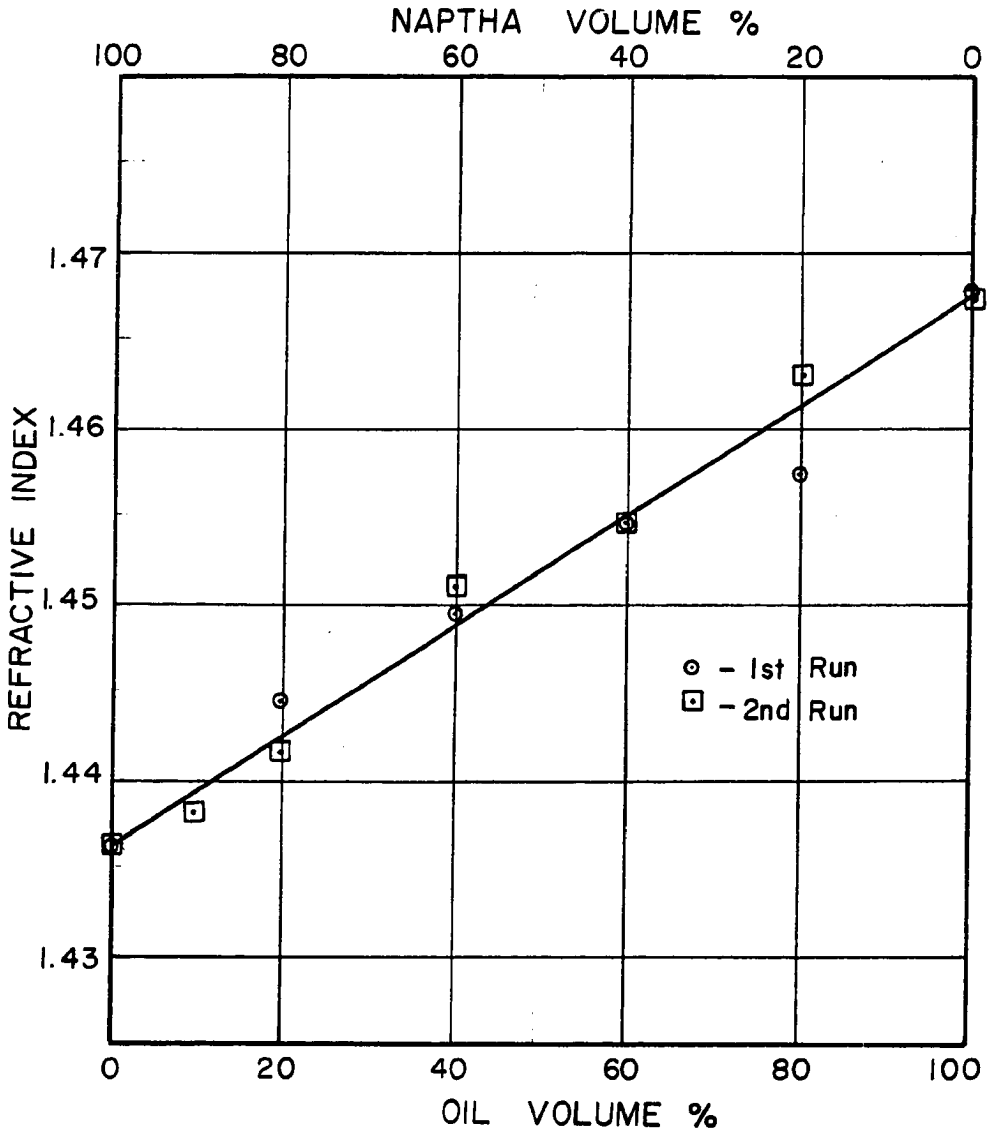

FIGURE 3 SAMPLE CALIBRATION CURVE FOR NAPTHA-1 AND CRUDE OIL

Refractive Indexes (R.I) versus percentages of oil-naptha mixture is presented in Appendix C to this report.

5. Inflow and Outflow System -

The injection and production system consisted of several small pieces of equipment as listed below:

(a) PVT (Pressure-Volume-Temperature) cell

(b) Positive Displacement Mercury Pump

(c) Gas Compressor

(d) Vacuum Pump

(e) Back Pressure Regulator

(f) Sampling tubes

(g) Production Equipment

(a) PVT Cell: The PVT cell used to inject/charge the reservoir with oil and gas in solution is basically a cylindrical container with a visual window on the top to check the mercury level while charging oil by the piston-like displacement of mercury within the cell. The PVT cell was used to measure the bubble point pressure of the oil and to recombine gas and crude oil. An actual reservoir condition was simulated by maintaining certain Gas Oil Ratio (GOR) of the initial saturating hydrocarbon. The glass window was also used to observe the liberation of gas

from the liquid below the bubble point pressure. The visual PVT cell has a standard volume of 650 cc and a pressure rating of 10,000 psi at 350°F. The visual PVT cell is mounted on a base that allows shaking of the cell. During the charging process of the reservoir the inlet of the cell is connected to the mercury pump and the outlet is connected to the reservoir model. The PVT cell is first charged with a precalculated amount of oil corresponding to the desired GOR, then the remaining volume of the cell is filled with gas compressed to a certain precalculated pressure by using a gas compressor. All inlet and outlet connections to and from the PVT cell are made with 1/8" stainless steel tubing.

(b) Positive Displacement Mercury Pump:

A Ruska model 2261 bench-mounted motorized pump was used to inject oil into the reservoir. The pump is equipped with an electric motor drive and is provided with adjustable travel-limited switches to stop the motor when the plunger reaches a preset point in either direction of travel. This pump has a single cylinder with a capacity of 100 cc and is able to generate a maximum injection pressure of 25000 psi. The dial resolution is 0.01 cc and the resolution of the scale is 1 cc. The pump is provided with 5 outlets with a 1/8" NPT thread. The mercury pump is connected to a PVT cell, a mercury container, and a pressure gauge as shown in Figure 1.

(c) Gas Compressor: A gas compressor manufactured by C. A. Mathey Machine Works was made available for this study by the University of Oklahoma. The gas compressor was used to pressurize gas while injecting into the PVT cell to obtain the desired Gas in Solution (GOR). The inlet to the compressor was connected to a natural gas supply cylinder with 1/4" stainless steel tubing. The outlet from the compressor was connected to the PVT cell by 1/8" stainless steel tubing.

(d) Vacuum Pump: A vacuum pump manufactured by Cenco Megavar pump was used in this experiment. The location and connection of the vacuum pump is shown in Figure 1.

(e) Back Pressure Regulator:

The direct operating pressure reducing valve type DR10D originally installed in the equipment was changed because this valve was not suitable for this investigation. A back-pressure regulator, manufactured by TESCOM Corporation, with handknob adjustments, model 26-3220-24 was installed at the effluent part of the reservoir model as shown in Figure 1. The maximum back-pressure setting was limited to 5,000 Psi. The working temperature was between -4.0 to +160°F. The back pressure of the system was held constant at 2,000 Psi for all the tests performed for the sandpack reservoir model.

(f) Sampling Tubes:

To measure the effluent concentration of oil and naptha during the miscible flooding process samples were collected at intervals of 2 - 8 minutes. Each of these samples had to be analyzed by using the refractometer. Due to short sampling intervals samples were stored during the displacement process in small glass tubes capped with plastic caps for refractometer analyses. The effluent percentage composition of naptha and oil in each of the samples representing different positions of the flood front is then determined with the help of the refractometer. All sampling tubes were properly marked to reflect the sequence of their collection. Records of time for all samples were also maintained during the experiment by using a stop watch.

(g) Production Equipment:

i. Graduated Cylinder -

A graduated cylinder, 1,000 cc. capacity, modified to work as liquid-gas separator was installed in the producing end of the reservoir model as shown in Figure 1.

ii. Gas Filter - A filter made of silica gel was installed immediately after the graduated cylinder.

iii. Gas-Metering Apparatus - As shown in figure 1, a Sargent wet test meter, manufactured by Precision Scientific Co. was used to determine the amount of gas produced during displacements. The scale resolution is 0.0001 SCF.

6. Additional Equipment:

In order to determine fluid properties other instruments were used. The instruments used were: Fann viscosimeter, KIMRAY Gas Gravitometer, Hydrometers, etc..

Materials:

The materials used in this experimental setup were: Insulation material, medium material, light oil, natural gas and standard gas samples.

The outside insulation material used in this investigation to cover the 15" O.D. casing was a Thermo Saver Commercial fiberglass insulation blanket. This material has a thermal conductivty of 0.12 BTU/hr. ft^2 ^oF. The section of the stainless steel tube containing the porous medium was insulated using commercial urethane. This material has a density of 1.9 Lb/ft^3 and a thermal conductivity of 0.15 BTU/hr. ft^2 ^oF.

The porous medium used in this invetigation was an artificially consolidated sandpack. The sand used was clean Oklahoma sand, number 1 with 100 mesh size. Data and calculation of

absolute permeability for this porous medium are shown in Appendix A.

The oil selected for this study was Tenneco's South Lone Elm Field light oil. The same oil and the equipment setup was also used by C .A. Alarcon[1] in his investigation on enhanced oil recovery by Nitrogen injection. This field is located in Noble County, Oklahoma. Table 1 shows properties and some PVT characteristics of oil from the South Lone Elm field.

The natural gas used in these experiments was sampled from the South Lone Elm Field, Noble County, Oklahoma. The natural gas was collected at 70 psi in a small gas cylinder. For safety sake it was necessary to collect a limited number of natural gas samples and consequently several field trips for this purpose were needed.

Other Materials:

Throughout the experiments, tap water, naphtha and mercury were used.

Procedure of Investigation and Techniques for Setup #1:

Different experimental procedures and techniques were required in this investigation. The

TABLE 1 PHYSICAL PROPERTIES AND PVT CHARACTERISTICS OF CRUDE OIL FROM SOUTH ELM UNIT

PARAMETERS	Gas in Solution(GOR) 200 Scf/Stb	GOR 400 Scf/Stb	GOR 575 Scf/Stb
Formation Volume Factor, B_o @ 2000 psi	1.1	1.2	1.29
Bubble point Pressure @ 70°F	750	1550	1790
Avg. Stock Tank Oil Gravity @ 60°F (°API) 42.4			
Sp. Gravity @ 60°F 0.814			
Oil Viscosity @ 70°F (cp) 3.2			

experimental procedure for this setup are subdivided as follows:

1. Recombination process.
2. PVT analysis.
3. Saturation of the reservoir model.
4. Oil recovery by nitrogen injection.
5. Oil recovery by naptha injection.

1. Recombination Process:

In this experiment a visual PVT cell with a capacity of 650 cc. was used for the recombination process. The two major advantages in using the visual PVT cell were 1) visual PVT Cell could be shaken and, 2) the amount of recombination during a test is reduced. Figure 4 shows the recombination system used in this experiment in conjunction with the Enhanced Oil Recovery (EOR) project by N_2 injection[1]. The visual PVT Cell is connected to the inlet of the reservoir model through a 1/8" stainless steel tube. The bottom of the visual PVT Cell is connected to the gas compressor, vacuum pump, oil-feed pump, and to the mercury pump.

The following steps will describe the recombination procedure:

Step 1: Selection of the Gas in Solution (GOR) to work with.

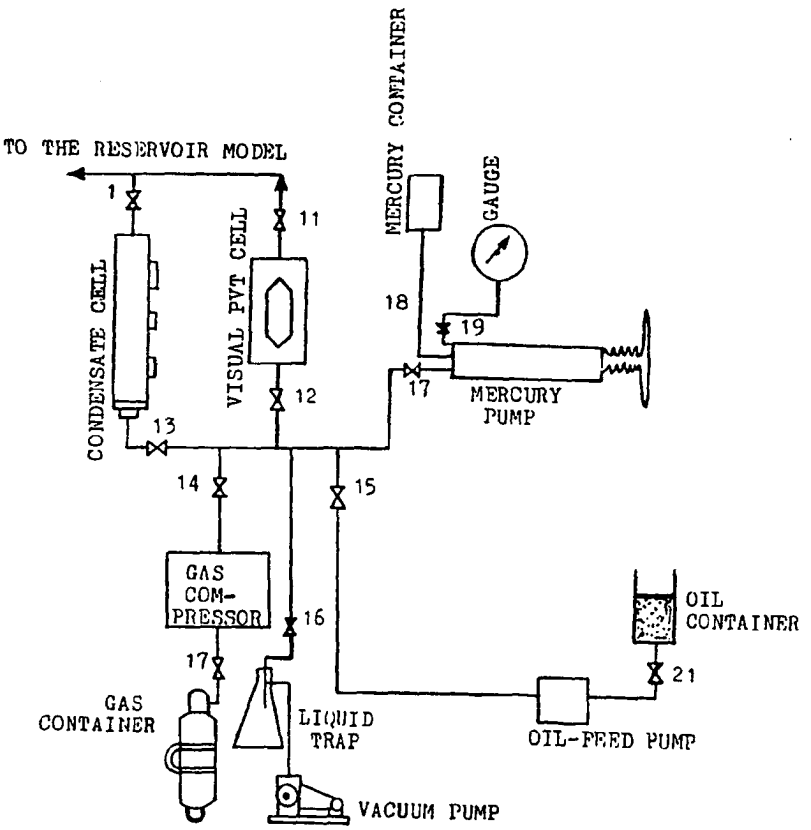

FIGURE 4 DETAILS OF THE RECOMBINATION SYSTEM

Step 2: Calculation of the maximum amount of oil that can be recombined depending upon the desired GOR.

Step 3: Calculation of the injection pressure of the compressor to attain the desired GOR.

Step 3: Vacuum the visual PVT Cell for at least 2 hours.

Step 4: Charging the PVT cell with oil according to the calculation done in step 2 by using the vacuum created in the cell

Step 5: By using the gas compressor inject natural gas into the cell. The amount of gas and the required injection pressure is determined mathematically by using an equation of state for real gases.

Step 6: By using the mercury pump inject mercury into the cell up to 2000 Psi. At that pressure the content of the cell is considered to be a single phase fluid.

After step 6 , the recombined oil is ready to be injected into the reservoir model for saturation.

2. Procedure for PVT Analysis

The bubble-point pressure of a hydrocarbon reservoir fluid is defined as the pressure at which the first bubble of gas is separated from the liquid hydrocarbon. This bubble-point pressure is determined in the laboratory by means of the visual PVT Cell (Pressure-Volume-Temperature cell) and the formation volume factor as well. In order to obtain bubble-point pressure (also saturation pressure) and formation volume factor in the laboratory, the following steps are followed:

Step 1: Follow all the first six steps for recombination process.

Step 2: After step 1, the cell is already charged. Then shake the visual PVT Cell for 5 minutes, and open the bottom valve which communicates with the mercury pump and raises the pressure to a value above the average pressure of the reservoir. This value has to be known before hand.

Step 3: Close the bottom valve of the cell and take the first gauge reading. Shake for 5 minutes and reduce the pressure 10 Psi.

Step 4: Look through the glass window to check for the appearance of gas bubble.

Step 5: Repeat the above procedure for several pressures until the first bubble of gas appears in the visual PVT cell. When the bubble-point pressure is detected, go to the next step.

Step 6: Go several times above and below the saturation pressure to confirm that the gauge pressure reading of the bubble point is right.

It may be noted that the volume of mercury removal from the PVT cell has to be measured with reference to one reference pressure to avoid error due to the expansion of mercury or infiltration of gas in the system.

The results of the PVT analyses for a GOR of 575 Scf/STB and 400 Scf/STB are shown in Figures 5 and 6 respectively. The variation in bubble point pressures corresponding to different GOR of the solution could be easily observed in these Figures.

3. Saturation of the Reservoir Model

The reservoir model was first saturated with water and then displaced with oil and gas in solution. The initial water saturation helps the system to closely represent a natural water wet reservoir. The saturation process was very time-consuming due to the long reservoir model and low permeability of the consolidated sandpack. The procedure used for saturation of the reservoir model is succinctly detailed in the following paragraph.

The reservoir is first water saturated by injecting water with the help of the high pressure positive displacement pump as shown in Figure 1. Thereafter, upon completion of the recombination process in the visual PVT cell as described previously, the recombined oil with gas in

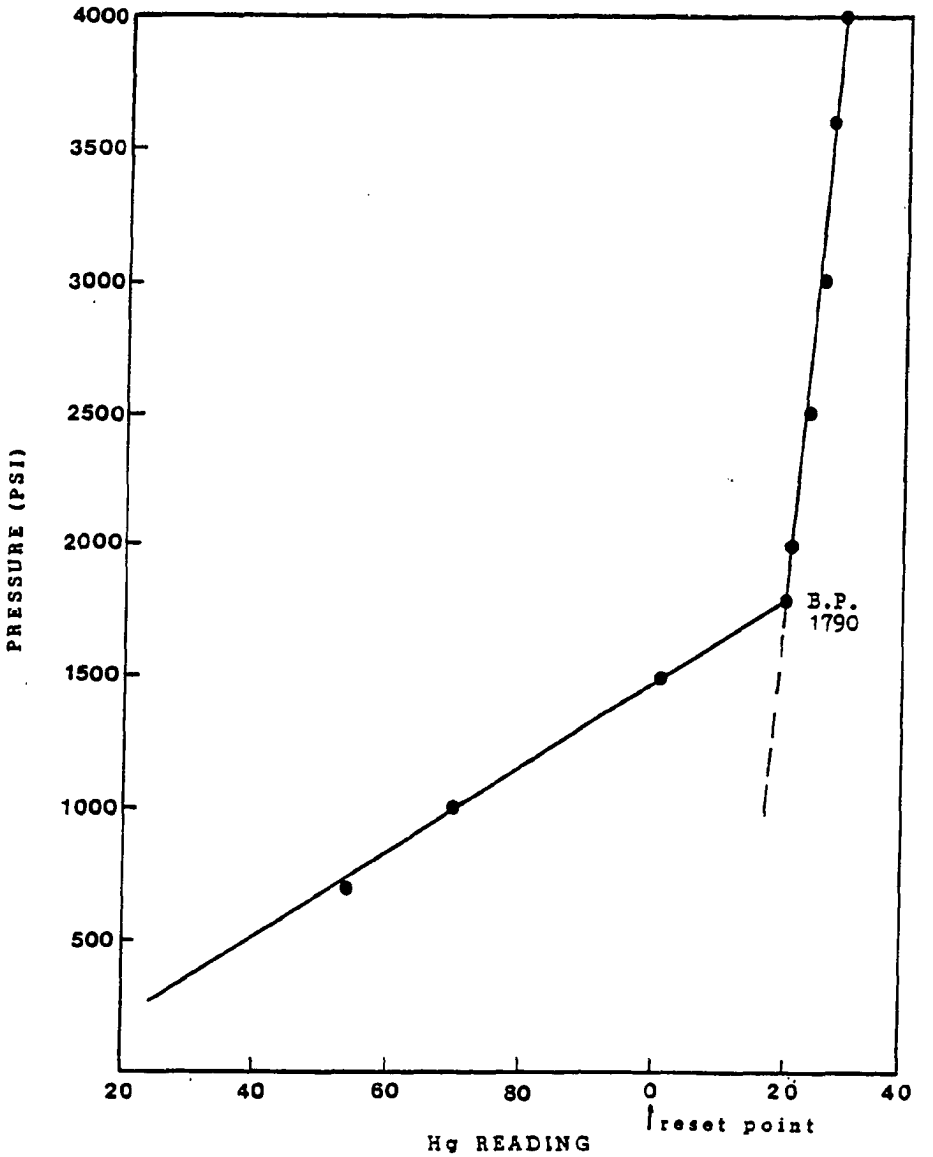

BUBBLE POINT: 1790 PSI

FIGURE 5 SATURATION PRESSURE CURVE FOR SOUTH LONE ELM CRUDE OIL RECOMBINED WITH NATURAL GAS (GOR = 575 scf/stb)

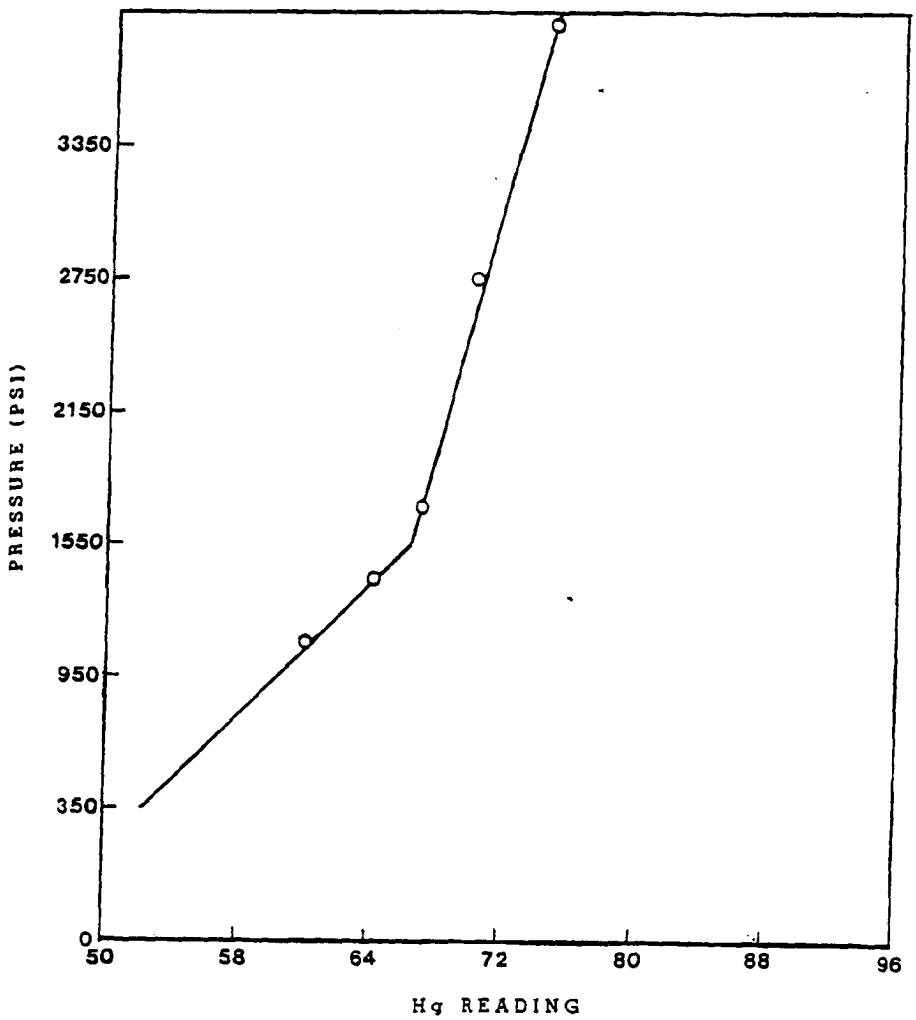

FIGURE 6 SATURATION PRESSURE CURVE FOR SOUTH LONE ELM CRUDE OIL RECOMBINED WITH NATURAL GAS (GOR = 400 scf/stb)

solution is injected into the reservoir model with the help of the mercury pump, which works through the PVT cell to make a piston like displacement of oil into the reservoir. Since the capacity of the PVT cell is much smaller than the pore volume of the reservoir model, about three full volumes of the recombined oil and gas had to be injected from the PVT cell for obtaining the maximum possible oil saturation in the reservoir physical model. The connate water saturation in the reservoir was found to be fairly consistent during the test runs.

4. Oil Recovery by Nitrogen Injection

After saturation of the reservoir model with oil, Nitrogen was injected at a pressure of about 4000 psi to displace the oil from the reservoir model. The high pressure Nitrogen formed a limited miscible slug in the reservoir and the recovery from the flood was collected in a graduated cylinder. The vapor samples from the effluent composition was analyzed by C. F. Alarcon[1] for determining the hydrocarbon and other outflowing vapor composition.

5. Oil Recovery by Naptha Injection

After completion of the secondary recovery process by Nitrogen injection, the remaining oil saturation in the reservoir model was often found to be more than 20 percent.

To recover that oil from the reservoir tertiary flooding was performed by using naptha as a miscible flooding liquid. The high pressure positive displacement pump was used to inject naptha into the reservoir while maintaining the reservoir pressure above the bubble point with the help of the back pressure regulator. The effluent concentration of naptha and oil during the naptha flood were determined by using the refractometer as shown in Figure 7.

Another experimental setup was later made for testing the dispersivity of Berea sandstone as shown in Figure 7. This later setup for this investigation will be hereinafter referred to as Setup #2. Similar displcement method as described for Setup #1 is used in Setup #2. Each component of this experimental setup is detailed in the following paragraphs.

(A) Epoxy Coated Core:

A Berea sandstone core, 2 inches (5.08 cm) Dia., 7.75 inches (19.69 cm) long with a cross sectional area of 3.141593 in^2 (20.26 cm^2) was used in this experimental setup. The Berea sandstone core was obtained from the Cleveland Quarries in Amhurst, Ohio and was coated with an epoxy coating to form a square shaped outer surface. This epoxy coating was tested to withstand 50 psig. The ends of the core were kept open for fitting in the core holder and for making necessary displacement experiments.

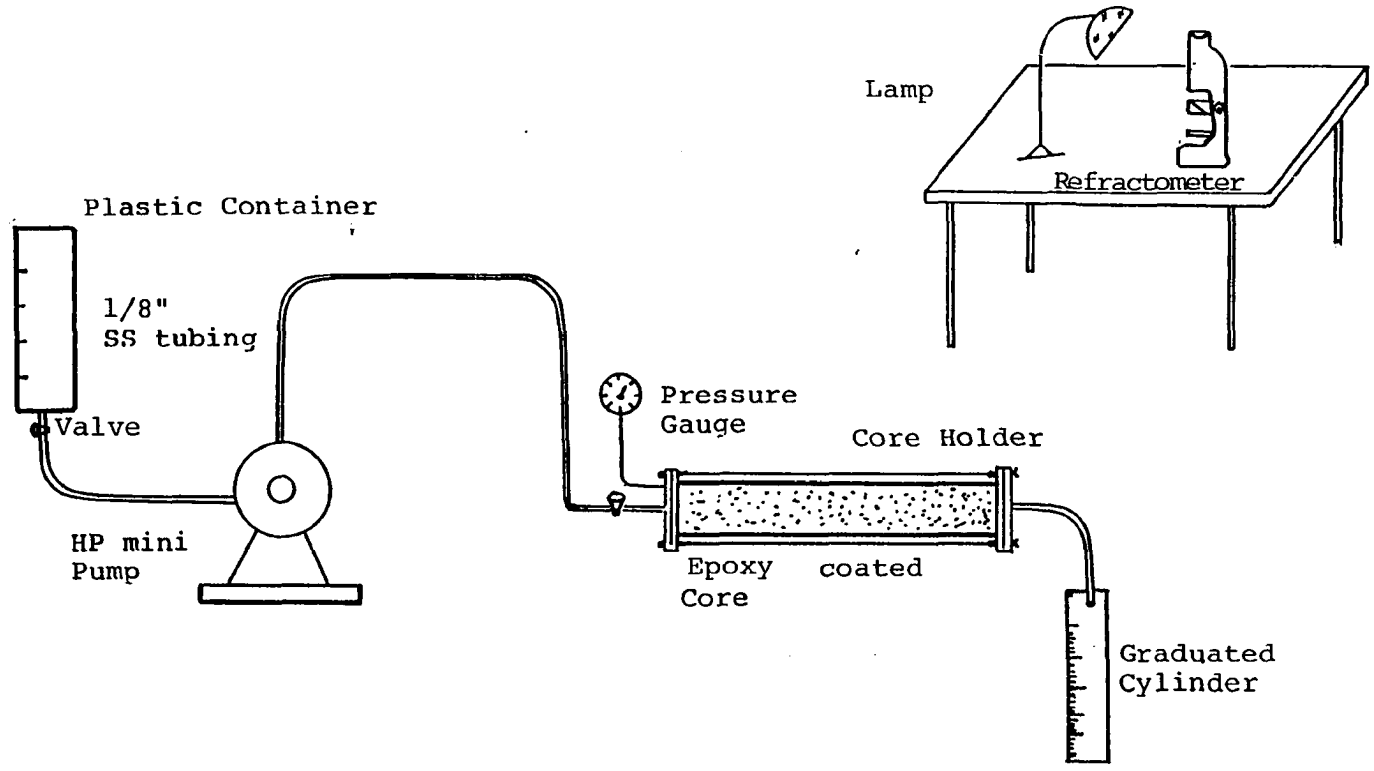

FIGURE 7 SCHEMATIC DIAGRAM OF EXPERIMENTAL SETUP #2

(B) Core Holder:

A core holder was made at the University of Oklahoma with two fiberglass endpieces to fit into the square shaped coating and were held together by four iron rods connected at the four corners with the help of hexagonal nuts. The weight of the epoxy-coated core and the core holder with all attachment was found to be 4.64 lbs (2105.2 gms), and the dry weight of the core was found to be 3.40 lbs (1540.5 gms).

(C) High Pressure Mini Pump:

The High Pressure (HP) mini pump used for setup #1 was also used in this experimental setup #2. The details of the pump is described previously under setup #1.

(D) Graduated Epoxy Container: One 1200 cc epoxy container was used as a liquid storage for feeding into the inlet of the HP mini pump, which was used to inject into the reservoir model.

(E) Pressure Gauge:

A Matheson pressure gauge, P/N 63-3412, of 100 psi capacity was used in this experimental setup as shown in Figure 7 for recording the inlet pressure of the displacing liquid. The inlet pressure was found to drop with the advancement of the flood front.

(F) Refractometer:

An Abbe refractometer was made available by the University of Oklahoma for this experimental study. The same refractometer was used in Setup #1. The use of the refractometer was described previously under Setup #1. The operational procedure of the refractometer is described stepwise hereunder:

1. Connect the refractometer to a cold flowing water tap to maintain a constant temperature during the experiment.
2. Wait until the temperature reading is constant.
3. Record temperature.
4. Place a small amount of liquid sample on glass plate.
5. Turn the lamp on.
6. While looking through the eyepiece, adjust the lamp to maximum brightness.
7. Adjust knob so as to form a clear interface between the light and dark areas.
8. Place this line at the intersection of the cross hairs in the eyepiece by turning the handwheel (on the side of the meter).
9. Hold switch down, the refractive index (R.I) can be read directly from the scale.
10. Clean the sample plate with distilled water, dry gently with a soft towel, place a soft, dry towel between plates.

11. Repeat the same procedure from step 4 for next sample, if any.

12. Turn the waterflows and the lamp off at the end of operation.

The third experimental setup, hereinafter referred to as Setup #3 was similar to Setup #2 except that the reservoir model used in Setup #3 was an unconsolidated sandpack. There was a close similarity between Setup #2 and Setup #3 in terms of the core length, fluid type, injection pressure, and temperature. The average interstitial velocity was quite high in Setup #3 due to its exceedingly high permeability compared to Setup #2.

A similar displacement method as described for Setup #2 is used in Setup #3. All components used in Setup #3 other than the sandpack were the same as used in Setup #2. The details of the unconsolidated sandpack used exclusively for this setup is furnished hereunder:

(A) Unconsolidated Sandpack:

An epoxy tube 4.44 cm (1.75 in.) I.D. was filled with clean dry sand and packed while filling. Length of the sandpack was 28.89 cm, and the cross sectional area was calculated to be 15.5179 cm^2. The ends of the core were fitted with valves to control injection and discharge from the sandpack.

3.0 THEORETICAL CORRELATION

Porous media can be visualized as a network of flow chambers, having random size and flow conductivity, connected together by openings of smaller size. These flow chambers, commonly known as flow paths conducts fluid through the medium. Some of these flow paths in the porous media are not interconnected and leads to dead end pore spaces.

The physical characteristics of the reservoir rock, such as porosity, permeability, tortuosity, and dispersivity plays a major role in the fluid flow through a porous media. The effect of dispersivity on the fluid flow through a porous media is studied and the dispersion coefficient/dispersivity is identified as a reservoir rock characteristic in this study.

Dispersion is considered as the macroscopic mixing caused by uneven laminar flow in fixed beds of real media. A variety of mechanisms on a macroscopic scale are considered to be responsible for the observable macroscopic dispersion as indicated by Greenkorn et al.[2]. Some of these

mechanisms which are considered to be responsible for dispersion are succinctly described below:

1. Eddy migration resulting from turbulent flow within the individual flow channels of the porous medium is one of the mechanisms which helps dispersion to occur.

2. Tortuosity is another important phenomenon which aids in occurrence of dispersion in a fluid flow through porous media. A tortuous porous medium means that the fluid elements starting at a given distance from each other and proceeding in the same direction will not remain the same distance apart as shown in Figure 8a.

3. Connectivity of the medium is also considered to be a factor responsible for dispersion in a porous media. All pores in the porous medium are not accessible to a fluid element after it has entered a particular flow path. The connectivity of the medium is thus not complete as shown in Figure 8b.

4. Flow Restrictions in a reservoir rock has a significant contribution to the dispersion in a fluid flow through a porous media. Recirculation arises from these flow restrictions. The conversion of pressure energy into kinetic energy gives a local region of low pressure, and if this region is accessible to fluid which has passed through the region previously, a recirculation similar to the

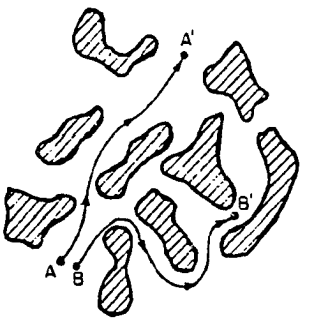

FIGURE 8a
MIXING DUE TO OBSTRUCTION

FIGURE 8b
INCOMPLETE CONNECTIVITY OF THE MEDIUM

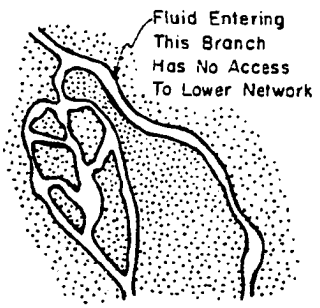

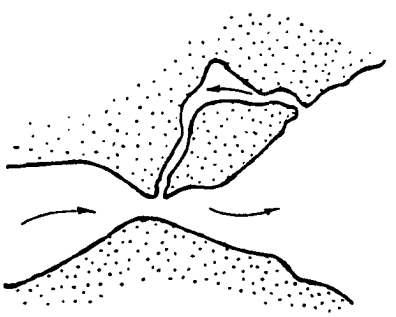

FIGURE 8c
RECIRCULATION CAUSED BY LOCAL REGIONS OF REDUCED PRESSURE

Source: 'FLUID FLOW THROUGH POROUS MEDIA', American Chemical Society Publications, Washington, D.C. (Ref. 2)

venturi-manometer combination is set up as shown in Figure 8c.

5. Dead-end Pore volumes cause dispersion in unsteady flow. As a solute-rich front passes the pore, diffusion into the pore occurs by molecular diffusion. After the front passes, this solute will diffuse back out, thus dispersing, for example, a step concentration input to the system. This dead-end pore space also causes confusion in the experimental interpretation because it is measured as porosity, but this porosity does not contribute to the available flow cross section for displacement of fluid through the porous media.

6. Adsorption is also found to contribute towards dispersion. It is considered to be an unsteady-state phenomenon. Similar to the dead-end pore volumes, due to adsorption a concentration front will deposit or remove material which tends to flatten concentration profiles in the interstitial fluid.

7. Adherence of the fluid to the wall also causes dispersion to occur. Macroscopic dispersion is produced in a capillary even in the absence of a molecular diffusion because of the velocity profile produced due to the adherence of the fluid to the wall. This causes fluid particles at different radial positions to move relative to

one another resulting to a dispersion by a series of mixing-cup samples at the end of the capillary.

Determination of dispersion coefficient has been attempted in the past by different investigators using various approaches such as statistical approach, continuum approach, and experimental approach. A few different models such as convective dispersion model, and dispersion-capacitance model, etc., have been investigated by different researchers for determining the dispersion coefficient. These investigations were conducted to determine the dispersion coefficients under different flooding conditions. Unlike all of these previous investigations, the objective of the present study is to identify dispersion as a reservoir rock characteristic.

The theoretical details of the dispersion phenomenon as uncovered by previous investigators using different approaches are furnished in the following paragraphs.

3.1 Statistical Approach:

The microscopic nature of the dispersion process reveals that the dispersion occurs not in one continuous medium, but in a medium which exhibits abrupt changes in fundamental properties when fluid flows from a fluid continuum to the porous structure and vice versa. For fluid flowing in a porous medium under conditions where the fluid

and the porous medium each behave individually as continua, if sufficient macroscopic parameters such as pressure drop, fluid-solid boundary location, etc. are specified, the problem is deterministic rather than stochastic in nature[2]. If complete information about the system is given, the detailed path of each fluid particle could be hypothetically calculated by using the basic statistical principles.

Such an approach is not feasible in practice due to the following reasons:

i. Determination of the precise solid-fluid boundary is impossible in most of the cases.
ii. The high tortuosity of a porous system renders problem for a mathematical solution.

Hence, a stochastic model of the porous system is found to be quite precise and in conformation with other approaches. A large number of fluid elements were fed to the stochastic model and information on the average flow rate, seepage velocity, etc., were averaged over the probability distribution of the model.

Almost all stochastic model focus on flow in elemental channels. A real porous medium consists of interconnecting passages and cul de sacs. The passage of fluid through the medium can be regarded as a series of steps in a random walk. The flow process can also be

regarded as analogous to turbulent flow, and the same mathematical model for turbulent flow may be applied. Similarly, the medium can be modeled by a network of capillaries built up of common subelements. Also by considering flow serially through a succession of capillaries drawn from some distribution of size, length, and orientation a model can be constructed.

A generalized statistical model of randomly oriented pores is exemplified by the works of Scheidegger[23], Saffman[22], De Josselin De Jong[12], and Haring et al.[14]. Scheidegger treated the statistical groundwork for the models of Saffman and De Josselin De Jong which were developed independently. Saffman considered an ensemble of randomly mixed straight pores. The pressure gradient in the medium was taken as linear with distance with an imposed fluctuation described by a Gaussian and isotropic probability density function. A random walk was taken with this model, assuming that successive steps were statistically independent. The lateral and longitudinal dispersions were then calculated and compared with the data.

The model of Saffman and De Josselin De Jong has been extended by Haring and Greenkorn[14] to the case of nonuniform media by use of the beta distribution, both for the radius and for the length distribution individually.

Capillary pressure, permeability, and longitudinal and transverse dispersion are calculated in terms of the parameters of the beta distribution. In this model, they assume an elemental pore as shown in Figure 9. The length, radius, and orientation angles θ and Y are assumed independent.

The dimensionless length $l^* = l/L$, where L is the longest pore and dimensionless radius $r^* = r/R$, where R is the largest radius pore and pores are distributed according to the beta function. The choice of the beta function is arbitrary and was made since it is a distribution which gives a range of skew and symmetric shapes, depending on values of the parameters. It is also conveniently normalized.

The probability distribution functions for l^* and r^* are defined by the following equations[14]:

$$f(l^*) = \frac{(a + b + 1)!}{a!b!} (l^*)^a (1-l^*)^b \quad ..(1)$$

$$g(r^*) = \frac{(\alpha + \beta + 1)!}{\alpha!\beta!} (r^*)^{\alpha} (1-r^*)^{\beta} \quad ..(2)$$

Where:
α and β are parameters of beta distribution.

The effect of nonuniformity on dispersion during the flow was focused in the investigation of Haring et al.[14]

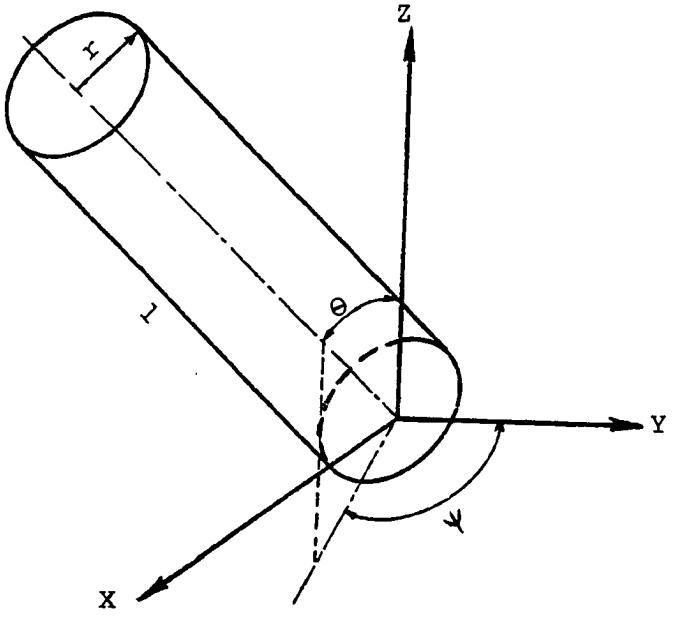

FIGURE 9 ELEMENTAL PORE FOR STATISTICAL MODEL

Source: "Flow Through Porous Media", American Chemical Society Publications, Washington, D.C. (Ref. 2)

The probability of existence of a pore with properties in the range l^* to $l^* + dl^*$, r^* to $r^* + dr^*$, θ to $\theta + d\theta$, Ψ to $\Psi + d\Psi$ is given by:

$$dE = \frac{1}{2\Pi}[f(l^*)dl^*][g(r^*)dr^*]Sin\theta d\theta d\Psi \quad ...(3)$$

If marked particle is assumed to take a random walk through the model then selecting pores proportional to volumetric flow rate, the probability of pore selection can be represented by the following equation:

$$dP = \frac{q}{M} dE = \frac{v\Pi r^2}{M} dE \quad .....(4)$$

Where:

q = Flow rate; v = velocity of flow; and

M is the normalization constant. The dispersion can be considered to be the variance of the average position of a marked particle; thus the longitudinal dispersion can be expressed as:

$$D_L = \frac{\overline{(Z - \tilde{V}T)}^2}{2T} \quad .....(5)$$

Where: $\tilde{V}$ is a velocity of fluids as defined later by eq. (19)
The transverse dispersion can be expressed as:

$$D_T = \frac{\overline{X}^2}{2T} = \frac{\overline{Y}^2}{2T} \quad .....(6)$$

Where:

T = Total time
X = Rectangular Coordinate
Y = Rectangular Coordinate

The position of a marked particle at the end of a number of steps

can be expressed as:

$$Z_n = \sum_{i=1}^{n} z_i \quad \ldots\ldots\ldots\ldots\ldots\ldots\ldots\ldots\ldots\ldots\ldots\ldots(7)$$

The average position can be expressed as :

$$\bar{Z}_n = nL \int_{P_1}^{P_2} 1^* \cos\theta \, dP \quad \ldots\ldots\ldots\ldots\ldots\ldots\ldots\ldots\ldots\ldots(8)$$

Likewise

$$\bar{X}_n = \bar{Y}_n = 0 \quad \ldots\ldots\ldots\ldots\ldots\ldots\ldots\ldots\ldots\ldots\ldots\ldots(9)$$

and

$$\bar{T}_n = nL \int_{P_1}^{P_2} \left(\frac{1^*}{v} \right) dP \quad \ldots\ldots\ldots\ldots\ldots\ldots\ldots\ldots\ldots\ldots(10)$$

The variance and co-variance may also be found by

$$\overline{(Z_n - \bar{Z}_n)^2} = n \int_{\rho} (z - \bar{z}) dP = nL^2 \sigma_z^2 \ldots(11)$$

and from similar integration over Pressure (P) -

$$\bar{X}_n^2 = nL^2 \sigma_x^2 \quad \ldots\ldots\ldots\ldots\ldots\ldots\ldots\ldots\ldots\ldots\ldots\ldots(12)$$

$$\overline{(T_n - \bar{T}_n)^2} = \frac{nL^2 \sigma_T^2}{v^2} \quad \ldots\ldots\ldots\ldots\ldots\ldots\ldots\ldots(13)$$

$$\overline{(Z_n - \bar{Z}_n)(T_n - \bar{T}_n)} = \sigma_{zT}^2 \ldots\ldots\ldots\ldots\ldots\ldots\ldots\ldots(14)$$

The expressions for the dispersion coefficients in terms of the parameters of the distribution function can be written as:

$$D_L = \frac{1}{12} \frac{(a+2)(a+b+2)}{(a+1)(a+b+3)J^2} \langle 1 \rangle \, VC_1 \quad ..(15)$$

where,

$$C_1 = \ln \left[\frac{27}{2} \frac{(a+b+2)^2 \, VT}{(a+1)^2 J^3 \langle 1 \rangle} \right]$$

and

$$D_T = \frac{3}{16} \frac{(a+2)(a+b+2)\langle 1 \rangle V}{(a+1)(a+b+3)J} \quad .....(16)$$

and

$$\frac{D_L}{D_T} = \frac{4}{9} J \ln \left[\frac{27}{2} \frac{(a+b+2)^2 \, VT}{(a+1)^2 J^3 \langle 1 \rangle} \right] \quad ..(17)$$

where

$$J = \frac{(\alpha+1)(\alpha+2)(\alpha+\beta+4)(\alpha+\beta+5)}{(\alpha+3)(\alpha+4)(\alpha+\beta+2)(\alpha+\beta+3)} \quad ...(18)$$

α and β = Beta Distribution parameters

TABLE 2 CALCULATED VALUES OF DISPERSION COEFFICIENT CORRESPONDING TO VARIOUS VALUES OF BETA DISTRIBUTION PARAMETERS[+*]

a	b	α	β	$K_L \times 10^3$ (cm^2/sec)	$K_T \times 10^4$ (cm^2/sec)	K_L/K_T
2	2	0	0	1.77	4.85	3.66
2	2	$-\frac{1}{2}$	$-\frac{1}{2}$	7.28	7.87	9.37
2	2	$-\frac{1}{2}$	1	33.20	16.80	19.80
2	2	2	4	4.82	6.54	7.40
2	2	2	2	3.78	5.87	6.42
2	2	4	2	2.43	4.89	4.96
2	2	1	1	4.54	6.32	7.18
2	2	2	4	3.96	5.15	7.70
2	4	1	1	4.78	4.96	9.65
4	2	1	1	7.95	11.60	6.85
2	4	4	2	2.02	4.00	5.05
4	2	4	2	4.26	8.95	4.76
1	1	4	2	1.98	4.28	4.68
1	1	2	4	3.54	5.75	6.16

+ - These calculated values are taken from Greenkorn et al.[2]

* - The interstitial velocity was taken as 0.1 cm/sec for calculating the values of dispersion coefficients

The dispersion coefficient for the model are definitely functions of the nonuniformity as shown in Table 2. It was noted that the particle following the most probable path does not travel at the Darcy velocity but at a velocity given by the following equation:

$$\tilde{V} = \frac{v}{J} \qquad (19)$$

where:

v is the darcy velocity

The model predicts a linear dependence of dispersion on velocity.

3.2 Continuum Approaches:

According to Darcy's equation, the flux is proportional to the velocity of flow. Hence, dispersion coefficient must be dependent on the velocity of flow.

If the interfacial tension between two fluids is non-zero the fluids do not mix then a distinct fluid-fluid interface always separates the fluids. Coexistence of two fluids in this manner is conventionally termed as immiscible

fluids. On the other hand, if the interfacial tension between two fluids is zero then a distinct fluid-fluid interface does not exist and the fluids are miscible.

If two fluids are miscible then molecules of one fluid can diffuse into the other fluid. This is a spontaneous process. It can be thought of as occurring by the following mechanism.

Consider two fluids brought into contact at a plane. Within either fluid the molecules have a random motion which is dependent upon the absolute temperature. This motion is isotropic; that is, in any homogeneous region there are equal numbers of molecules moving in all directions with the same distribution of velocity.

At the plane of separation there are molecules of kind 1 on the left, say, and molecules of kind 2 on the right. Due to the random motion some molecules of kind 1 cross the plane to the right and some of kind 2 cross to the left. This process expands in both directions until a homogeneous mixture of the two kinds of molecules exists. This process is termed "molecular diffusion."

If the fluids are immiscible, the molecules of kind 1 attempting to move right across the plane of separation would be acted on by a force field in the neighborhood of the interface which would restrain them.

Thus no mixing by diffusion would occur.

The heuristic description of diffusion given leads to the law of diffusion termed Fick's law. It is evident that the rate of movement of molecules should depend on the relative concentration. Thus the rate of movement across a plane should depend on the difference in concentration across the plane. More specifically, the rate of movement can be represented by

$$dn/dt = -D_o A \frac{dC'}{dx} \quad \text{.....(20)}$$

Where dn/dt is the number of molecules crossing the area A per unit time in the direction of increasing x, C' is the concentration in molecules per volume of molecules of the kind being considered and D_o is a factor called the diffusion coefficient, or the diffusion constant. The dimensions of D_o are length squared per unit time (cm^2/sec in c.g.s. units). Generally D_o is not exactly a constant. Not only does D_o depend upon the absolute temperature but it also varies somewhat with concentration. Furthermore the value of D_o for a particular kind of molecule depends upon what other kinds of molecules are present. However, in the majority of applications D_o can be treated as a constant for a particular problem.

Often the diffusion of a material substance is expressed in mass per unit time. If equation (20) is multiplied by M/L where M if the molecular weight of the diffusing substance and L is Avagadro's number, the number of molecules per mole, we get the following expression:

$$dm/dt = -D_o M \frac{A}{L} \frac{\partial c'}{\partial x} \quad \text{.....(21)}$$

Here dm/dt is mass per unit time diffusing across A. If the concentration, C', is expressed in the more common units of mass of diffusing material per mass of total substance, we have

$$C = MC'/L\rho \quad \text{.....(22)}$$

Where ρ is the mass density of total substance. If ρ is treated as being constant, independent of composition of the substance, then Fick's law can be written in the form:

$$dm/dt = -D \frac{A\, dC}{dx} \quad \text{.....(23)}$$

where $D = \rho D_o$
= the diffusion constant expressed in mass/length-time. The common units are gm/cm-sec.

Fick's law can be written for a general geometry in the multidimensional case, as

$$\dot{m} = -D \nabla C \quad \text{.....(24)}$$

Where:

$\dot{m}$ = mass flux density vector, mass per unit time per unit area.

This is the form most often employed in applications to flow problems.

To illustrate some of the microscopic features of miscible displacement in porous materials we consider first the problem of the displacement of a fluid from a straight circular capillary tube by another fluid which is miscible with the resident fluid.

If the two fluids have the same viscosity and density the distribution of fluid velocity within the tube does not depend on the distribution of the two fluids within the tube. For slow steady flow at the mean velocity, v, the velocity at a point a distance r from the axis of the tube can be expressed as:

$$v(r) = 2\bar{v}(1 - r^2/a^2) \quad \text{.....(25)}$$

Where:

a = radius of the tube.

The fluid at the wall does not move and the fluid on the axis of the tube has the maximum speed. Thus, if a group of marked particles lies on a plane perpendicular to the axis at time zero they will lie on the surface of a paraboloid of revolution at any later time by convection alone.

If at time t = 0 the concentration distribution of injected fluid is C(x,r), where x is measured along the axis, then at time t the concentration is given by

$$C = C(x - vt, r) \quad \ldots\ldots\ldots\ldots\ldots\ldots\ldots\ldots (26)$$

The value of v used in equation (26) is given by equation (25). Thus the convection alone produces a dispersion of injected fluid.

Several investigators have undertaken to construct a mathematical theory describing the dispersion phenomenon. Scheidegger[23] and Saffman[22] have treated the problem in terms of random walk formulation in analogy to Einstein's theory of Brownian motion. Saffman[22] has also treated the problem by the method of Lagrangian correlation functions.

Kramers and Alberda[17] rationalized that on the basis of a cell-mixing model the equation for concentration in a packed tube with uniform flow can be expressed as:

$$\frac{\partial C}{\partial T} = D \frac{\partial^2 C}{\partial x^2} - v_x \frac{\partial C}{\partial x} \quad \ldots\ldots\ldots\ldots (27)$$

The solution for this problem yields the same frequency response diagram as a number n of perfect mixers, each with the same residence time. Thus, if a packed bed is divided into n equal parts, the average residence time can be expressed as L/nv_x and the dispersion time constant can be expressed as $L^2/2Dn^2$.

Based upon the continuum approach, two flexible and generalized models on dispersion coefficient, namely the Covective Dispersion Model and the Dispersion-Capacitance Model, were developed in the past by Perkins and Johnston[20], and Coats and Smith[10], respectively. Theoretical details of these models are furnished in the following paragraphs.

(A) Convective Dispersion Model :

The mathematical formulation of the dispersion model and the mixing phenomenon is detailed in this section. The use of the model in calculating the slug size requirements is also demonstrated by an example after the theoretical details.

The mixing process may be demonstrated by considering the following idealized linear displacement:

i. A linear tube is uniformly packed with sand.
ii. The sandpack is homogeneous and isotropic.
iii. The sandpack is completely saturated with oil.
iv. The oil is displaced by a solvent having the same density and viscosity as the oil.

Such a displacement is shown in Figure 10. Because the displaced and the displacing fluids have the same density and viscosity, and the porous medium is isotropic, the flood front is stable and the displacement is essentially piston-like. The change in the solvent concentration at the oil/solvent interface as the oil moves through this ideal system is also depicted in Figure 10. At the system inlet the interface is initially sharp. As the solvent travels through the sandpack, a mixing develops with a resultant S-shaped concentration profile. This mixing zone becomes progressively larger with distance traveled.

Molecular Diffusion and convective dispersion are the two distinct mechanisms which contribute to the growth of the mixing zone. Even in the absence of the gross fluid movement a mixing zone would develop due to the random thermal motion of the molecules - this mechanism is referred to as molecular diffusion. The dispersed zone is much larger with fluid movement than with molecular diffusion. The additional mixing is due to convective dispersion, a mechanism resulting from uneven flow paths brought about by microscopic heterogeneities.

The general dispersion equation describing the

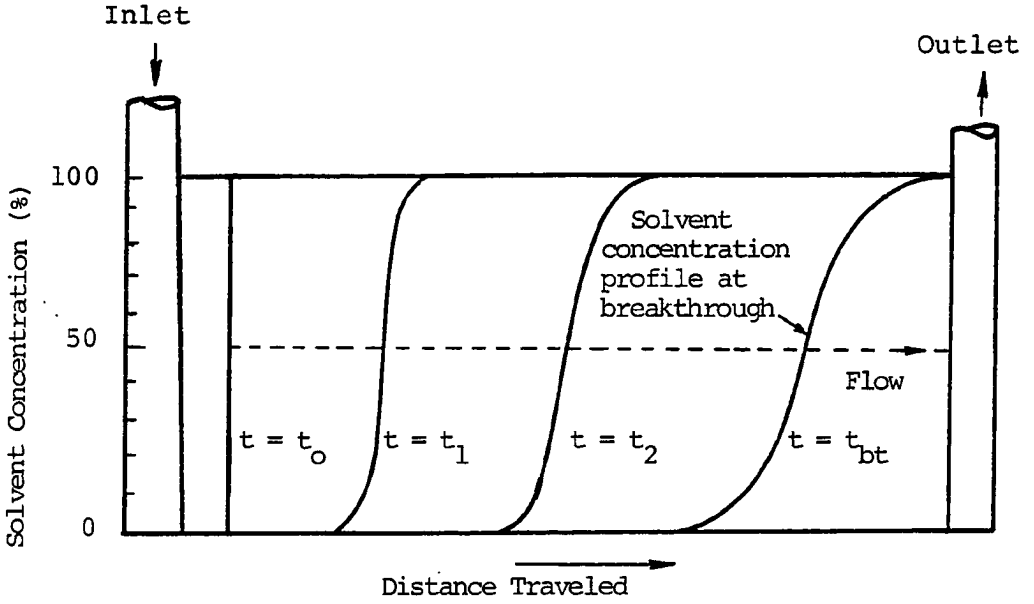

FIGURE 10 SOLVENT CONCENTRATION PROFILE IN AN IDEALIZED LINEAR DISPLACEMENT

Source: S. M. Chen et al. (Ref. 7)

overall transport and mixing of fluids flowing through a porous medium can be written as:

$$\nabla.(K.\nabla C) - (V.\nabla C) = \frac{\partial C}{\partial t} \quad \ldots\ldots\ldots\ldots\ldots\ldots (28)$$

Where:

C = Solvent concentration
K = Effective Dispersion coefficient
V = Average Interstitial Velocity
  = Q/Ao
A = Cross-sectional area of the core
o = Porosity of the medium

For the idealized linear displacement described above, Equation (28) takes the following form:

$$K.\frac{\partial^2 C}{\partial x^2} - V.\frac{\partial C}{\partial x} = \frac{\partial C}{\partial t} \quad \ldots\ldots\ldots\ldots\ldots (29)$$

Where:

K = D + E
D = Effective molecular diffusion coefficient
E = Convective dispersion Coefficient

A considerable effort has been devoted towards the development of a quantitative relationship describing the

effective dispersion coefficient as a function of various displacement parameters. Perkins and Johnston[20] developed the following equation for effective dispersion coefficient:

$$K = \frac{D_o}{F\phi} + 0.5V\sigma\, dP, \quad 4 < \frac{V\sigma\, dP}{D_o} < 50 \qquad (30)$$

It was observed that at low flow rates ($V\sigma\, dP < 0.1$) mixing is almost entirely due to molecular diffusion, whereas at high flow rates ($V\sigma\, dP > 4.0$) convective dispersion dominates the mixing process, and at intermediate flow rates ($0.1 < V\sigma\, dP < 4.0$), both the mechanisms contribute to the mixing process.

Analytical solutions to Equation (29) have been derived for various boundary conditions by Brigham[7] . For the idealized displacement above, and ignoring higher order terms, the solution for solvent concentration can be written in the form:

$$C = 0.5\ \mathrm{erfc}\left\{ \frac{x - Vt}{2(Kt)^{0.5}} \right\} \qquad (31)$$

This equation describes the growth of the zone in which C varies from zero to unity.

Because of the asymptotic behavior of the

complementary error function, it is not practical to define the mixing zone as that in which C ranges from zero to unity. Instead, it is customary to select arbitrary values of concentration, such as 0.10 to 0.90, to define the mixing zone boundaries. By substituting the above values for C in equation (31), we can solve for the zone boundaries as follows:

$$X_{10} = 0.9062.2(Kt)^{0.5} + Vt \quad \text{.....(32a)}$$

and

$$X_{90} = -0.9062.2(Kt)^{0.5} + Vt \quad \text{.....(32b)}$$

Where:

X_{10} = Distance to the 10% solvent concentration
X_{90} = Distance to the 90% solvent concentration

If the mixing boundaries are arbitrarily defined at C values of 0.05 and 0.95, the distances to the zone boundaries become:

$$X_5 = 1.163.2(Kt)^{0.5} + Vt \quad \text{.....(33a)}$$

and

$$X_{95} = -1.163.2(Kt)^{0.5} + Vt \quad \text{.....(33b)}$$

Where:

X_5 = Distance to the 5% solvent concentration
X_{95} = Distance to the 95% solvent concentration

The mixing zone length (MZL) corresponding to Equations (32a) and (32b) can be expressed as:

$$MZL_{10-90} = X_{10} - X_{90} = 3.625(Kt)^{0.5} \quad ...(34)$$

The mixing zone length of the effluent is measured experimentally and equation (34) is used to solve for the effective dispersion coefficient, K.

In a miscible slug process, as shown in Figure 11, two distinct mixing zones develop at the interface between oil and solvent, and between solvent and chase gas. In this case it is apparent that the sum of the two mixing zones with concentration cut-offs of 0.10 and 0.90 can be expressed as:

$$X_{10} - X_{90} = 3.625\{(K_{o/s}.t)^{0.5} + (K_{s/g}.t)^{0.5}\} \quad .....(35)$$

Where:

$K_{o/s}$ = Effective dispersion coefficient for the oil/solvent system

$K_{s/g}$ = Effective dispersion coefficient for the solvent/chase gas system

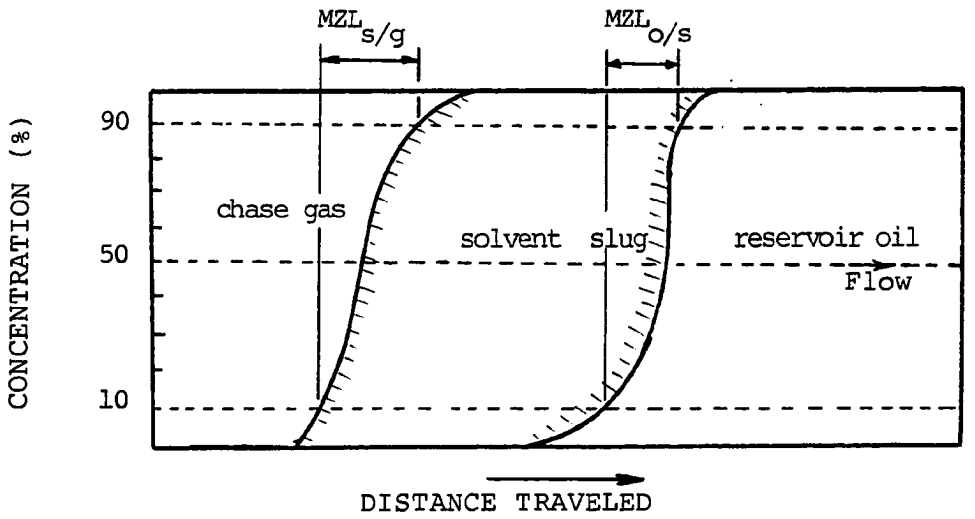

MZL - Mixing Zone Length

FIGURE 11 MIXING ZONES IN A MISCIBLE SLUG PROCESS

Source: S. M. Chen et al. (Ref. 7)

If 90% solvent concentration is sufficient to maintain miscibility, then the minimum slug requirement will be equal to the total volume of solvent within the mixing zone defined by equation (35) at solvent breakthrough. Since the concentration profiles are symmetric about the point C = 0.50, the required solvent volume is in fact equal to one half the total volume in the mixing zone. By dividing the MZL by the total length, L, the minimum slug size can be expressed as a function of the total pore volume as follows:

$$S_{min} = \frac{\text{MZL @ Breakthrough}}{\text{Total System Length}} \quad \ldots\ldots\ldots\ldots\ldots (36)$$

$$= \frac{3.625}{2L}\left\{(K_{o/s}.t_{bt})^{0.5}+(K_{s/g}.t_{bt})^{0.5}\right\}^{2}$$

Where:

S_{min} = minimum solvent slug size required
t_{bt} = Breakthrough time

A sample calculation of slug size requirements using representative dispersion coefficients, and for a variety of well spacings, is shown in Table 3.

Two general observation can be made from this sample calculation:

i. The slug requirements are typically quite small.

ii. With increasing system length, the slug size, expressed as a fraction of the total pore volume decreases.

(B) Dispersion-Capacitance Model:

Significant deviation from the symmetrical effluent concentration profiles of an ideal system is observed in an actual reservoir condition. Most of the tests carried out on actual reservoir rock were characterized by:

i. Breakthrough of the 50% concentration prior to the injection of one pore volume of solvent, and

ii. An asymmetrical solvent concentration profiles.

These characteristics are illustrated in Figure 12. It was postulated that such results must be due to capacitance effects. The porous medium in these tests must contain a stagnant or dead-end pore volume which contributes to the total pore volume, but which can not flow. This dead-end pore volume is considered to be the main reason for the early breakthrough of the 50% concentration. The asymmetrical profile is a result of mass transfer between the by-passed stagnant volume and the solvent.

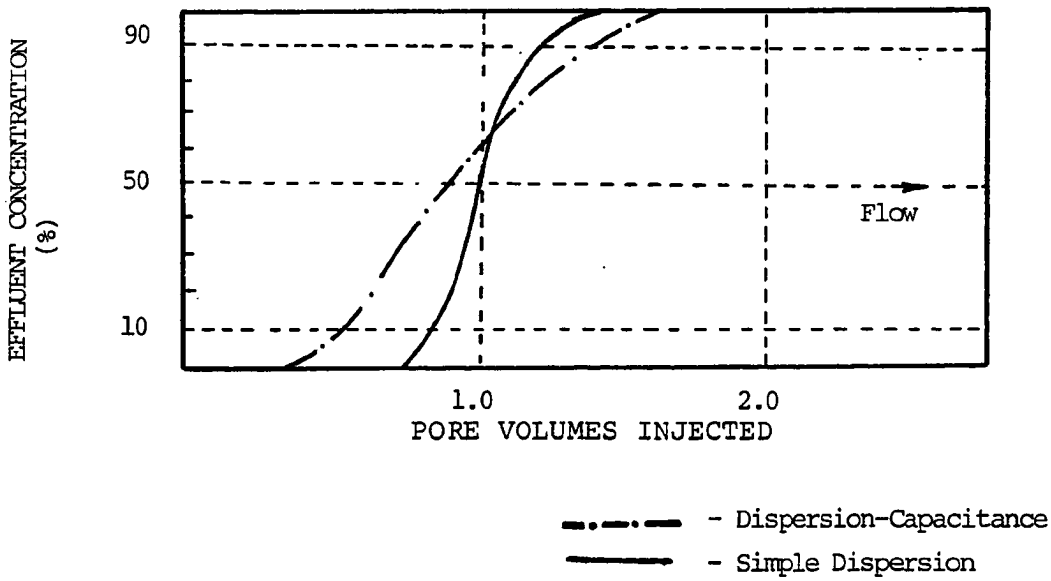

FIGURE 12 EFFLUENT CONCENTRATION PROFILES SHOWING CAPACITANCE EFFECTS

Source: S. M. Chen et al. (Ref.9)

TABLE 3 CALCULATION OF THE SLUG SIZE USING THE DISPERSION MODEL*

S (ha)	L (m)	V (cm/s)	$K_{o/s}$ (cm^2/s)	$K_{s/g}$ (cm^2/s)	t_{bt} (sec)	S_{min} (%HCPV)
8.1	201	0.000113	0.00003	0.00052	$2.52x10^8$	4.1
16.2	284	0.000159	0.00004	0.00053	$2.52x10^8$	3.0
32.4	402	0.000225	0.00005	0.00054	$2.52x10^8$	2.2
64.8	569	0.000319	0.00007	0.00056	$2.52x10^8$	1.6

* Source: S. M. Chen et al.[9]

S = Well spacing, Hectare; L = Interwell Distance;

V = Interstitial velocity; $K_{o/s}$ = Oil-solv. dispersion coeff.

$K_{s/g}$ = Solvent-Gas dispersion coeff.;

t_{bt} = Breakthrough time; S_{min} = Min. Slug size

Displacement parameters

Five Spot Pattern

F = 20; O = 0.10; $_{dp}$ = 0.36 cm; $(D_o)o/s = 2x10^{-5}$ cm^2/sec

$(D_o)s/g = 1x10^{-3}$ cm^2/sec

A mathematical model, namely the dispersion-capacitance model, has been developed by Coats and Smith[10] to take into account the effect of the dead-end pore volume on the mixing zone. Equation (29) representing the simple dispersion model was modified as follows:

$$K.\frac{\partial^2 C}{\partial x^2} - V.\frac{\partial C}{\partial x} = f.\frac{\partial C}{\partial t} + (1-f).\frac{\partial C^*}{\partial t} \quad .(37)$$

and

$$(1-f).\frac{\partial C^*}{\partial t} = M(C - C^*) \quad .....(38)$$

Where:

f = Flowing volume fraction
M_* = Mass transfer coefficient
C^* = Solvent concentration in stagnant volume

It may be noted that this equation reduces to Equation (29) for f = 1.

It may be noted that the parameters K, f, and M, as defined in the previous paragraph, can be adjusted to match the effluent concentration profiles according to this capacitance model rather than just one parameter (K) in a simple dispersion model. Because of this flexibility the

dispersion-capacitance model should be able to fit the experimental data more closely than a simple dispersion model. However, this better match is still not considered to be a proof that the capacitance is an actual physical phenomenon by Coats and Smith[10], who considers it to be a concept only.

The Dispersion Capacitance model was further modified by Baker[3] and Batycky et al.[4] for simulating the dual porosity systems exhibited commonly by carbonate and limestone reservoirs. The flowing fraction of the pore volume represent the interconnected vug-microfracture porosity system, and the stagnant volume represents the intergranular matrix porosity system. However, since the intergranular porosity system normally exhibits a very low permeability, it is not entirely correct to consider this volume as totally stagnant. This phenomenon is considered as a predominant factor when the microfractures are not continuous from injector to the producer. In this case, an injected fluid must eventually flow through parts of the matrix porosity in order to reach the producer.

The solvent first enters the vug-microfracture porosity in such a system, but since the fractures are discontinuous, the solvent is forced to flow through at least a part of the

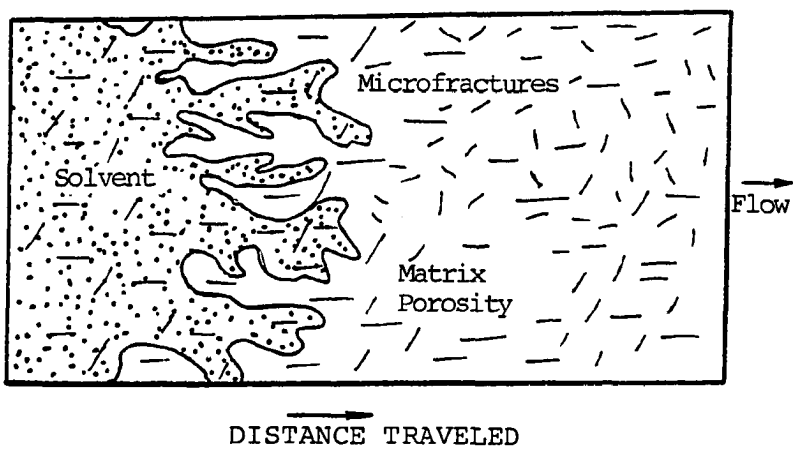

FIGURE 13 DISPLACEMENT OF SOLVENT IN A DUAL POROSITY SYSTEM (Ref. 9)

intergarnular porosity. This type of displacement of solvent in a dual porosity system is shown in Figure 13.

Therefore, it seems that in applying the dispersion-capacitance model to a dual porosity system, the parameter M represents not only mass transfer effects, but also takes into account actual fluid flow through the two porosity systems. If laboratory-derived parameters using a dispersion-capacitance model are to be applied to flow in the reservoir, it is important to distinguish the relative contributions of mass transfer and interflow between porosity systems. Hence, equations (37) and (38) of the dispersion-capacitance model were retained in the same way and the parameter f in these equations was modified in the following way:

$$f = f_1 + f_2 \quad \text{.....(39)}$$

Where:

f_1 = Volume fraction occupied by vug microfracture porosity

f_2 = Fraction of matrix porosity swept by solvent

The term f_1 can be considered as constant in equation (39) since solvent will flow through most of the microfractures. However, the term f_2 may depend on

several parameters, such as the ratio of microfracture porosity to matrix porosity, distribution of microfractures, injection patterns, etc. The term f_2 is a function of time and can be estimated from the sweep efficiency.

Greenkorn and Kessler[2] gave a detailed description of the microscopic dispersion in porous media as detailed previously in this report. Scheidegger[23] showed that there are two possible extremes for the form of dispersion coefficient K, one directly proportional to velocity v, the other proportional to the square of the velocity. The former relation reflects the situation where there is enough time for complete mixing of the fluids, while the later one represents incomplete mixing. Most investigators prefer a similar form, with the exponent of velocity between one and two.

Blackwell[6] expressed (K/D_o) as a function of $(d_p v/2D_o)$, where D_o is the molecular diffusion coefficient, giving

$$K/D_o = 0.67 \quad \text{for} \quad \frac{d_p v}{2D_o} < 0.04 \qquad \ldots\ldots\ldots\ldots (40)$$

and

$$K/D_o = 8.8\left(\frac{d_p v}{2D_o}\right)^{1.17} \text{for} \quad \frac{d_p v}{2D_o} > 0.5 \qquad \ldots (41)$$

Brigham et al.[8] proposed a general expression of the following form

$$K/D_o = 1/F\phi + a\left(\frac{d_p v}{D_o}\right)^{1.20} \quad \text{.....(42)}$$

Where:

F = Formation resistivity factor.
ϕ = porosity

In equation (42) d_p is calculated from the following relation:

$$d_p = 6\sqrt{(8kT^2/\phi)} \times 10^{-4} \quad \text{.....(43)}$$

Where:

T = Tortuosity

k = permeability of the medium in Darcies

The equations used in calculating the dispersion coefficient from the experimental observation in this study were originally developed by Brigham et al.[8] . Theoretical equations initially derived by Taylor[25] showed that if one fluid were displaced by another fluid under these conditions where diffusion could nearly damp-out radial concentration variations, then a symmetrical longitudinal mixed zone would be established. The mixed zone would travel with the mean speed of the injected fluid and would be dispersed as if there were a constant dispersion coefficient given by the following equation:

$$K_l = D_o + \frac{U^2 a^2}{48 D_o} \quad \text{.....(44)}$$

Where:

K_l = Longitudinal dispersion Coefficient, in cm^2/sec.

a = Radius of the capillary in cm

U = Average Interstitial Velocity in cm/sec
= $Q/A\phi$

A = Cross-sectional area of the core in cm^2
ϕ = Average porosity of the medium
Q = Volumetric injection rate or discharge rate in cm^3/sec

Brigham et al.[8] have shown a convenient method for determining the dispersion coefficient from experimental data obtained from miscible displacement. With a given pore volume, V_p, of the porous media, and any volume, V, during displacement through the porous media, a parameter λ is defined as follows:

$$\lambda = [(V/V_p) - 1)]/\sqrt{V/V_p} \quad \text{.....(45)}$$

A plot of λ against concentration on arithmetic probability paper results in a straight line, from which the values of corresponding to 90% and 10% displacing liquid

concentrations are read. The dispersion coefficient K is then calculated from the following equation:

$$K = U L \frac{(\lambda_{90} - \lambda_{10})^2}{(3.625)^2} \quad \text{.....(46)}$$

Where:

L = Length of the core in cm.

$\lambda_{90} = [(V/V_p) - 1]/\sqrt{V/V_p}$, when effluent contains 90% displacing fluid

After determining the dispersion coefficient, K, from equation (46), the mixing coefficient α_d is calculated by using the following equation:

$$\alpha_d = (K - D)/U \quad \text{.....(47)}$$

Where:

D = Diffusion coefficient
U = Average interstitial velocity

In a miscible flooding process both the displaced and the displacing fluids are in dynamic condition and hence the diffusion effect is very small and negligible. Hence, the mixing coefficient, called the Dispersivity, for a purely dispersing system can be expressed by the following equation:

$$\alpha_d = K/U \quad \text{.....(48)}$$

Where:

α_d = Dispersivity, cm
K = Dispersion coefficient in cm^2/sec
U = Average interstitial velocity, cm/sec

To calculate the amount of oil recovered during two observations the following equation was developed in the early stage of this study:

$$Oil_i = Rx(1 - efc_i)x(V_2 - V_1) \quad \ldots\ldots(48)$$

Where:

Oil_i = Amount of oil recovered during two susbsequent observations, cc

R = Random number between 0.5 and 0.9

efc_i = Effluent solvent concentration at the first observation point.

$V_{1,2}$ = Volume injected, cc at the time of observations 1 and 2

Due to random variation of the effluent concentration of crude oil as observed during the experiment, a random correction factor is introduced in equation (48) to compute the amount of crude oil produced during two subsequent observations. Cumulative oil recovered by tertiary flooding is then calculated by the following equation:

$$Q = \sum_{i=1}^{n} Oil_i \quad \ldots\ldots(49)$$

Where:

Q = Cumulative oil recovered

In the later stage of this study the cumulative oil recovered by Naptha flood was determined by measuring the area under the crude oil concentration curves. Crude oil concentration curves for each run are shown separately in Figures D-1 through D-8 as enclosed in Appendix-D to this report. This method of computing the crude oil volume was found to be more precise.

Efficiency of the tertiary flooding is then calculated by using the following equation:

$$\eta = (Q \times 100)/OILIN \quad \ldots\ldots\ldots\ldots\ldots (50)$$

Where:

η = Efficiency, %

OILIN = Oil in place before the beginning of naptha injection, cc

4.0 EXPERIMENTAL RESULTS

The basic physical properties of the reservoir model were first determined in this study which was done in conjunction with the enhanced oil recovery project by Nitrogen injection[1]. The porosity, and the permeability of the reservoir model were the two important parameters needed to be determined before any other test could be performed.

Using standard testing procedure the absolute permeability of the reservoir model for Setup #1 was determined to be 910 mD, and the average porosity for Setup #1 was found to be 32%. The absolute permeability of the consolidated Berea core used in Setup #2 was found to be 80 mD, and the corresponding porosity was determined to be 14%. The absolute permeability of the unconsolidated Sandpack used in Setup #3 was found to be 66,800 mD, and the corresponding porosity was determined to be 41.7%.

Details of calculation and experimental observations in attaining these aforementioned values of porosity and permeability of the reservoir models are furnished in Appendix A to this report.

The experimental condition under Setup #1 was changed after the first four runs. The reservoir model was modified to include a heating system and the experimental run for the next four tests were conducted at an elevated temperature of 120 °F. Actual reservoir condition was better represented in this modified condition. No heating system was involved in the second setup.

The first two tests were conducted by monitoring the effluent from point C of the reservoir model of Setup #1 as shown in Figure 1. This point represents 60% of the total model length. The third and the fourth tests were conducted by monitoring the effluent from point E, the producing end, of the reservoir model maintaining other experimental conditions similar to the first two tests.

The fifth and the sixth tests were conducted at an elevated reservoir model temperature of 120 °F. The seventh test was conducted in a different experimental setup with a consolidated reservoir core as shown in Figure 7.

A computer program 'DISCAL' was written to compute the value of λ (lamda) for each experimental observation by using equation (45). The values of λ_{10} and λ_{90} corresponding to 10% and 90% effluent solvent concentration respectively were then determined by the program using

average gradient based upon arithmetic probability. This determination was possible only graphically before. So, this program introduces a new method of computing λ_{90} and λ_{10}. The values of Dispersion coefficient and Dispersivity is then determined by the program by using equations (46) and (47) respectively.

This program also has the option to calculate the amount of oil recovered during the flood when the decline in oil concentration do not follow a regular trend, and an average oil concentration for two subsequent observations by arithmetic averaging would not yield correct results. However, the amount of oil recovered during the Naptha flood was graphically determined in this study for attaining better precision.

The efficiency of the tertiary recovery is then computed by using equation (50). The initial oil in place was noted at the beginning of each experimental Run. A flowchart for the computer model 'DISCAL' is shown in Figure 14. A listing of 'DISCAL' computer model is furnished in Appendix D to this report.

Experimental data pertaining to each test for these two different setups and the observations therefrom are furnished separately under each experiment number in the following pages of this report.

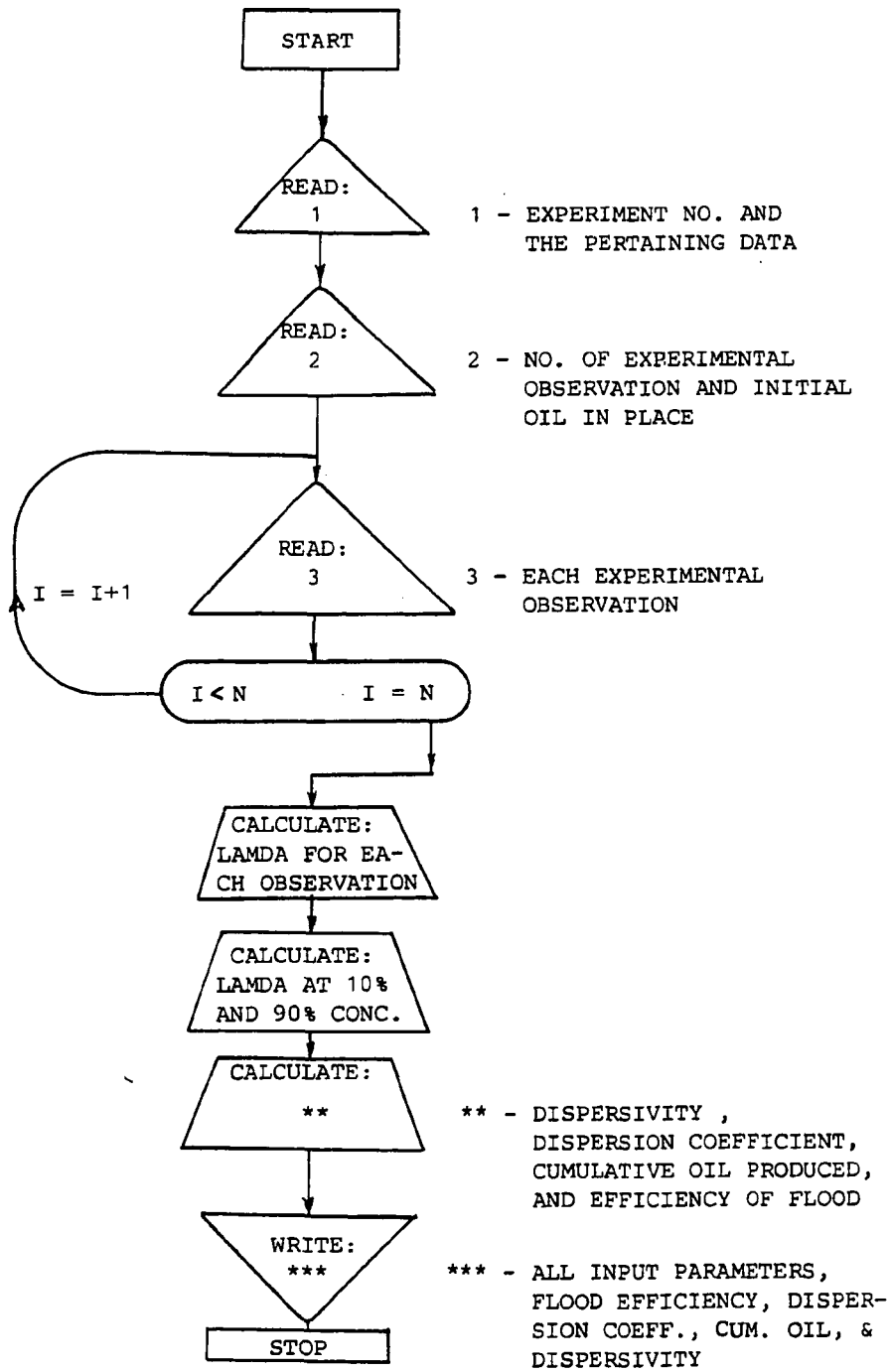

FIGURE 14 FLOWCHART FOR THE COMPUTER PROGRAM 'DISCAL'

RUN # 1

EXPERIMENTAL SETUP # 1

Length of the Core	=	2286.00 cm
Average Interstitial Velocity	=	0.3837 cm/sec
Displacing Fluid	=	Naptha
Displaced Fluid	=	Crude Oil
Reservoir Model Temp.	=	72.0 F
Permeability of the Core	=	910.00 mD
Cross-sectional Area	=	0.9588 sq. cm
Pore Volume	=	702.25 cc
Porosity	=	32%
Injection Pressure	=	4000 psi
Cumulative Oil Recovered By Tertiary Flooding	=	92.00 cc
Efficiency of Tertiary Flooding	=	88.92%

Initial Saturations before Naptha Flood: S_w = 23%; S_o = 14.7%; S_g = 62.3%

The output of the computer model showing the detail experimental condition of test #1 and the computed values of average interstitial velocity, cumulative crude oil produced, and efficiency of the flood is listed in the previous page under Run #1. The computed values of lamda for each experimental observation is listed in Table 4.

The computed values of Dispersion Coefficient and Dispersivity is listed after the Table as shown in the following page. The effluent concentration of the displacing fluid (Naptha) is plotted against the calculated values of lamda as shown in Figure 15.

The effluent concentration is also plotted against time as shown in Figure 16 which is indicative of the movement of the floodfront during the miscible flooding process.

The efficiency of tertiary flooding was found to be 88.92% in this experimental Run. Comparison of the results obtained from this test with the results from other tests is reviewed in detail in the next section of this report under Discussion.

TABLE 4

EXPERIMENTAL OBSERVATION # 1

Refractive Index	Naptha Injected (cc)	Time (Sec.)	Calculated Lamda	Effluent Naptha Conc. (%)
1.4663	525.00	3100.	-0.1575	4.00
1.4600	580.00	3193.	-0.0577	21.50
1.4580	596.00	3450.	-0.0305	30.00
1.4510	610.00	3693.	-0.0073	57.40
1.4470	622.00	3900.	0.0122	66.50
1.4450	628.00	4000.	0.0218	72.00
1.4440	646.00	4300.	0.0500	73.50
1.4410	688.00	5000.	0.1131	84.10
1.4395	724.00	5600.	0.1642	87.50
1.4390	736.00	5800.	0.1807	90.00

Calculated Value of:

DISPERSION COEFFICIENT = 6.3862 sq cm/sec
DISPERSIVITY = 16.646 cm

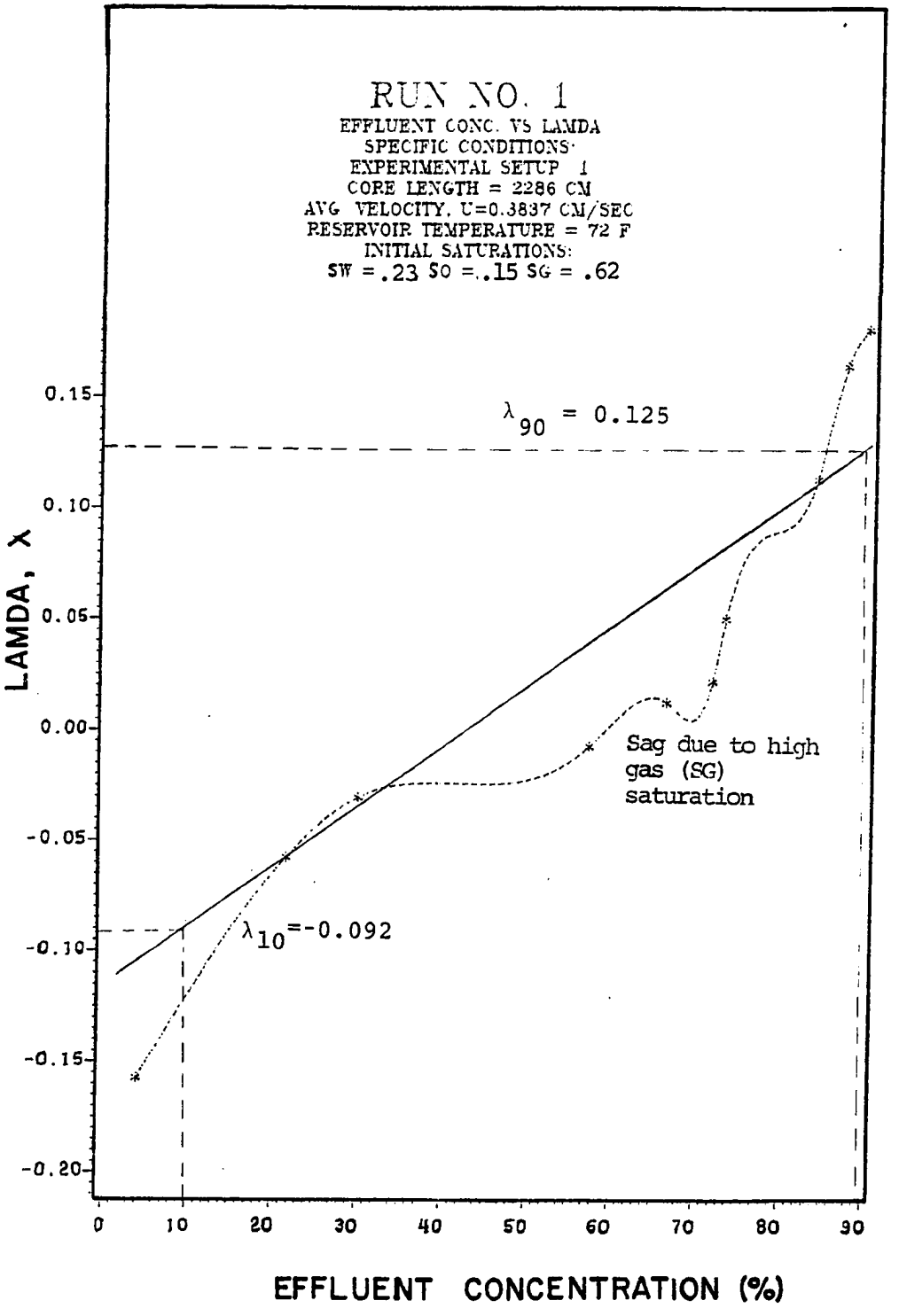

FIGURE 15 CALCULATED LAMDA VS EFFLUENT SOLVENT CONCENTRATION FOR RUN #1

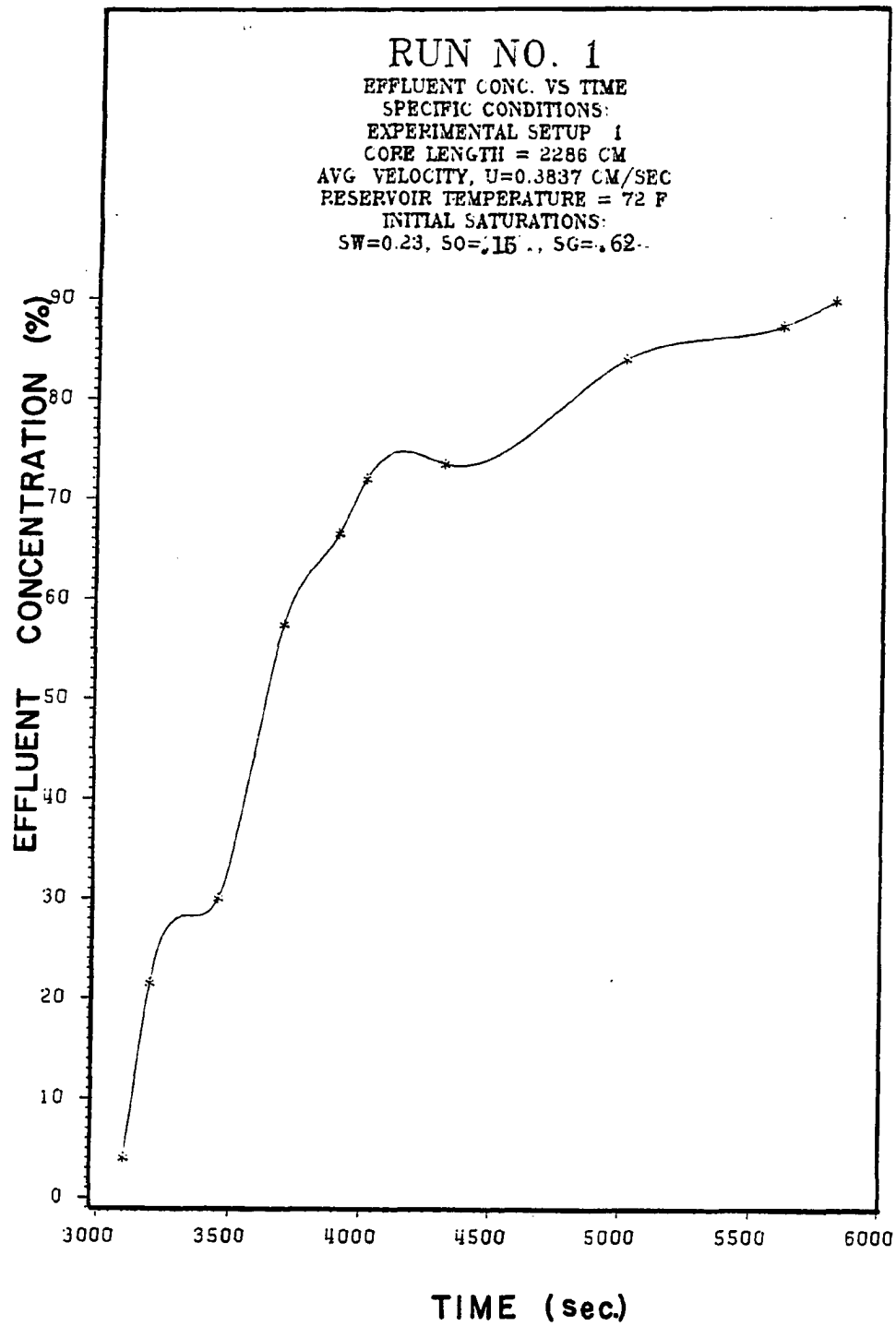

FIGURE 16 EFFLUENT SOLVENT CONCENTRATION VS TIME FOR RUN #1

RUN # 2

EXPERIMENTAL SETUP # 1

Length of the Core	=	2286.00 cm
Average Interstitial Velocity	=	0.2347 cm/sec
Displacing Fluid	=	Naptha
Displaced Fluid	=	Crude Oil
Reservoir Model Temp.	=	69.5 F
Permeability of the Core	=	910.00 mD
Cross-sectional Area	=	0.9588 sq. cm
Pore Volume	=	702.25 cc
Porosity	=	32%
Injection Pressure	=	4000 psi
Cumulative Oil Recovered By Tertiary Flooding	=	92.93 cc
Efficiency of Tertiary Flooding	=	80.21 %

Initial Saturations before Naptha flood: S_w = 23.6%; S_o = 16.5% ; S_g = 59.9%

The detail experimental condition of test #2 and the computed values of average interstitial velocity, cumulative oil produced, and efficiency of the flood is listed in the previous page under Run #2. The computed values of lamda for each experimental observation is listed in Table 5.

The computed values of Dispersion Coefficient and Dispersivity is listed after the Table as shown in the following page. The effluent concentration of the displacing fluid (Naptha) is plotted against the calculated values of lamda as shown in Figure 17.

The effluent concentration is also plotted against time as shown in Figure 18 which is indicative of the movement of the floodfront during the miscible flooding process.

The efficiency of tertiary flooding is found to be 80.2% in this experimental Run. Comparison of the results obtained from this test with the results from other tests is reviewed in detail in the next section of this report under Discussion.

TABLE 5

EXPERIMENTAL OBSERVATION # 2

Refractive Index	Naptha Injected (cc)	Time (Sec.)	Calculated Lamda	Effluent Naptha Conc. (%)
1.4658	530.00	3250.	-0.1480	7.00
1.4650	540.00	4044.	-0.1293	9.00
1.4510	600.00	4680.	-0.0238	57.10
1.4460	610.00	4840.	-0.0073	69.00
1.4450	630.00	5157.	0.0250	71.50
1.4430	645.00	5395.	0.0485	78.50
1.4420	665.00	5712.	0.0790	81.00
1.4410	705.00	6347.	0.1375	84.10
1.4398	740.00	7061.	0.1862	88.00
1.4390	760.00	7220.	0.2130	90.00

Calculated Value of:

DISPERSION COEFFICIENT = 4.5789 sq cm/sec
DISPERSIVITY = 19.513 cm

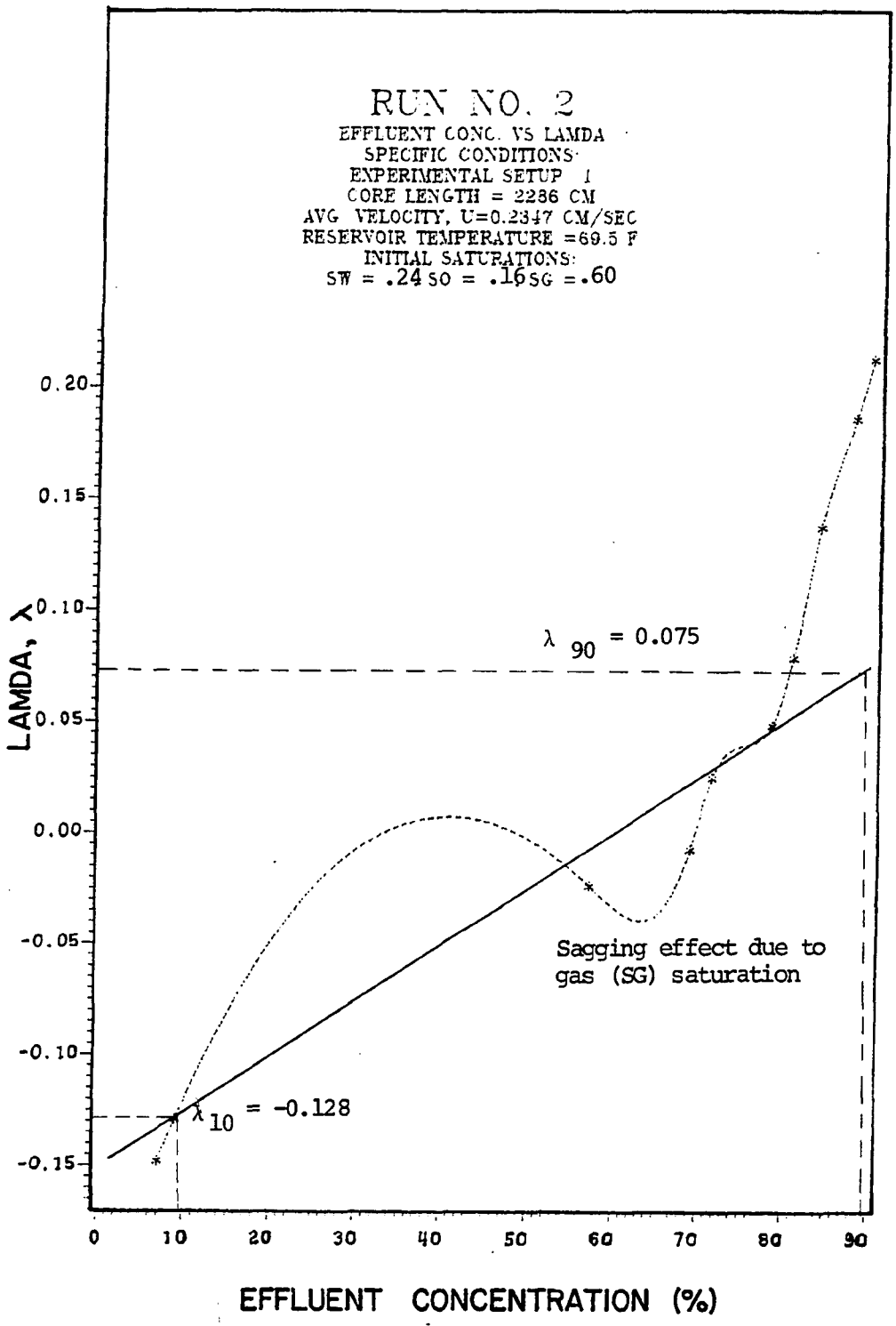

FIGURE 17 CALCULATED LAMDA VS EFFLUENT SOLVENT CONCENTRATION FOR RUN #2

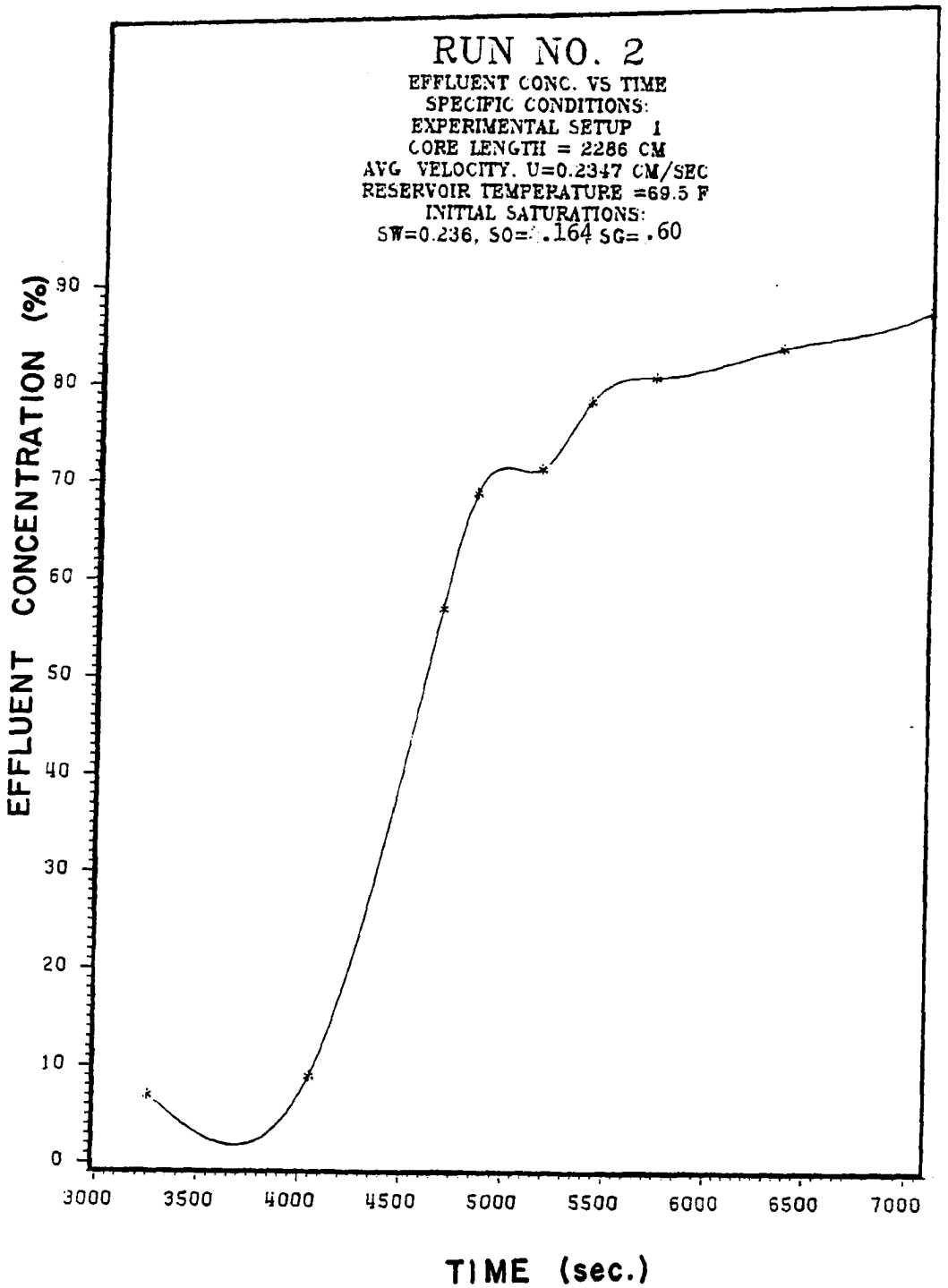

FIGURE 18 EFFLUENT SOLVENT CONCENTRATION VS TIME FOR RUN #2

RUN # 3

EXPERIMENTAL SETUP # 1

Length of the Core	=	3810.00 cm
Average Interstitial Velocity	=	0.0815 cm/sec
Displacing Fluid	=	Naptha
Displaced Fluid	=	Crude Oil
Reservoir Model Temp.	=	70.5 F
Permeability of the Core	=	910.00 mD
Cross-sectional Area	=	0.9588 sq. cm
Pore Volume	=	1170.00 cc
Porosity	=	32.0 %
Injection Pressure	=	4000 psi
Cumulative Oil Recovered By Tertiary Flooding	=	163.13 cc
Efficiency of Tertiary Flooding	=	87.23 %

Initial Saturations before Naptha Flood: S_w = 22%; S_o = 16.0% ; S_g = 62.0%

The detail experimental condition of test #3 and the computed values of average interstitial velocity, cumulative oil produced, and the efficiency of the flood is listed in the previous page under Run #3. The computed values of lamda for each experimental observation is listed in Table 6.

The computed values of Dispersion Coefficient and Dispersivity is listed after the Table as shown in the following page. The effluent concentration of the displacing fluid (Naptha) is plotted against the calculated values of lamda as shown in Figure 19.

The effluent concentration is also plotted against time as shown in Figure 20 which is indicative of the movement of the floodfront during the miscible flooding process.

The efficiency of tertiary flooding is found to be 87.23 % in this experimental Run. Comparison of the results obtained from this test with the results from other tests is reviewed in detail in the next section of this report under Discussion.

TABLE 6

EXPERIMENTAL OBSERVATION # 3

Refractive Index	Naptha Injected (cc)	Time (Sec.)	Calculated Lamda	Effluent Naptha Conc. (%)
1.4655	810.00	11380.	-0.3698	8.50
1.4618	900.00	14460.	-0.2631	20.00
1.4605	910.00	14640.	-0.2520	22.00
1.4525	945.00	14935.	-0.2140	47.50
1.4630	965.00	15580.	-0.1929	18.50
1.4625	970.00	15650.	-0.1877	18.80
1.4580	980.00	15860.	-0.1774	29.80
1.4620	1035.00	16455.	-0.1227	19.00
1.4600	1050.00	17000.	-0.1083	21.50
1.4520	1080.00	17300.	-0.0801	55.00
1.4500	1095.00	17550.	-0.0663	58.00
1.4390	1130.00	18190.	-0.0348	90.00

Calculated Value of:

DISPERSION COEFFICIENT = 2.1713 sq cm/sec
DISPERSIVITY = 26.648 cm

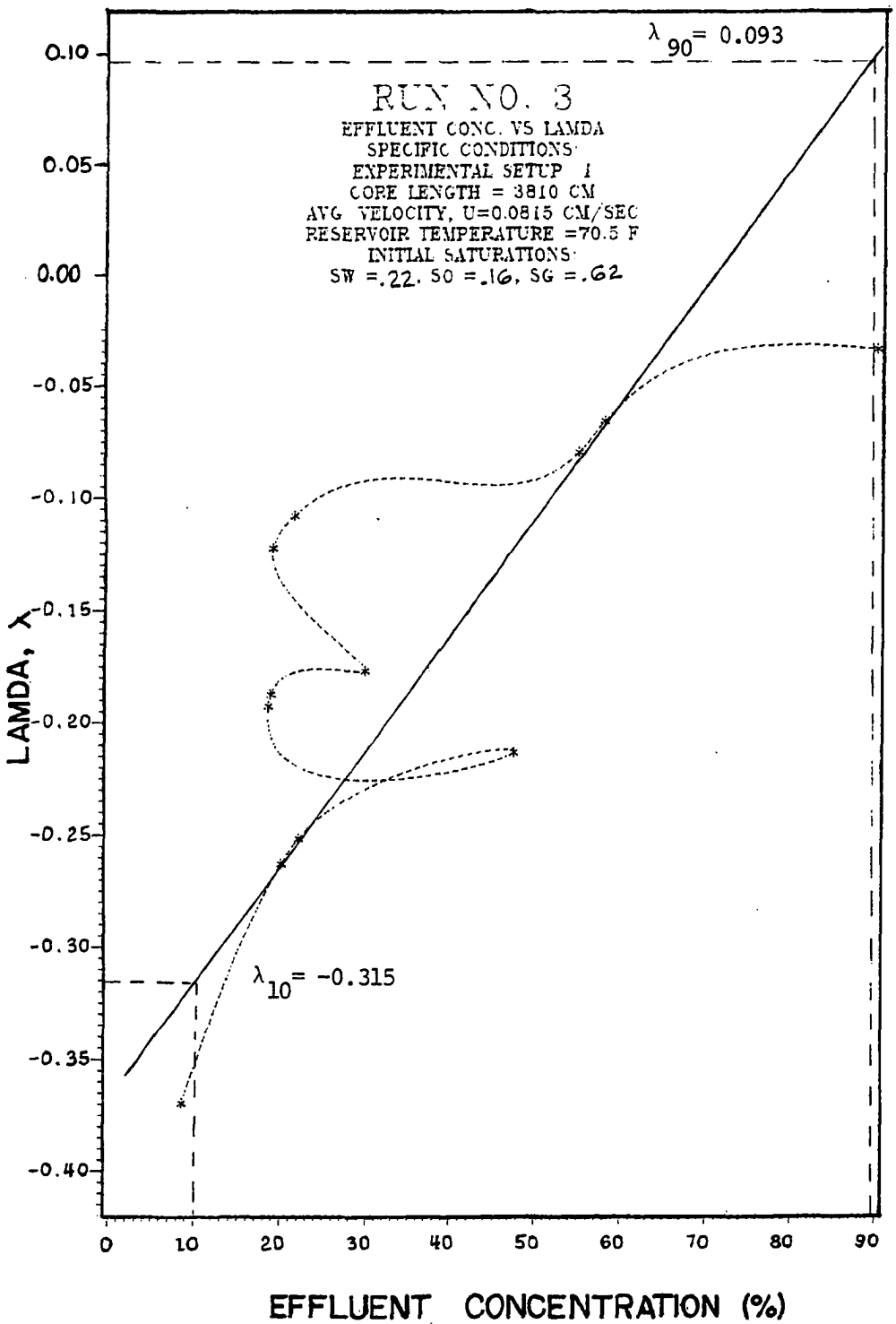

FIGURE 19 CALCULATED LAMDA VS EFFLUENT SOLVENT CONCENTRATION FOR RUN #3

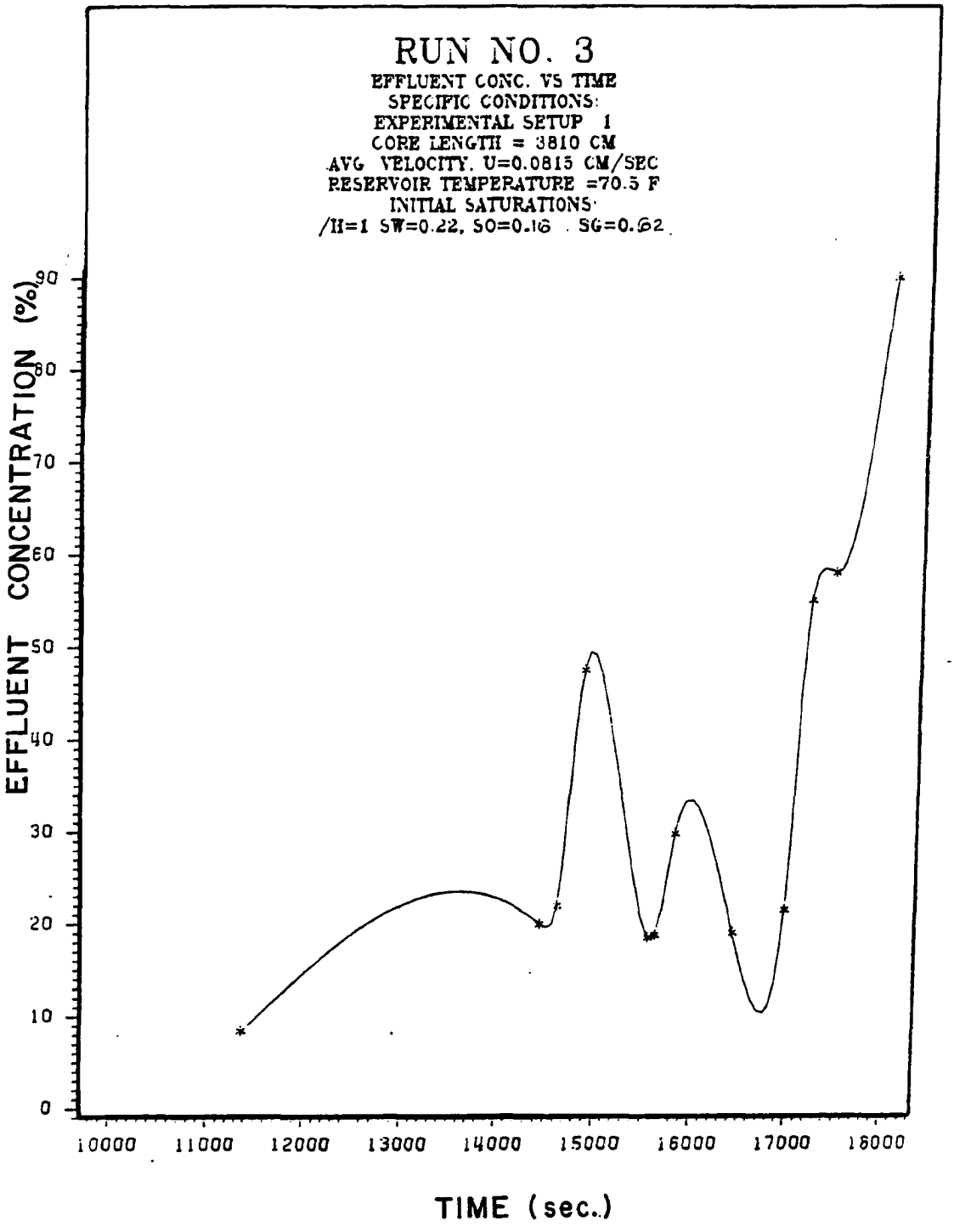

FIGURE 20 EFFLUENT SOLVENT CONCENTRATION VS TIME FOR RUN #3

RUN # 4

EXPERIMENTAL SETUP # 1

Length of the Core	=	3810.00 cm
Average Interstitial Velocity	=	0.0913 cm/sec
Displacing Fluid	=	Naptha
Displaced Fluid	=	Crude Oil
Reservoir Model Temp.	=	69.5 F
Permeability of the Core	=	910.00 mD
Cross-sectional Area	=	0.9588 sq. cm
Pore Volume	=	1170.00 cc
Porosity	=	32.0 %
Injection Pressure	=	4000 psi
Cumulative Oil Recovered By Tertiary Flooding	=	251.67 cc
Efficiency of Tertiary Flooding	=	90.20 %

Initial Saturations before Naptha Flood: S_w = 23%; S_o = 23.8% ; S_g = 53.2%

The detail experimental condition of test #4 and the computed values of average interstitial velocity, cumulative oil produced, and the efficiency of the flood is listed in the previous page under Run #4. The computed values of lamda for each experimental observation is listed in Table 7.

The computed values of Dispersion Coefficient and Dispersivity is listed after the Table as shown in the following page. The effluent concentration of the displacing fluid (Naptha) is plotted against the calculated values of lamda as shown in Figure 21.

The effluent concentration is also plotted against time as shown in Figure 22 which is indicative of the movement of the floodfront during the miscible flooding process.

The efficiency of tertiary flooding is found to be 90.20% in this experimental Run. Comparison of the results obtained from this test with the results from other tests is reviewed in detail in the next section of this report under Discussion.

TABLE 7

EXPERIMENTAL OBSERVATION # 4

Refractive Index	Naptha Injected (cc)	Time (Sec.)	Calculated Lamda	Effluent Naptha Conc. (%)
1.4665	750.00	11120.	-0.4484	4.00
1.4653	820.00	12548.	-0.3573	5.80
1.4639	875.00	14435.	-0.2916	18.00
1.4612	905.00	15120.	-0.2575	21.00
1.4563	945.00	15946.	-0.2140	37.50
1.4632	995.00	16435.	-0.1622	17.50
1.4645	1040.00	17576.	-0.1179	11.00
1.4573	1080.00	18680.	-0.0801	32.00
1.4538	1120.00	19710.	-0.0437	48.00
1.4392	1150.00	20530.	-0.0172	89.20
1.4370	1280.00	23430.	0.0899	97.50

Calculated Value of:

DISPERSION COEFFICIENT = 2.0878 sq cm/sec
DISPERSIVITY = 22.878 cm

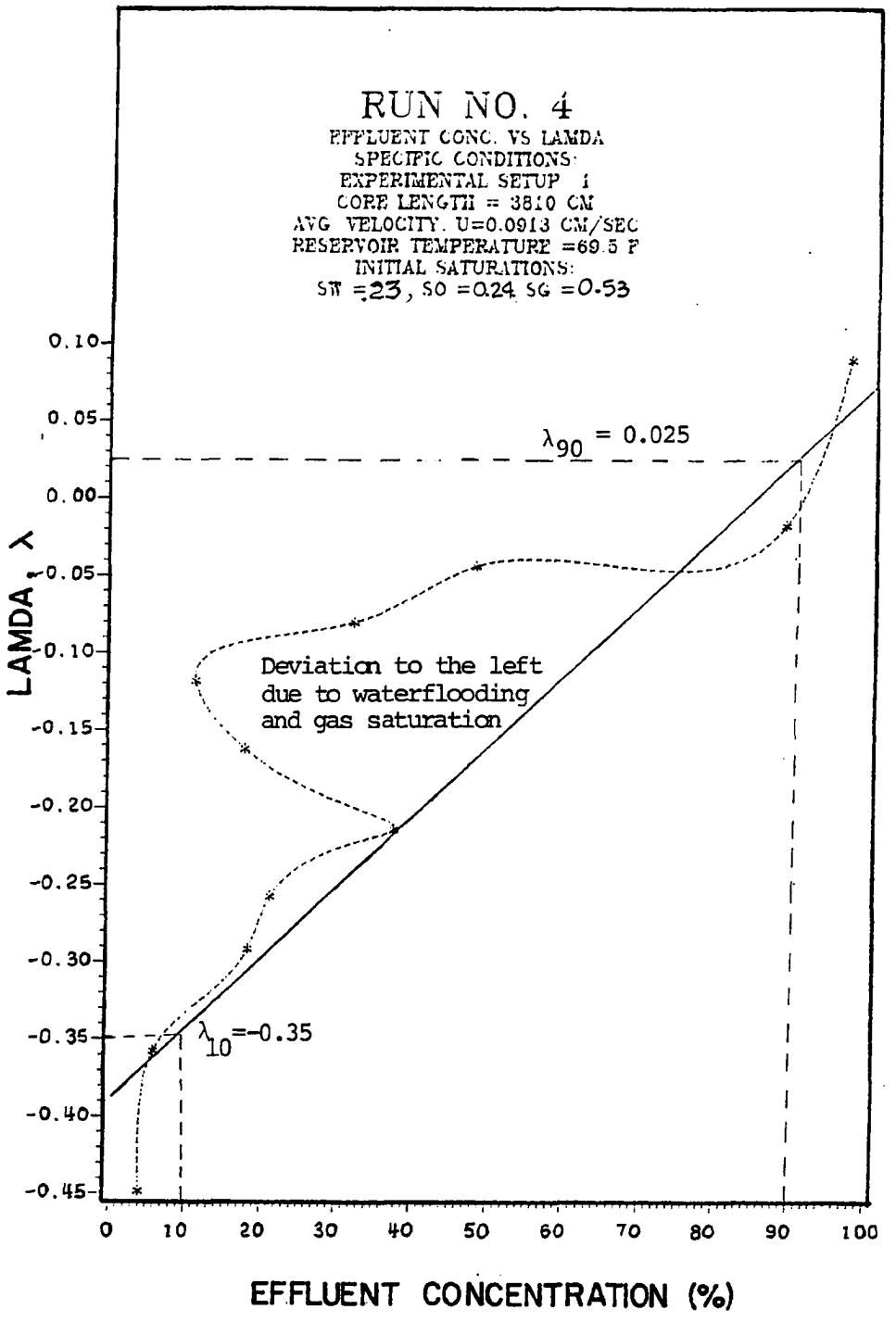

FIGURE 21 CALCULATED LAMDA VS EFFLUENT SOLVENT CONCENTRATION FOR RUN #4

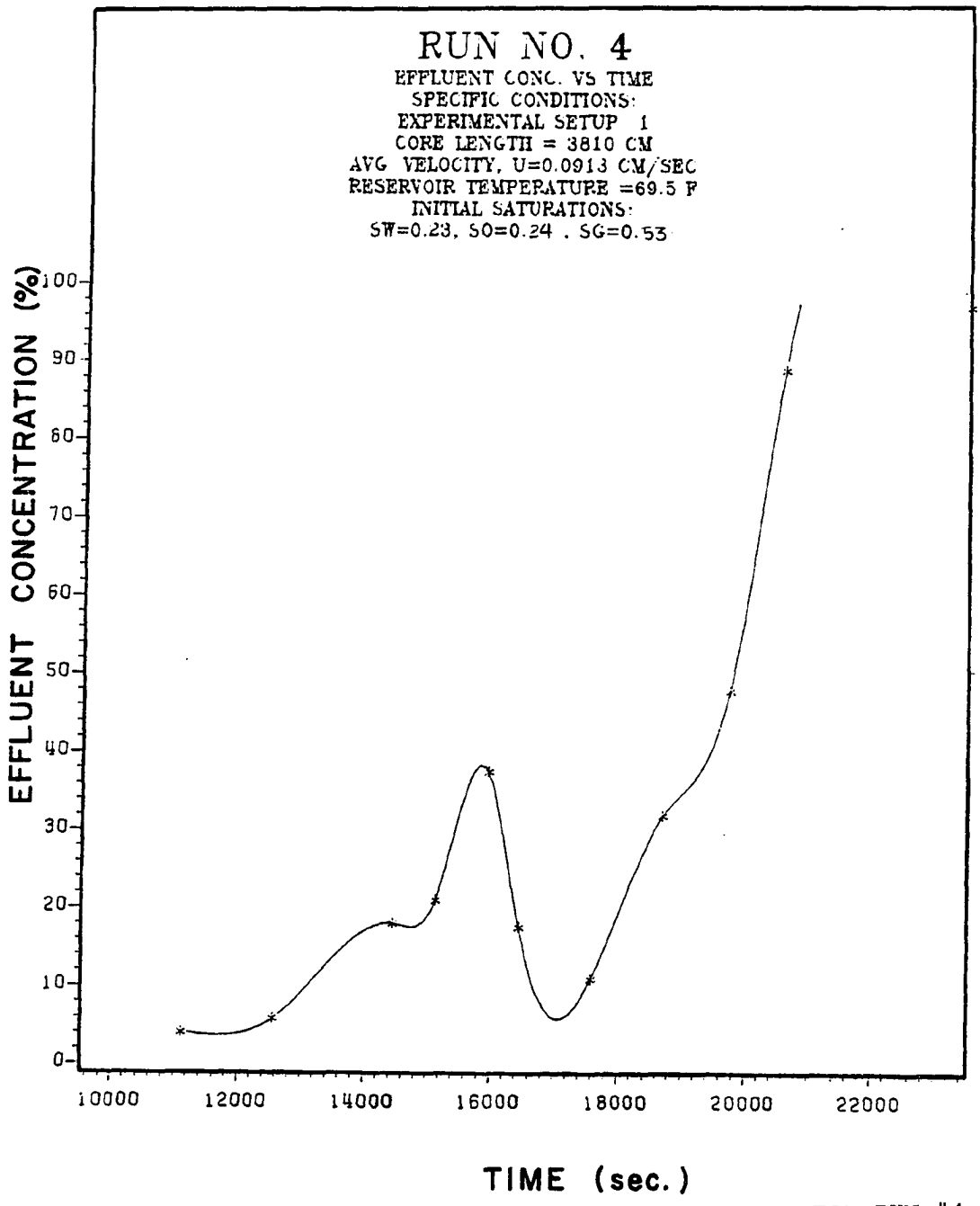

FIGURE 22 EFFLUENT SOLVENT CONCENTRATION VS TIME FOR RUN #4

RUN # 5

EXPERIMENTAL SETUP # 1

Length of the Core	=	3810.00 cm
Average Interstitial Velocity	=	0.1173 cm/sec
Displacing Fluid	=	Naptha
Displaced Fluid	=	Crude Oil
Reservoir Model Temp.	=	120.0 F
Permeability of the Core	=	910. mD
Cross-sectional Area	=	0.9588 sq. cm
Pore Volume	=	1170.00 cc
Porosity	=	32.0 %
Injection Pressure	=	4000 psi
Cumulative Oil Recovered By Tertiary Flooding	=	93.52 cc
Efficiency of Tertiary Flooding	=	89.92 %

Initial Saturations before Naptha Flood: S_w = 19.8%; S_o = 18.8 %; S_g = 61.4%

The detail experimental condition of test #5 and the computed values of average interstitial velocity, cumulative oil produced, and efficiency of the flood is listed in the previous page under Run #5. The computed values of lamda for each experimental observation is listed in Table 8.

The computed values of Dispersion Coefficient and Dispersivity is listed after the Table as shown in the following page. The effluent concentration of the displacing fluid (Naptha) is plotted against the calculated values of lamda as shown in Figure 23.

The effluent concentration is also plotted against time as shown in Figure 24 which is indicative of the movement of the floodfront during the miscible flooding process.

The efficiency of tertiary flooding is found to be 89.90% in this experimental Run. Comparison of the results obtained from this test with the results from other tests is reviewed in detail in the next section of this report under Discussion.

TABLE 8
EXPERIMENTAL OBSERVATION # 5

Refractive Index	Naptha Injected (cc)	Time (Sec.)	Lamda	Effluent Naptha Conc. (%)
1.4650	700.00	10950.	-0.5193	4.50
1.4632	720.00	11780.	-0.4903	11.20
1.4610	780.00	13420.	-0.4082	20.00
1.4565	810.00	14180.	-0.3698	38.00
1.4555	840.00	14690.	-0.3329	39.50
1.4548	860.00	15200.	-0.3090	41.00
1.4534	920.00	16800.	-0.2410	45.50
1.4481	1010.00	18260.	-0.1472	60.00
1.4390	1070.00	18720.	-0.0894	87.50
1.4370	1150.00	19230.	-0.0172	93.00
1.4368	1210.00	20230.	0.0336	97.50

Calculated Value of:

DISPERSION COEFFICIENT = 5.5110 sq cm/sec
DISPERSIVITY = 46.969 cm

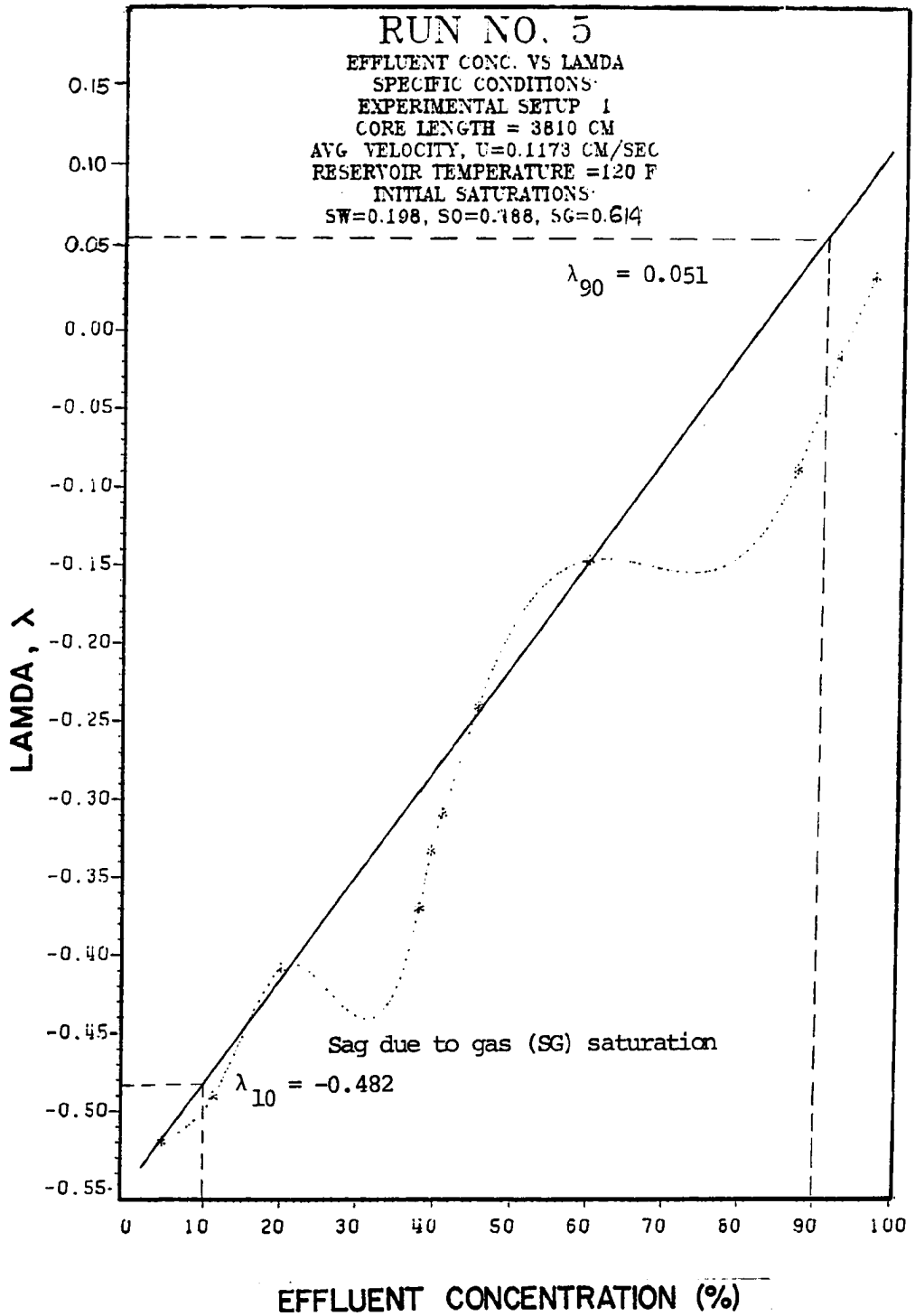

FIGURE 23 CALCULATED LAMDA VS EFFLUENT SOLVENT CONCENTRATION FOR RUN #5

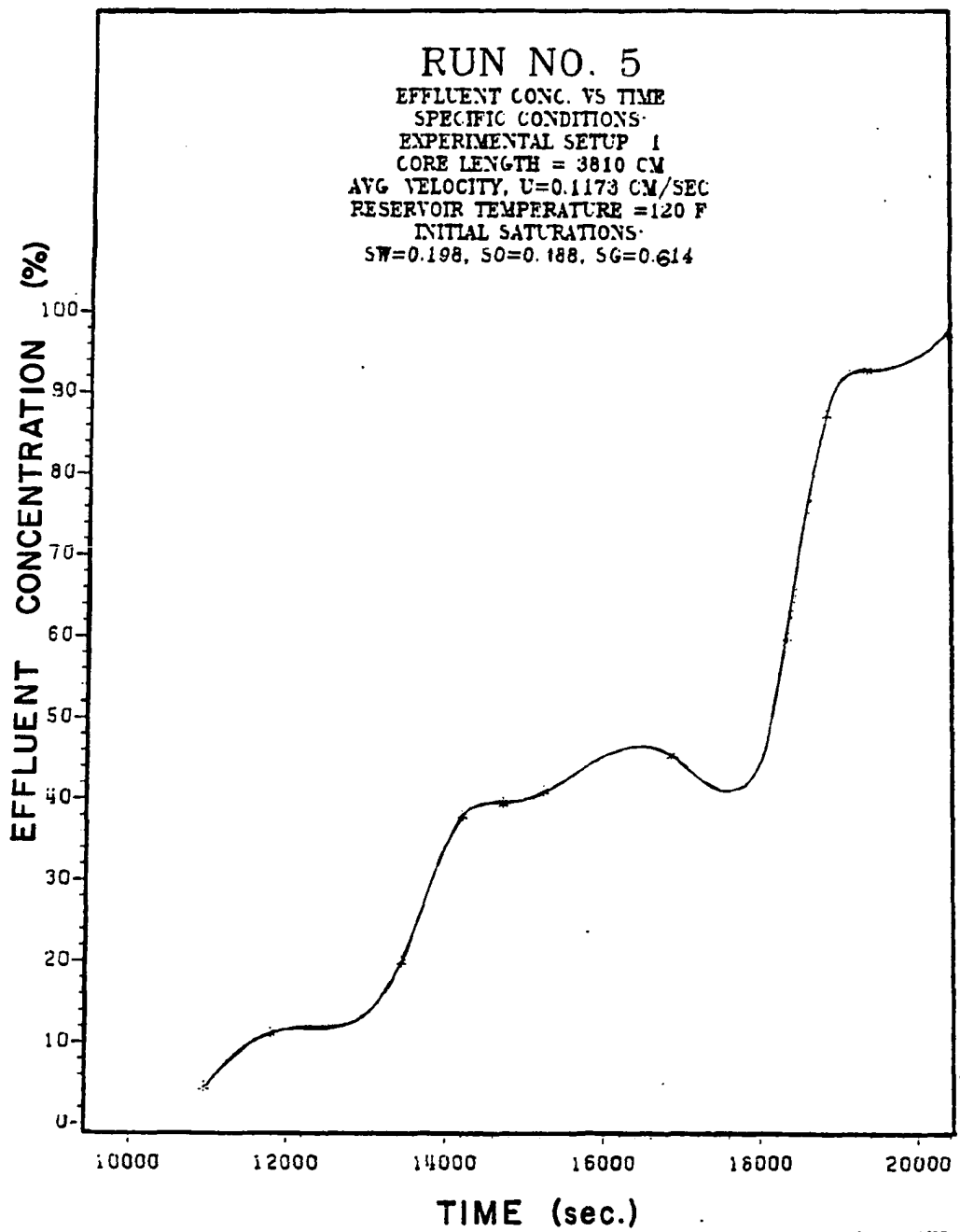

FIGURE 24 EFFLUENT SOLVENT CONCENTRATION VS TIME FOR RUN #5

RUN # 6

EXPERIMENTAL SETUP # 1

Length of the Core	=	3810.00 cm
Average Interstitial Velocity	=	0.1043 cm/sec
Displacing Fluid	=	Naptha
Displaced Fluid	=	Crude Oil
Reservoir Model Temp.	=	120.0 F
Permeability of the Core	=	910.00 mD
Cross-sectional Area	=	0.9588 sq. cm
Pore Volume	=	1170.00 cc
Porosity	=	32.0 %
Injection Pressure	=	4000 psi
Cumulative Oil Recovered By Tertiary Flooding	=	206.77 cc
Efficiency of Tertiary Flooding	=	91.49 %

Initial Saturations before Naptha Flood: S_w = 19%; S_o = 19.3%; S_g = 61.7%

The detail experimental condition of test #6 and the computed values of average interstitial velocity, cumulative oil produced, and efficiency of the flood is listed in the previous page under Run #6. The computed values of lamda for each experimental observation is listed in Table 9.

The computed values of Dispersion Coefficient and Dispersivity is listed after the Table as shown in the following page. The effluent concentration of the displacing fluid (Naptha) is plotted against the calculated values of lamda as shown in Figure 25.

The effluent concentration is also plotted against time as shown in Figure 26 which is indicative of the movement of the floodfront during the miscible flooding process.

The efficiency of tertiary flooding is found to be 91.49% in this experimental Run. Comparison of the results obtained from this test with the results from other tests is reviewed in detail in the next section of this report under Discussion.

TABLE 9

EXPERIMENTAL OBSERVATION # 6

Refractive Index	Naptha Injected (cc)	Time (Sec.)	Calculated Lamda	Effluent Naptha Conc. (%)
1.4653	710.00	11100.	-0.5047	4.00
1.4630	730.00	11780.	-0.4761	11.00
1.4620	750.00	13420.	-0.4484	21.50
1.4570	770.00	14180.	-0.4214	31.00
1.4560	825.00	14690.	-0.3512	40.00
1.4550	900.00	15200.	-0.2631	42.00
1.4530	935.00	15350.	-0.2247	47.00
1.4470	980.00	16280.	-0.1774	57.00
1.4390	1160.00	16520.	-0.0086	87.50
1.4375	1230.00	17120.	0.0500	92.50
1.4365	1365.00	19750.	0.1543	97.20

Calculated Value of:

DISPERSION COEFFICIENT = 6.6198 sq cm/sec
DISPERSIVITY = 63.472 cm

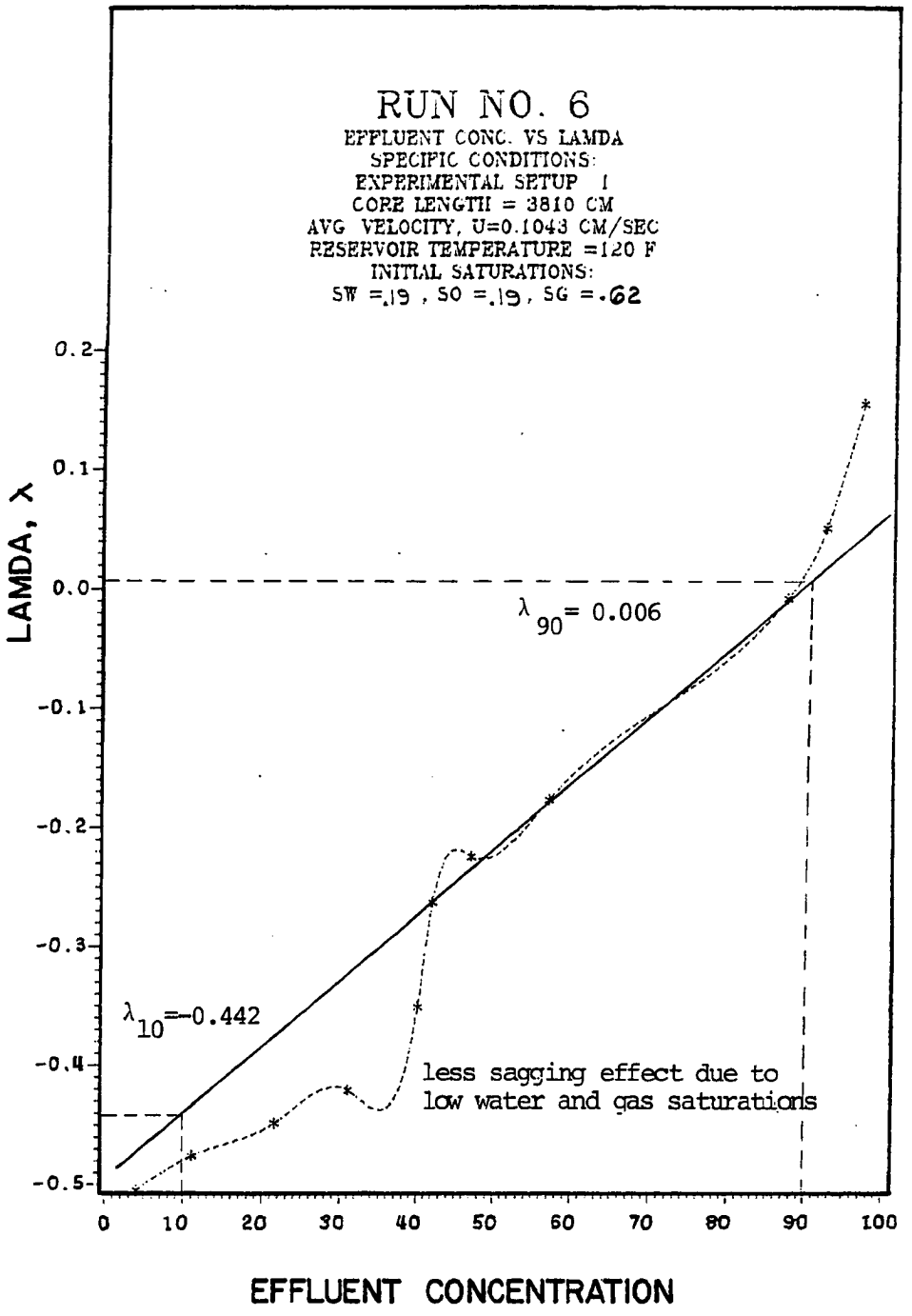

FIGURE 25 CALCULATED LAMDA VS EFFLUENT SOLVENT CONCENTRATION FOR RUN #6

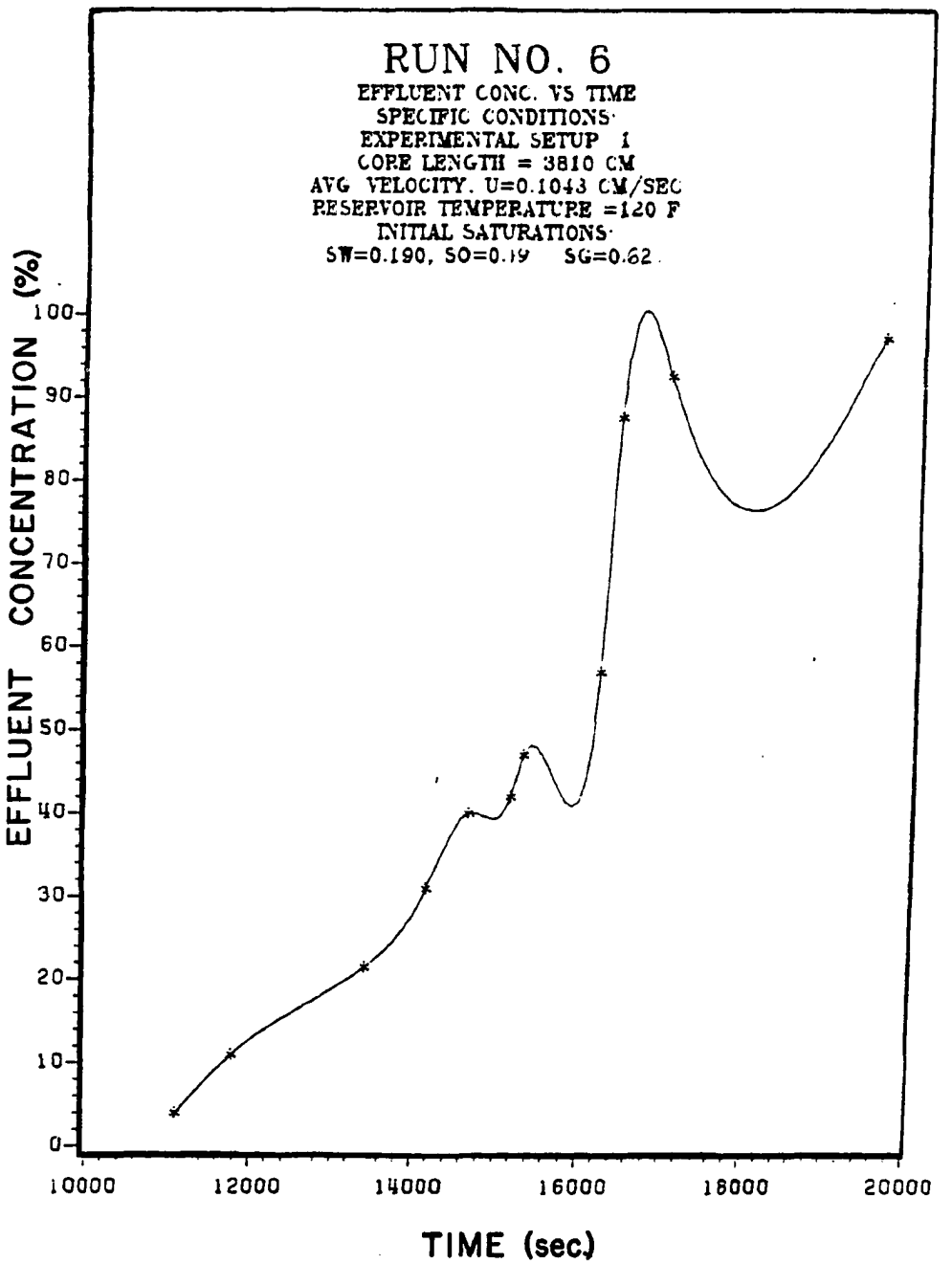

FIGURE 26 EFFLUENT SOLVENT CONCENTRATION VS TIME FOR RUN #6

RUN # 7

EXPERIMENTAL SETUP # 2

Length of the Core	=	19.69 cm
Average Interstitial Velocity	=	0.0067 cm/sec
Displacing Fluid	=	Naptha
Displaced Fluid	=	Crude Oil
Reservoir Model Temp.	=	70.0 F
Permeability of the Core	=	79.90 mD
Cross-sectional Area	=	20.2683 sq. cm
Pore Volume	=	55.85 cc
Porosity	=	14.000 %
Injection Pressure	=	15.00 psi
Cumulative Oil Recovered By Tertiary Flooding	=	32.53 cc
Efficiency of Tertiary Flooding	=	59.80 %

Initial Saturations before Naptha Flood: S_w = 2.6%. S_o = 97.40%

The detail experimental condition of test #7 and the computed values of average interstitial velocity, cumulative oil produced, and efficiency of the flood is listed in the previous page under Run #7. The computed values of lamda for each experimental observation is listed in Table 10.

The computed values of Dispersion Coefficient and Dispersivity is listed after the Table as shown in the following page. The effluent concentration of the displacing fluid (Naptha) is plotted against the calculated values of lamda as shown in Figure 27.

The effluent concentration is also plotted against time as shown in Figure 28 which is indicative of the movement of the floodfront during the miscible flooding process.

The efficiency of tertiary flooding is found to be 59.80% in this experimental Run. Comparison of the results obtained from this test with the results from other tests is reviewed in detail in the next section of this report under Discussion.

TABLE 10

EXPERIMENTAL OBSERVATION # 7

Refractive Index	Naptha Injected (cc)	Time (Sec.)	Calculated Lamda	Effluent Naptha Conc. (%)
1.4800	50.00	1688.	-0.1107	0.
1.4658	60.00	2120.	0.0717	3.50
1.4625	70.00	2531.	0.2263	13.50
1.4520	76.00	2869.	0.3093	44.50
1.4410	90.00	3207.	0.4817	67.10
1.4370	105.00	3545.	0.6418	72.00
1.4290	135.00	4558.	0.9115	87.10

Calculated Value of:

DISPERSION COEFFICIENT = 0.0054 sq cm/sec
DISPERSIVITY = 0.813 cm

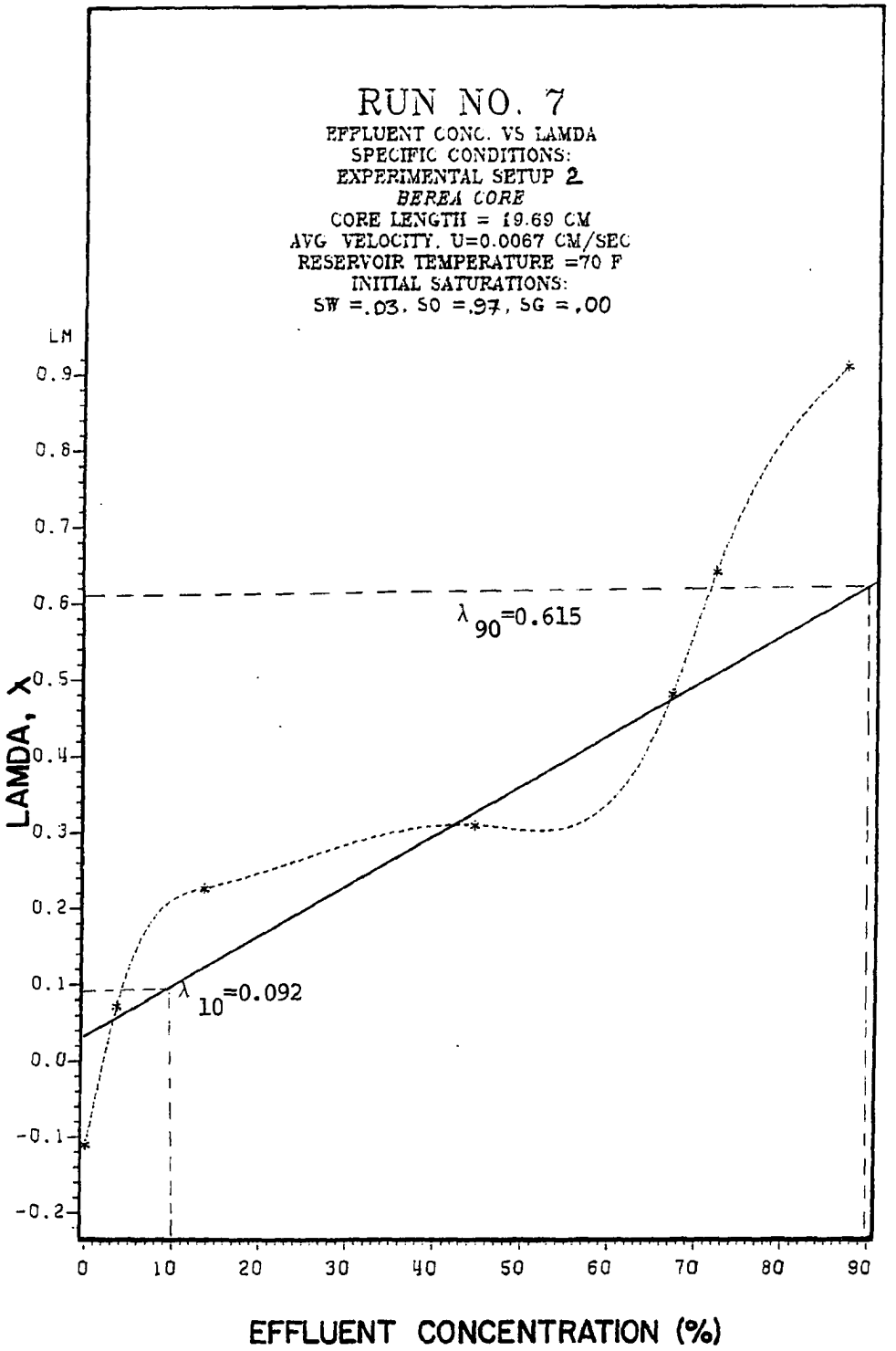

FIGURE 27 CALCULATED LAMDA VS EFFLUENT SOLVENT CONCENTRATION FOR RUN #7

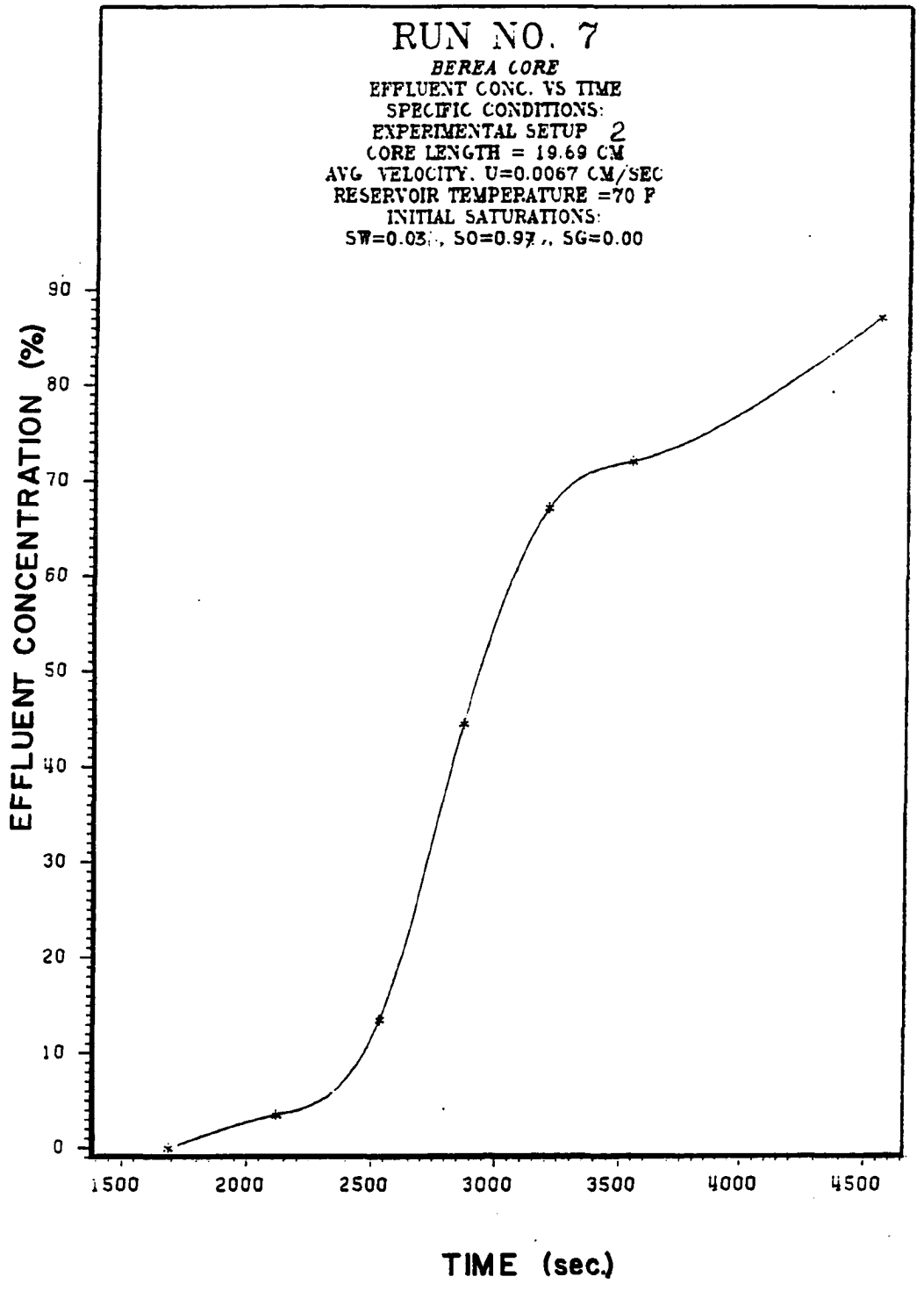

FIGURE 28 EFFLUENT SOLVENT CONCENTRATION VS TIME FOR RUN #7

RUN # 8

EXPERIMENTAL SETUP # 3

Length of the Core	=	28.89 cm
Average Interstitial Velocity	=	0.0966 cm/sec
Displacing Fluid	=	Naptha
Displaced Fluid	=	Crude Oil
Reservoir Model Temp.	=	70.0 F
Permeability of the Core	=	66800. mD
Cross-sectional Area	=	15.5179 sq. cm
Pore Volume	=	187.10 cc
Porosity	=	41.7 %
Injection Pressure	=	5 psi
Random Correction Factor	=	1.0
Cumulative Oil Recovered By Tertiary Flooding	=	53.40 cc
Efficiency of Tertiary Flooding	=	80.91 %

Initial Saturations before Naptha Flood : S_w = 64.8% ; S_o = 35.2%

LAMDA90 = 0.333960 LAMDA10 = -3.10364

The detail experimental condition of test #8 and the computed values of average interstitial velocity, cumulative oil produced, and efficiency of the flood is listed in the previous page under Run #8. The computed values of lamda for each experimental observation is listed in Table 11.

The computed values of Dispersion Coefficient and Dispersivity is listed after the Table as shown in the following page. The effluent concentration of the displacing fluid (Naptha) is plotted against the calculated values of lamda as shown in Figure 29.

The effluent concentration is also plotted against time as shown in Figure 30 which is indicative of the movement of the floodfront during the miscible flooding process.

The efficiency of tertiary flooding is found to be 80.91% in this experimental Run. Comparison of the results obtained from this test with the results from other tests is reviewed in detail in the next section of this report under Discussion.

TABLE 11

EXPERIMENTAL OBSERVATION # 8

Refractive Index	Naptha Injected (cc)	Time (Sec.)	Lamda	Effluent Naptha Conc. (%)
1.4750	15.00	16.	-3.2486	7.00
1.4440	44.00	45.	-1.5772	51.00
1.4350	94.00	101.	-0.7020	72.40
1.4270	144.00	147.	-0.2626	79.20
1.4240	194.00	204.	0.0362	82.60
1.4200	244.00	250.	0.2663	88.60
1.4160	344.00	355.	0.6185	96.00

Calculated Value of:

DISPERSION COEFFICIENT = 2.5093 sq cm/sec
DISPERSIVITY = 25.980 cm

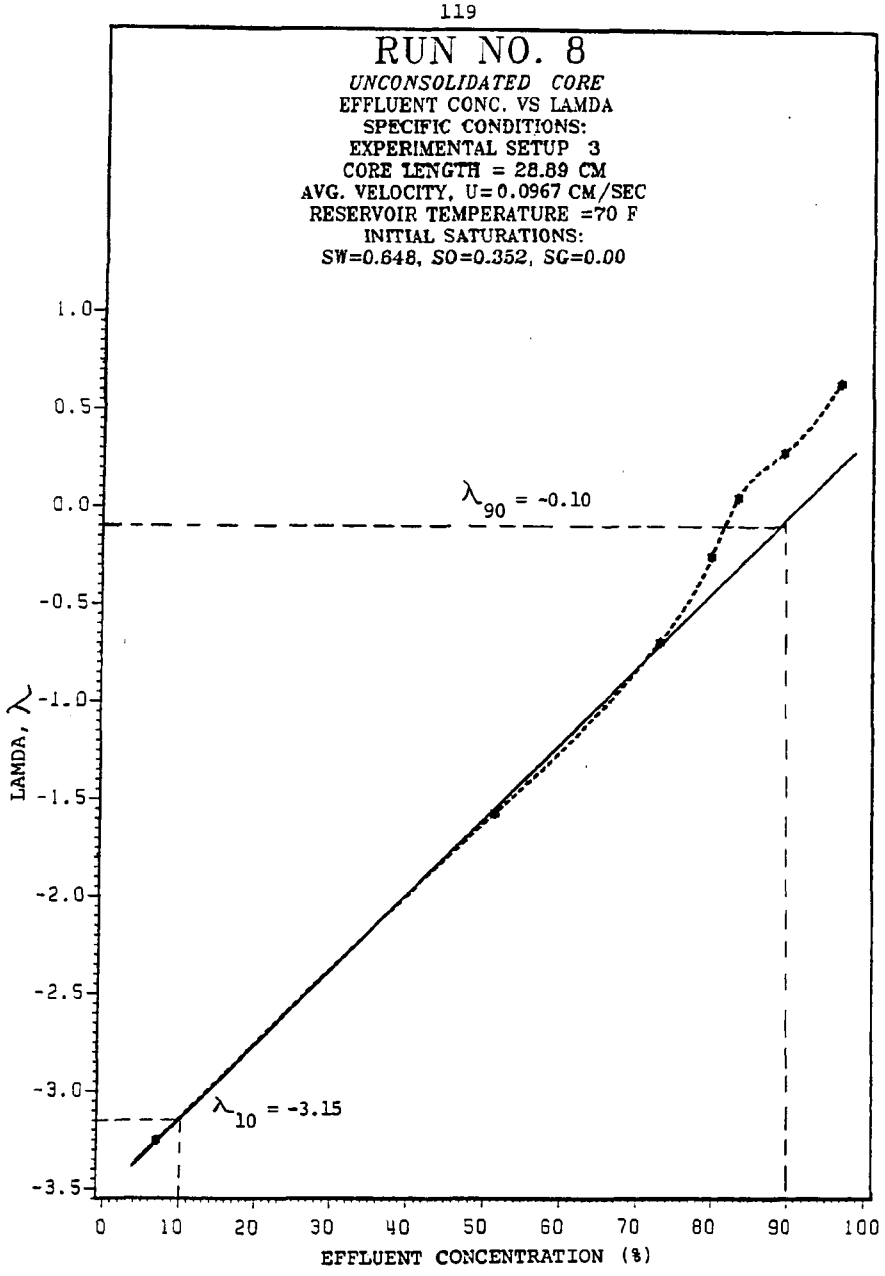

FIGURE 28 EFFLUENT CONC. PROFILE WITH LAMDA

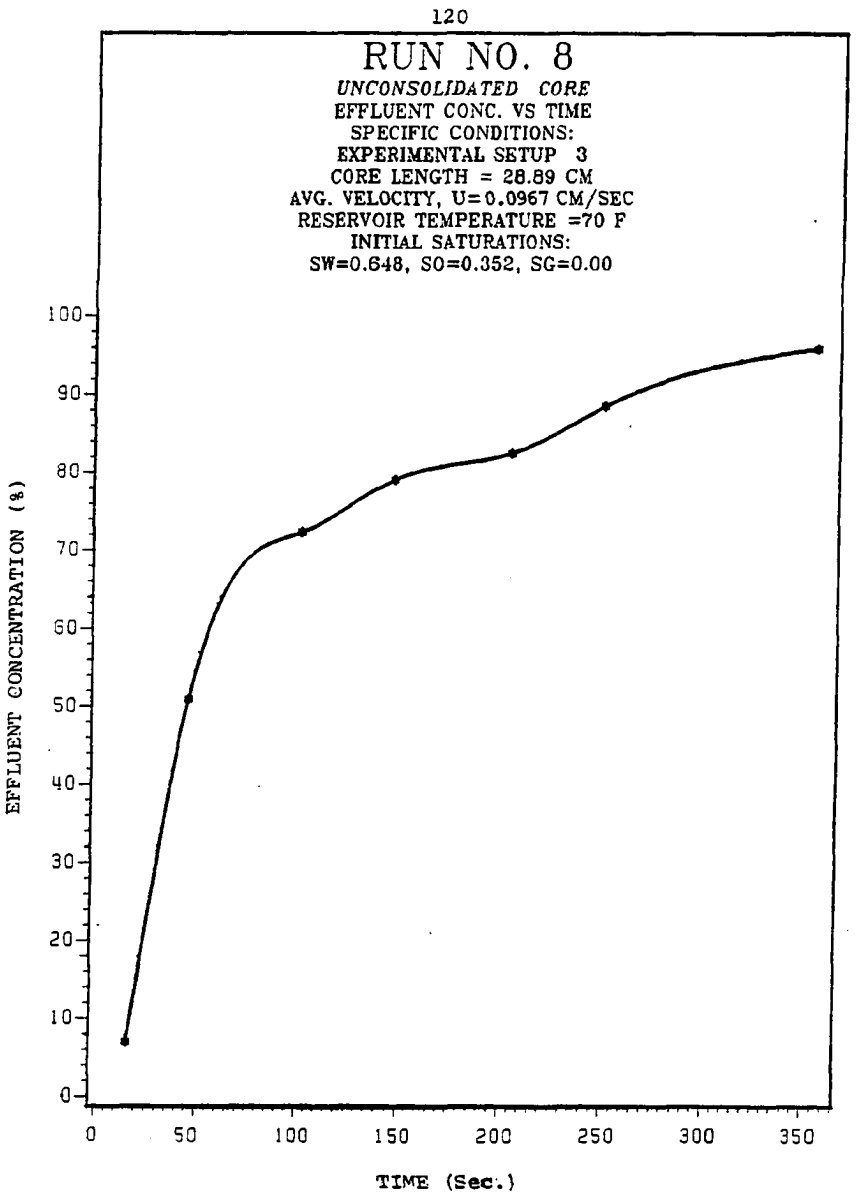

FIGURE 29 EFFLUENT CONC. PROFILE WITH TIME

5.0 DISCUSSION

Naptha was used as the displacing fluid (solvent) in this study for miscible displacement of oil from the reservoir model. For each experimental observation the effluent solvent concentration was determined by using the Refractometer as described in previous sections of this report.

In studying the problem of dispersion coefficient most investigators have filled a packed column with one fluid, displaced it with another fluid, and measured the effluent fluid composition as a function of displacement. Brigham, et al.,[8] has shown a typical effluent composition curve for a miscible displacement of a sand-packed column involving only two liquids. This typical curve involving two liquids and no gas saturation for miscible displacement of a sand-packed column is shown in Figure 31.

In the present investigation experimental conditions in most of the runs were quite different than what has been used by Brigham et al.[8]. However, in Run #8 (Setup #3) an unconsolidated sandpack was used which is comparable to that of Brigham et al.[8] . Three liquids (oil, water, and Naptha) were involved in the present investigation whereas only two liquids were used by Brigham et al.[8]. The close

resemblance of the effluent composition curve shown in Figure no. 29, pertaining to Run #8 of the present investigation, with typical effluent composition curve of Brigham et al[8] confirms that the deviation from the typical curve in Run #1 through #6 was mainly due to high gas saturation at the beginning of the miscible flood.

The experimental conditions were quite different and involved high gas saturations and higher temperatures for the first six Runs conducted with Setup #1. Setup #2 was also different and involved a consolidated reservoir core.

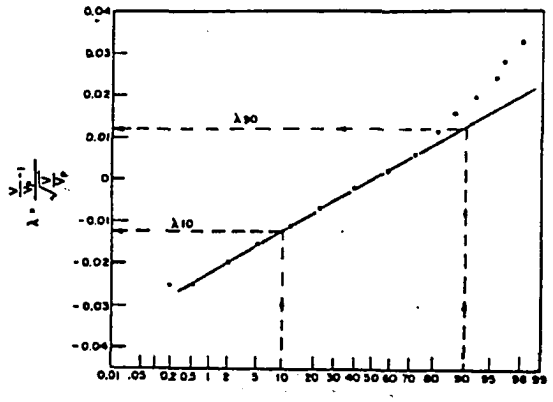

FIGURE 31 TYPICAL EFFLUENT-COMPOSITION CURVE FOR A MISCIBLE FLOOD

Source: Blackwell et al. (Ref. 8)

Also, the actual data points for Run #7 conducted with Setup #2 as shown in Figure 27 closely represented the typical curve pattern shown by Brigham, et al,[23] (Figure 29). This similarity verifies the typical curve pattern of (lamda) versus effluent solvent concentration.

The deviation from the typical curve pattern in Run nos. 1-6 was mainly due to the gas saturation in the reservoir model prior to the tertiary Naptha flood. The sagging effect and shift of the data points on the right side of the straight line as observed in Figure nos. 15 and 17, corresponding to Run nos. 1 and 2 respectively, can be attributed to the high initial gas saturations of the reservoir model.

A shift of the data points on the left side of the straight line as shown in Figure nos. 19 and 21, corresponding to Run nos. 3 and 4 respectively is mainly due to the presence of trapped water and gas in the effluent mixture as observed during sampling. Since the samples were taken from point E (Figure 1) of the reservoir model for these two Runs, water and gas from the last 25% of the reservoir model were also displaced along with oil by Naptha flood. This is also indicative of the fact that the reservoir model used in Setup #1 contains the most tortuous zone in the last quarter of the spiral layout.

In determining the dispersion coefficient, the values of λ (lamda) at 90% and 10% solvent concentrations were needed to be determined. The computer model 'DISCAL' developed for this study introduces a new method for determining λ_{90} and λ_{10} based upon the average gradient of effluent solvent concentration to the calculated λ for all the observations of a test Run. Only graphical solutions were available in the past for determining these values of λ needed for the calculation of dispersion coefficient.

The values of λ_{90} and λ_{10} determined by the computer model compares fairly well with the corresponding values obtained graphically. The following sample values from two different Runs are furnished for comparison.

The Values of λ_{90} and λ_{10} when determined graphically from Figure 15, Run #1, were found to be 0.125 and -0.092 respectively. These values match reasonably well with the values of λ_{90} and λ_{10} computed by the program 'DISCAL' as 0.180 and -0.128 respectively.

Also, the values of λ_{90} and λ_{10} when determined graphically from Figure 23, Run #5, were found to be 0.051 and -0.482 respectively. These values match closely with the values of λ_{90} and λ_{10} computed by the program 'DISCAL' as -0.066 and -0.468 respectively.

It is worth noting that the graphically determined values of λ_{90} and λ_{10} are subject to human discernment for selecting the best match, whereas the computer model arithmetically determines the average gradient. However, the maximum difference between the computed and graphical values of λ_{90} and λ_{10} for all the experimental Runs were found to be $\leqslant 0.4$. The maximum deviation of the computed values from the graphical values were observed for Run #7. This observation is indicative of the fact that when the effluent composition curve follows a typical pattern, it is more precise to use the graphically determined values for λ_{90} and λ_{10}.

The effluent solvent concentration was found to increase with time as expected, but this increase in effluent concentration did not consistently follow a definite or a linear pattern. The variations in the pattern of effluent solvent concentration are found to depend on the experimental conditions. Considering the major common features in the experimental Runs involved in this investigation, and based upon the closest resemblance with one another, a grouping of the experimental Runs are prepared, as shown in Table 12, for the purpose of determining the possible relationship between dispersion coefficient, dispersivity, average interstitial velocity, fluid saturations, and recovery.

TABLE 12 GROUPING OF EXPERIMENTAL RUNS BASED UPON SIMILAR EXPERIMENTAL CONDITIONS

Group No.	Run No.	Setup No.	Core Length (cm)	Temp. (°F)	K* cm^2/s	U+ (cm/sec)	Saturations Sw (%)	So (%)	Sg (%)	Remarks
1	1	1	2286.00	72.0	6.39	0.3837	0.23	0.16	0.61	Run #1
1	2	1	2286.00	69.5	4.58	0.2347	0.24	0.16	0.60	and #2 are similar
2	3	1	3810.00	70.5	2.17	0.0815	0.22	0.16	0.62	Run #3
2	4	1	3810.00	69.5	2.09	0.0913	0.23	0.24	0.53	and #4 are similar
3	5	1	3810.00	120	5.51	0.1173	0.20	0.19	0.61	Run #5
3	6	1	3810.00	120	6.62	0.1043	0.19	0.19	0.62	and #6 are similar
4	7	2	19.69	70.0	0.0054	0.0067	0.03	0.97	0.00	Berea Core
5	8	3	28.89	70.0	2.51	0.0966	0.65	0.35	0.00	Uncon-solidated sandpack

+ - U = Average Interstitial Velocity.
* - K = Dispersion Coefficient

Effluent solvent concentrations from four groups of experimental Runs are plotted against time, as shown in Figure 32. Since the total displacing time for Run #8 was very small compared to any other Runs of this investigation, for a better perspective and a convenient scale only the first four groups were plotted in Figure 32. Experimental data obtained from Run nos. 1, 4, 6, and 7 represents Group nos. 1, 2, 3, and 4 respectively in this Figure. It may be observed from the Figure that the overall change in effluent concentration with time follows the same pattern for Group #1 and Group #4. Smaller core length, similar temperature of the reservoir models, and short experimental time of displacement are considered to be the factors responsible for this similarity. Similar trend is followed by Group Nos. 2 and 3 as shown in Figure 32. However, the higher temperature effect is evident in case of Group #3 depicted by its steeper gradient.

It is evident from the experimental results that the dispersion coefficient and the dispersivity of the reservoir model have an effect on the recovery from miscible flooding. The efficiency of the miscible flooding for each experimental Run as shown in the Result section of this report reflects the recovery of the corresponding Run. The dispersion coefficients of all the experimental

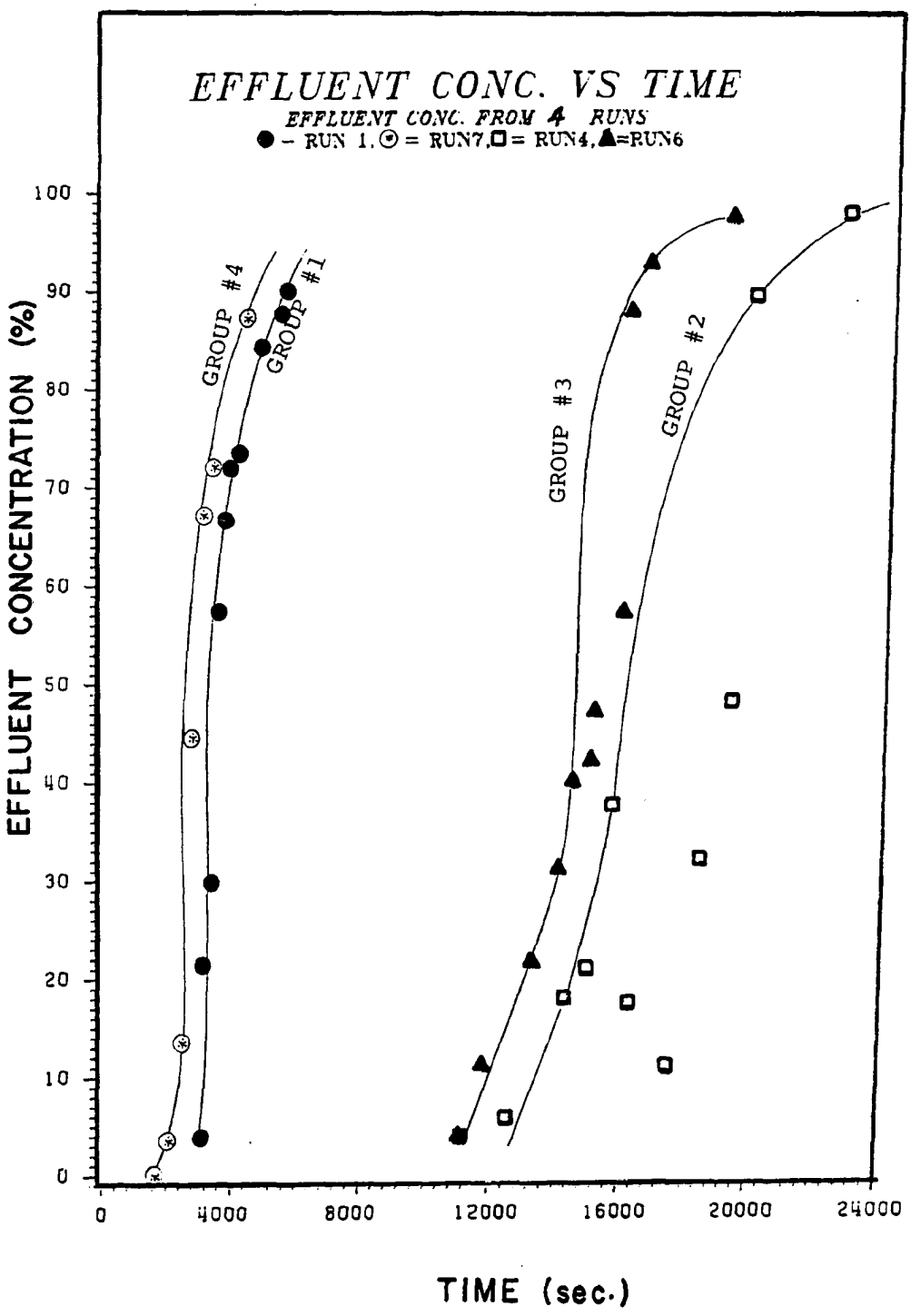

FIGURE 32 DIFFERENT SOLVENT EFFLUENT CONCENTRATION VS TIME

observations were plotted against the corresponding flood efficiencies for Setup #1 as shown in Figure 33.

The time-dependent behavior of the basic fluid flow through a porous media is reflected by the displacement velocity. The velocity dependence of the dispersion coefficient is theoretically established as discussed in the previous section of this report. Figure 34 shows the variation in dispersion coefficient, K, due to the change in average interstitial velocity, U. It may be noticed that in Group #1 of the experimental Runs there is comparatively a greater variation of dispersion coefficient with the change in average interstitial velocity, other conditions being the same.

A few other observations depicted in Figure 34 pertaining to Group #2 and #3 may be of some interest to the researchers in this area. Other conditions remaining almost the same in Group #2, it is observed that as initial gas saturation, S_g, increases, the dispersion coefficient, K, also increases under normal room temperature. This effect is observed to be reversed under high temperature as observed in the same Figure for Group #3. The temperature effect on dispersion coefficient evaluated with multiple fluids including gases needs more specific investigation to come to a generalized conclusion.

It may be noticed that in the last two Runs, which involved only liquids, the value of dispersion coefficient,

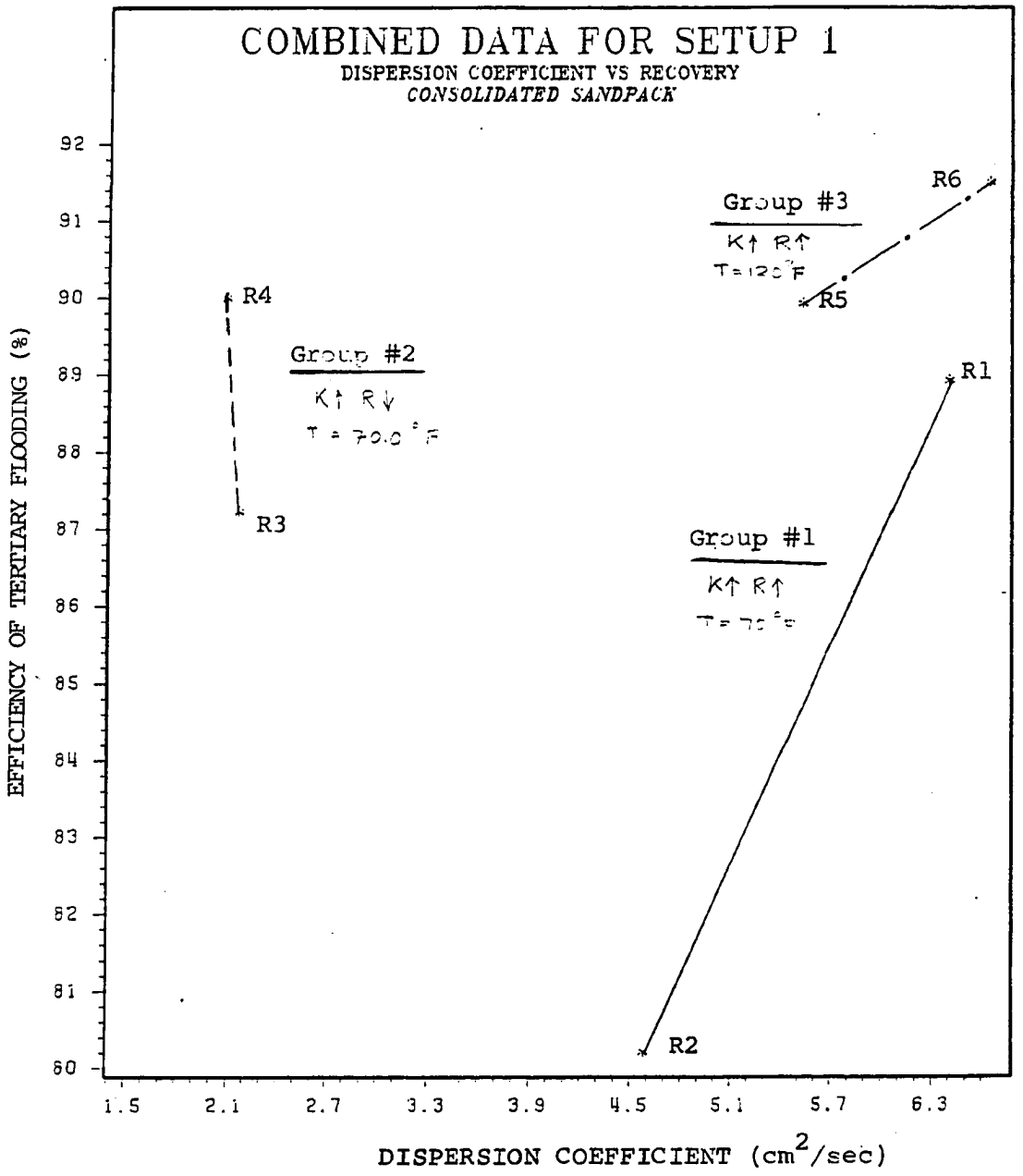

FIGURE 33 CRUDE OIL RECOVERY VS DISPERSION COEFFICIENT AS OBSERVED IN SETUP #1

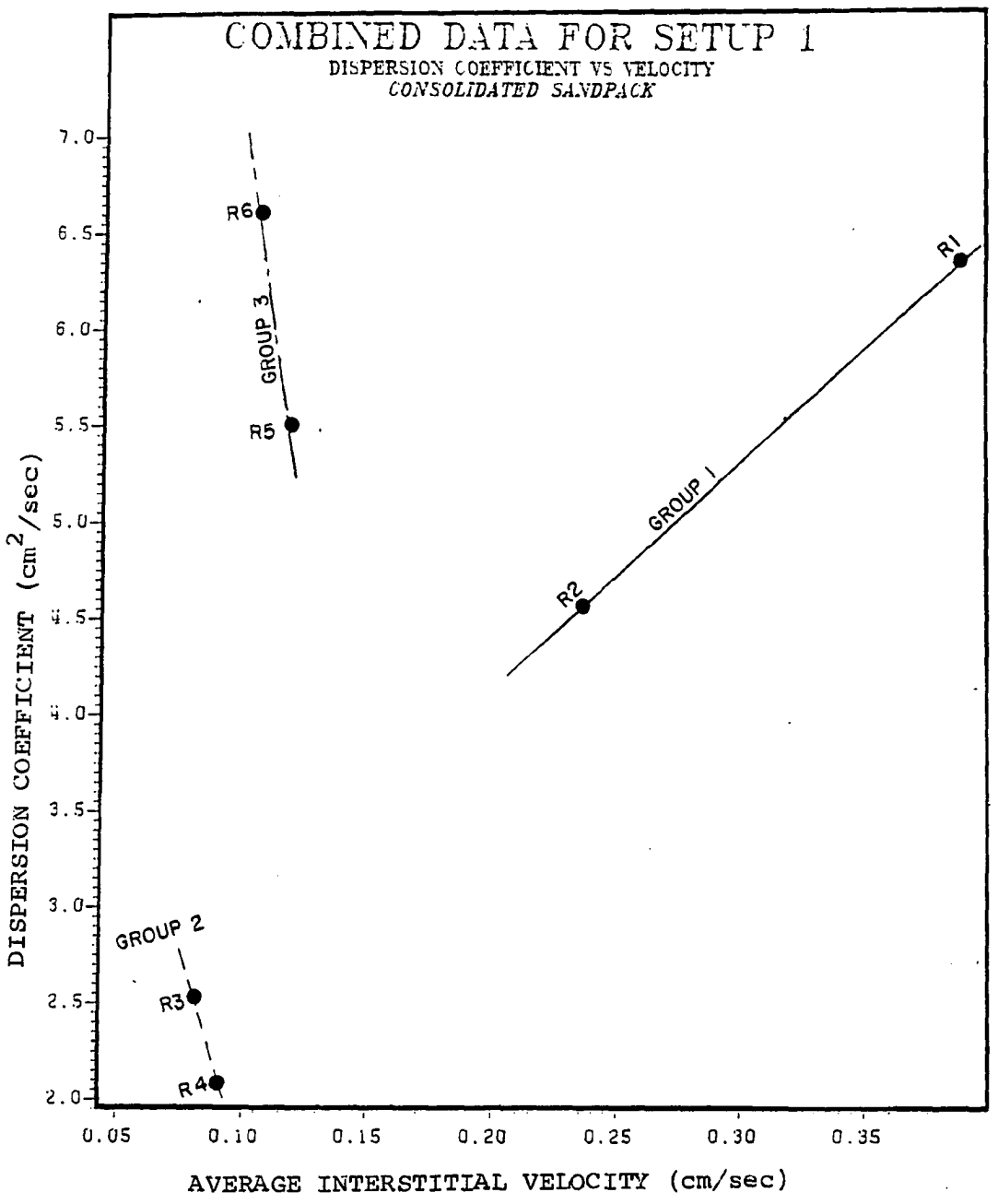

FIGURE 34 DISPERSION COEFFICIENT VS VELOCITY AS OBSERVED IN SETUP #1

K, showed an increase with initial water saturation, S_w. This observation matches quite well with the findings of Torcaso and Henderson[21].

The average interstitial velocity (U) of the displacing fluid in Setup #1 were also plotted against the corresponding dispersivity as depicted in Figure 35. The increase in average interstitial velocity in all the three Groups plotted in this Figure leads to a decrease in the dispersivity of the reservoir model. This observation is consistent with the theoretical equation (48) of dispersivity listed in the previous section of this report.

Since there was a substantial difference in length, type, temperature, and injection pressure between Setup #1 and Setup #2, hence the dispersivity, α and the dispersion coefficient, K, from Setup #1 is plotted against the average interstitial velocity (U) for all the Runs conducted in Setup #1 as shown in Figure 36. It is evident from the Figure that as U increases there is a decrease in dispersivity, α, and an increase in the dispersion coefficient, K. This increase in K is comparatively larger below an average interstitial velocity of 0.15 cm/sec. As U increases further the changes in α and K are very nominal but the increasing trend of K and decreasing trend of α can be observed in Figure 36.

It is interesting to note that as U increases further than 0.35 cm/sec the dispersivity and the dispersion

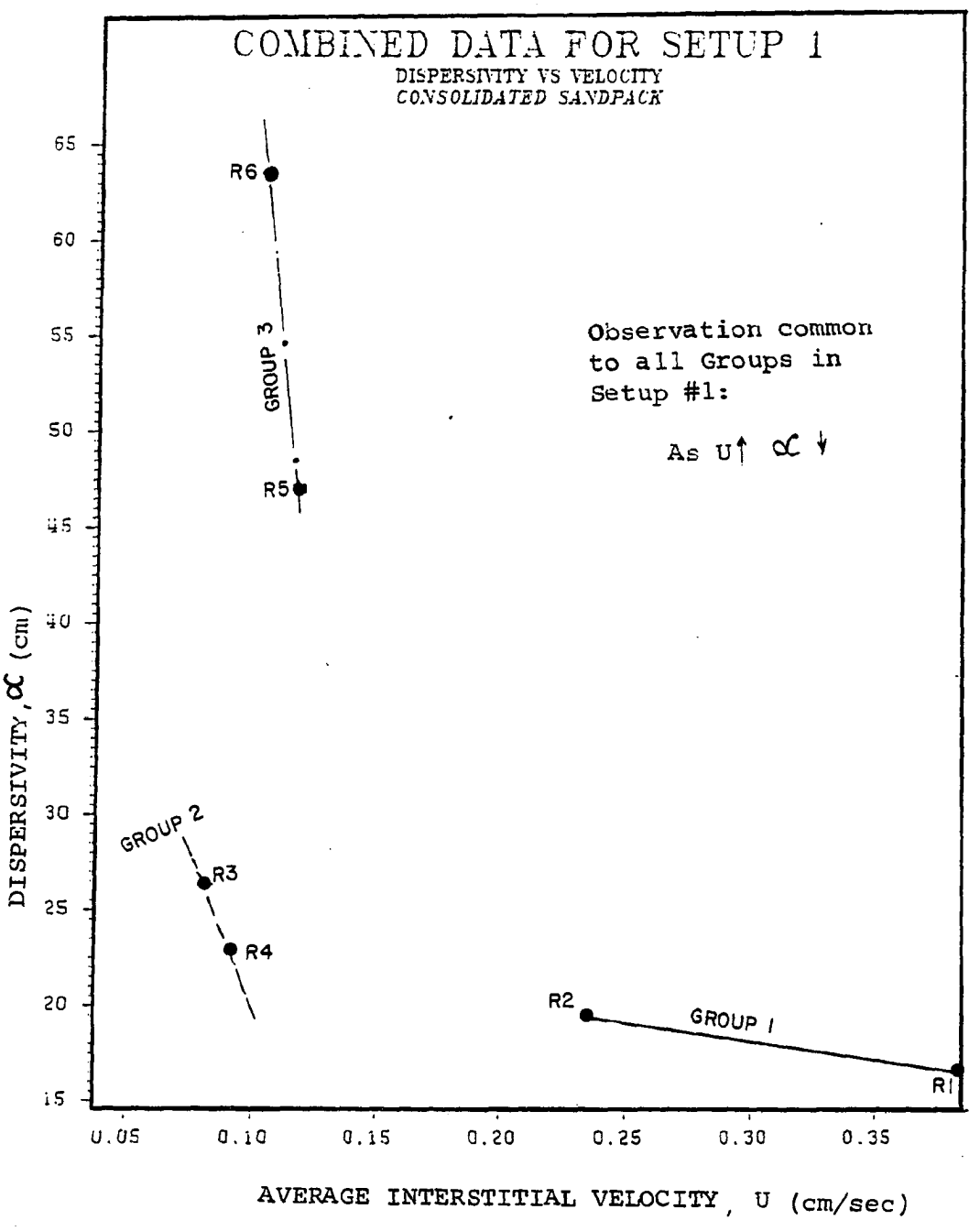

FIGURE 35 DISPERSIVITY VS VELOCITY AS OBSERVED IN SETUP #1

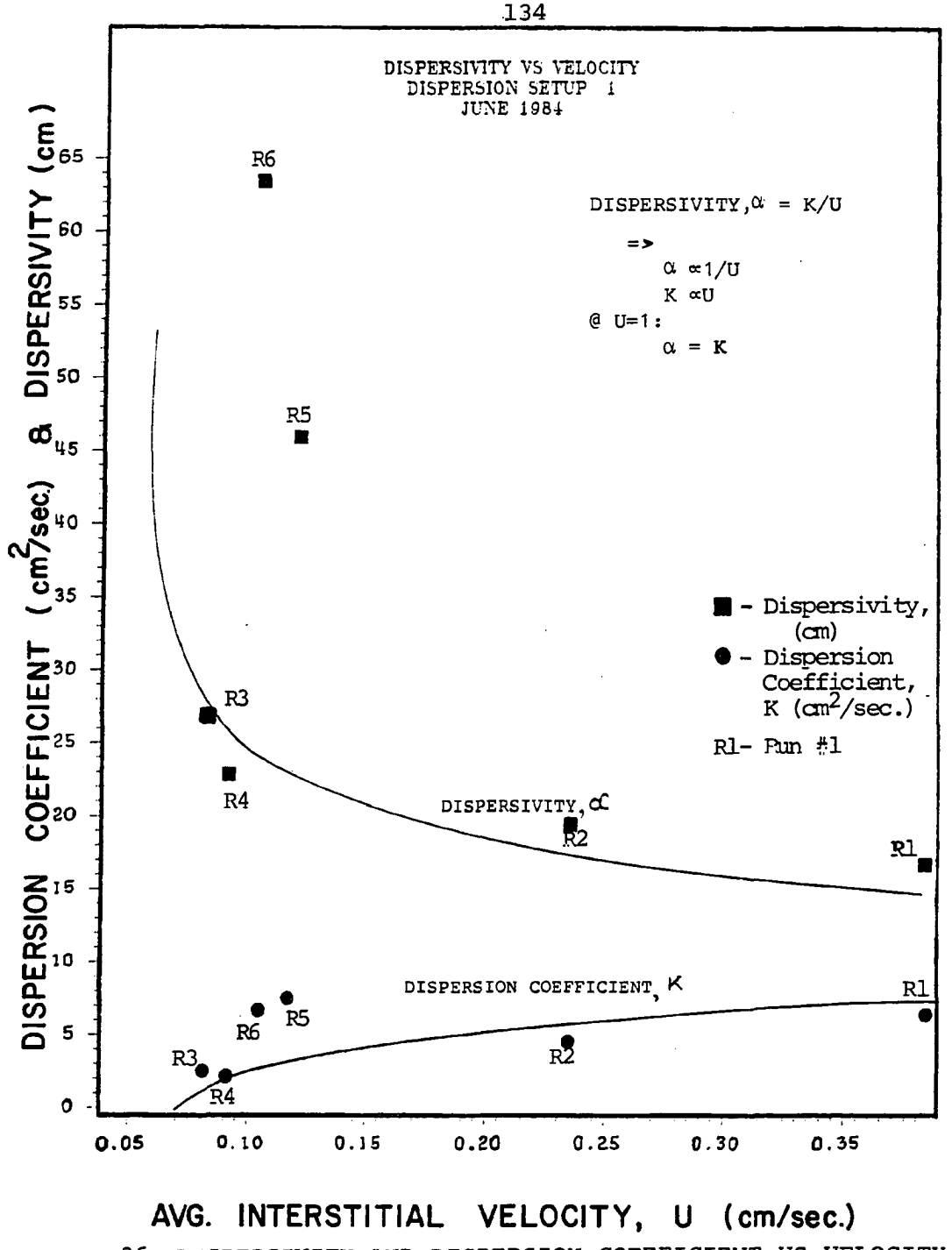

FIGURE 36 DISPERSIVITY AND DISPERSION COEFFICIENT VS VELOCITY FOR DIFFERENT EXPERIMENTAL CONDITIONS

coefficient seems to move towards a coinciding point. This experimental observation is theoretically true, since, at an average interstitial velocity of 1.0 cm/sec we have $K = \alpha$, as evident from equation (48) of this report.

The dispersivity of a reservoir rock is directly proportional to the dispersion coefficient as indicated by equation (48). From the experimental observations of this study the observed data points for different Groups are plotted and compared as shown in Figure 37. As depicted in this Figure by Group #2 and #3, it is evident that an increase in dispersion coefficient results in an increased dispersivity of the reservoir model. This observation is consistent with the findings of Kasraie et al.[15]. In their study of the role of immobile phase saturations in tertiary oil recovery they have shown similar variation in the mixing coefficient with the transition zone. The mixing coefficient used in their study is equivalent to the dispersivity, α, in this investigation. Eventhough, the transition zone does not represent the dispersion coefficient, K, but it is strongly dependent upon K. Hence, the varition of K with α as observed in this study is considered to be similar to the findings of Kasraie et al.[15].

The dependency of the dispersion coefficient on the core length can be clearly observed in Figure 37. This observation matches quite well with the findings of E. J. Koval[16].

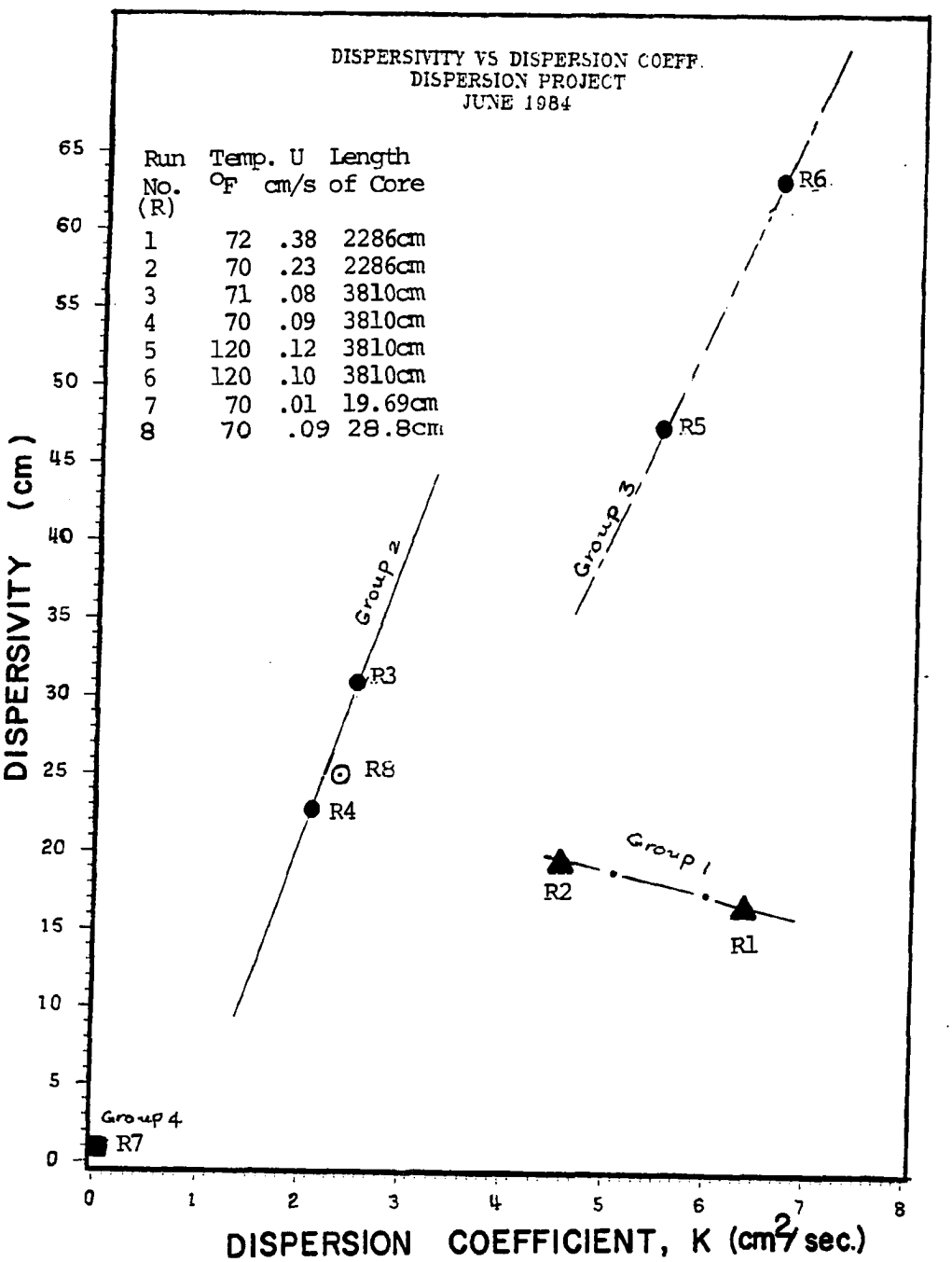

FIGURE 37 DISPERSIVITY VS DISPERSION COEFFICIENT FOR DIFFERENT EXPERIMENTAL CONDITIONS

The effect of immobile fluid saturation in the reservoir models can be easily seen in Figure Nos. 15 to 28. The oil, water, and gas saturations are specified in all of these Figures for better identification of the changes involved. The water saturation was nearly the same in the first six Runs, but the oil, and gas saturations varied considerably in some of the Runs conducted with Setup #1.

At very low recovery rates, the effect of dispersivity can be substantial. This increase in recovery due to higher dispersivity is attributed to the higher sweep area during the miscible flooding. Also, in case of recoveries over 90%, the effect of dispersivity is not significant. Hence, if the dispersivity of a reservoir rock is known, the effectivity of a flood in that reservoir can be roughly estimated by following the trend observed in this investigation. Figure 38 illustrates the effect of dispersivity on sweep area, which is directly related to the recovery from a reservoir rock in a flooding process. The different front positions corresponding to dimensionless time for a five-spot pattern theoretically developed by R. E. Collins[11] is shown in Figure 38 as the ideal base condition.

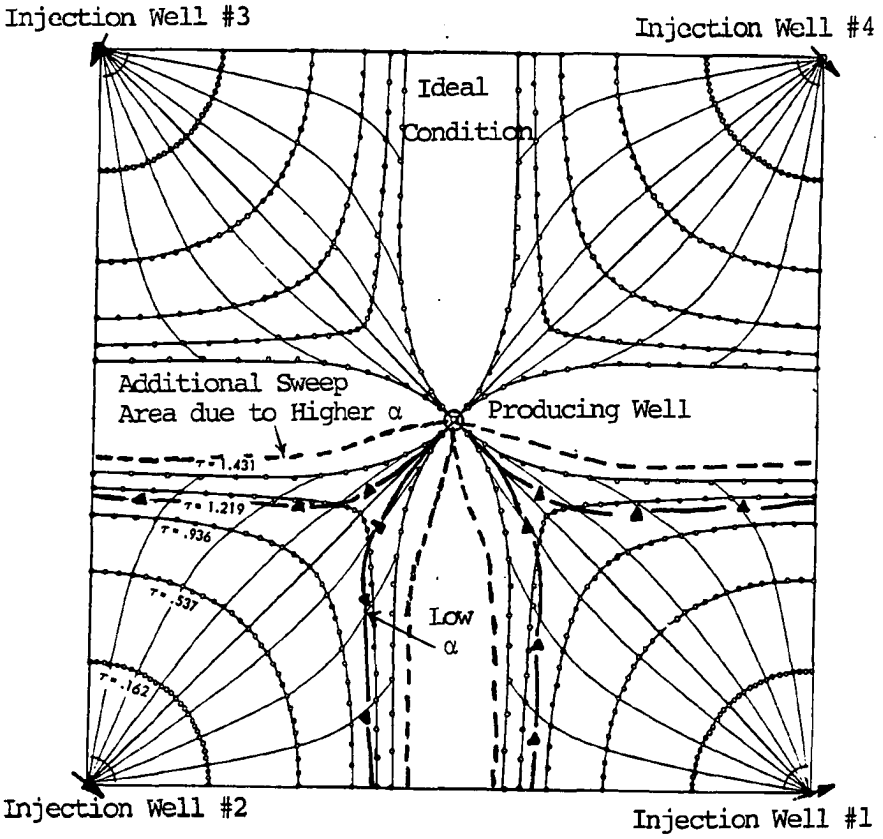

FIGURE 38 FLOODFRONT POSITIONS AS A FUNCTION OF DIMENSIONLESS TIME

Source for base pattern: Collins, R. E. (Ref. 25)

The sweep area shown in Figure 36 is changed in the same proportion to the observed change in recovery due to the corresponding change in dispersivity for Setup #1 and #2. Hence, more areal coverage of sweep area is expected to occur due to high dispersivity. The observed variation of dispersivity and its role as a reservoir rock property is further stressed in the next section of this report.

6.0 CONCLUSIONS AND RECOMMENDATIONS

Based upon the results of this study as discussed in the preceding section, it is evident that the dispersivity of a reservoir rock is one of the factors governing the areal sweep efficiency during a flooding process. Knowing the dispersivity of a reservoir rock the solvent slug size in a hydrocarbon miscible flooding can be determined by using conventional dispersion-capacitance model as described previously under Section 3.0 of this report. Selection of an optimum slug size is critical in the proper design of a hydrocarbon miscible flood. Hence the experimental determination of dispersivity of different reservoir rocks is considered to be equally important as compared to the determination of conventional physical properties of a reservoir rock such as porosity, and permeability, especially when a secondary or tertiary recovery process is considered.

The dispersivity of a reservoir rock also has a great influence on the effectivity of different fluid injection. A knowledge of the dispersivity of a reservoir prior to

the selection of the fluid to be injected will help in better design of the hydrocarbon miscible flood.

On the basis of this investigation it may be concluded that the dispersion coefficient or the dispersivity of a petroleum reservoir rock influences the recovery to a great extent when the recovery rate is very low in a reservoir. A low recovery rate could occur due to very low porosity and permeability of the reservoir rock or when significant dead-end pore spaces exist inside a reservoir. In the case of substantial dead-end pore spaces in a reservoir rock which could not be reached by normal immiscible flooding, a miscible flooding could be recommended if the dispersivity of the rock is high. The high dispersivity of such a reservoir rock will contribute substantially towards the recovery. The effect of dispersivity may be considered to be insignificant when the recovery from a secondary or a tertiary flooding is high due to other favorable conditions of the reservoir.

In order to have a better understanding of the dispersion phenomena the following recommendations are made for future work:

(1) The effect of physical properties of the displacing and the displaced fluid on the dispersion coefficient or the dispersivity of the reservoir rock should be further studied.

(2) This investigation leads to a completely new direction of possible study involving correlation of the pore size distribution of a reservoir rock with the dispersivity and the corresponding changes in the behavioral pattern for several rocks with different permeabilities.

(3) Correlating the Heterogeneity factor, H, as introduced by Koval[26], with the dispersivity of a reservoir rock for a miscible flood is also suggested for future investigation.

(4) Determination of the dispersivity of a rock by both miscible and immiscible flooding and further investigation into the dispersion mechanism by analyzing the cause of deviations in results, if any, due to two different flooding conditions.

So, further investigation into the dispersion phenomena as necessitated by this study is expected to aid the petroleum industry in designing more efficient Enhanced Oil Recovery (EOR) method.

NOMENCLATURE

A = Cross-sectional area, cm^2
D = Diffusivity, $cm^2/sec.$
H = Heterogeneity factor
K = Dispersion Coefficient, $cm^2/sec.$
k = Permeability, millidarcy
q = Volumetric flow rate, cc/sec.
Q = Cumulative flow, cc
L = Length, cm
S = Saturation, % of pore volume
t = Time, sec.
T = Temperature, ^oF
U = Average interstitial Velocity, cm/sec
V = Velocity, cm/sec
W = Weight, gms.
X = Rectangular coordinate axis (X)
Y = Rectangular Coordinate axis (Y)
Z = Cylindrical Coordinate axis (Z)
P = Pressure, psi

Greek Letters:

α = Dispersivity, cm
β = parameter of beta distribution
ϕ = porosity, %
μ = viscosity, cp
δ = partial differential operator

Subscripts:

1,2,3 = for Setup #1, 2, and 3 respectively
g = gas
o = oil
w = water
n = number of steps

BIBLIOGRAPHY

1. Alarcon, Carlos, A., "A Laboratory Study to Determine the Effect of High-Pressure Nitrogen Injection on Enhanced Oil Recovery., Ph. D. Thesis, 1982, and SPE/DOE, Fourth symposium on Enhanced Oil Recovery, Tulsa convention center, Tulsa, Oklahoma, Vol. 2, April 1984.

2. American Chemical Society Publications, Flow Through Porous Media, Washington, D.C., October 1970.

3. Baker, L.E. "Effects of Dispersion and Dead-End Pore Volumes in miscible Flooding", SPE Journal, march 1964.

4. Batycky, J.P., Maini, B.B., and Fisher, D.B., "Simulation of Miscible Displacement in Full Diameter Carbon Cores, "SPE Journal, October, 1982.

5. Blackwell, R.J., Terry, W.M., Rayne, J.R., Lindley, D.C., "Recovery of Oil by Displacement with water-solvent mixtures", Reprint series, SPE, Dallas, 1965.

6. Blackwell, R.J., "Laboratory Studies of Microscopic Dispersion Phenomena", SPE Journal, March 1962

7. Brigham, W.E., "Mixing Equations in Various Geometries", Paper SPE 4585, Las Vegas, Sept. 30, 1973.

8. Brigham, W.E., Reed, Phillip, W. and Dew, John N., " Experiments on mixing during miscible displacement in porous media", SPE Journal, March 1961.

9. Cheng, Shing-Ming, Allard D.R., and Anli Jun, " Factors Affecting Solvent Slug Size Requirements in Hydrocarbon Miscible Flooding", SPE/DOE, Vol. 1, April 1984.

10. Coats, K.H. and Smith, B. D., "Dead-End Pore Volume and Dispersion in Porous Media." SPE Journal, March 1964.

11. Collins, R.E., Flow of Fluids Through Porous Materials, The Petroleum Publishing Company, Tulsa, Oklahoma 1976.

12. De Josselin De Jong, G., ibid. 1958.

13. Giordano, R.M. and Salter, S.J., "Comparison of Simulation and Experiments for Compositionally well-defined Corefloods. SPE/DOE, Fourth symposium on Enhanced Oil Recovery, Tulsa convention center, Tulsa, Oklahoma, Vol. 1, April 1984.

14. Haring, R.E., and Greenkorn, R.A., A.I.Ch.E. Journal, 1970.

15. Kasraie, Mahnaz and Ali Farouq S. M., " Role of Immobile phase saturations in Tertiary Oil Recovery", SPE/DOE, Fourth symposium on Enhanced Oil Recovery, Tulsa convention center, Tulsa, Oklahoma, Vol. 1, April 1984.

16 Koval, E. J., "A Method for Predicting the Performance of Unstable Miscible Displacement in Heterogeneous Media", SPE Journal, June 1963, p. 145-154

17. Kramers, H, and Alberda G., Chem. Eng. Science, 1953.

18. Moskowitz, Joyce, ME News Roundup, Mechanical Engineering, July 1981, p. 62-63.

19. Orlob, G.T., and Radhakrishna, G.N., "The Effect of Entrapped Gas on Hydraulic Characteristics of Porous Media", Trans. AGU, Aug. 1948.

20. Perkins, T. K. and Johnston, O.C., "A Review of Diffusion and Dispersion in Porous Media", SPE Journal, March, 1963, p. 70-84.

21. Raimondi, P., Torcaso, M.A., and Henderson, J.H., "The Effect of Interstitial Water on the Mixing of 9 Hydrocarbons During a Miscible Displacement Process". Min. Ind. Expt. Station Cir. 61, Penn State U. (Oct. 1961).

22. Saffman, P.G., Fluid Mechanics, 1959.

23. Scheidegger, A.E., Can. Mining Metallurgical Bulletin, 1959.

24. Stalkup, F.I., "Miscible Displacement Monograph Series, SPE, Dallas, 1983.

25. Taylor, G.I., "Dispersion of Soluble Matters in Solvent Flowing Slowly Through a Tube", Proc. Roy. Society, Vol 219, 186.

26. Thomas, G.H., Countryman, G.R., and Fatt, I, "Miscible Displacement in a Multiphase System", SPE Journal, Sept. 1963.

A P P E N D I C E S

APPENDIX A

CALIBRATION OF THE LDG MINIPUMP

CALIBRATION OF THE LDG MINIPUMP

A1: DESCRIPTION:

The LDG minipump model 396 (duplex) is a reciprocating plunger, positive displacement type pump. It is designed to produce liquid flow in precise quantities against pressure up to 6,000 PSIG. The duplex version consists of two pump bodies. The pump has two manual micrometer dial controls to fix the stroke length of the pump. Adjustment of the flow rate may be made while the pump is shutdown.

A2: CALIBRATION:

Since the flow rate is proportional to the motor speed and stroke length it was necessary to perform a test to obtain data to determine relationships between micrometric dial position and the flow rate. The performance data for the minipump is given in table A1 and the calibration curve is shown in figure A1.

TABLE A1

Performance Data for the LDG Minipump

TIME (SEC)	RECOVERY VOLUME (MIN) RATE	LDG MINIPUMP DIAL SETTING
0	-	0
480	10	10
960	20	10
206	10	20
412	20	20
979	70	30
1116	80	30
1437	110	35
1555	120	35
1699	130	35
330	30	40
440	40	40
550	50	40
177	20	50
145	20	60
327	45	60

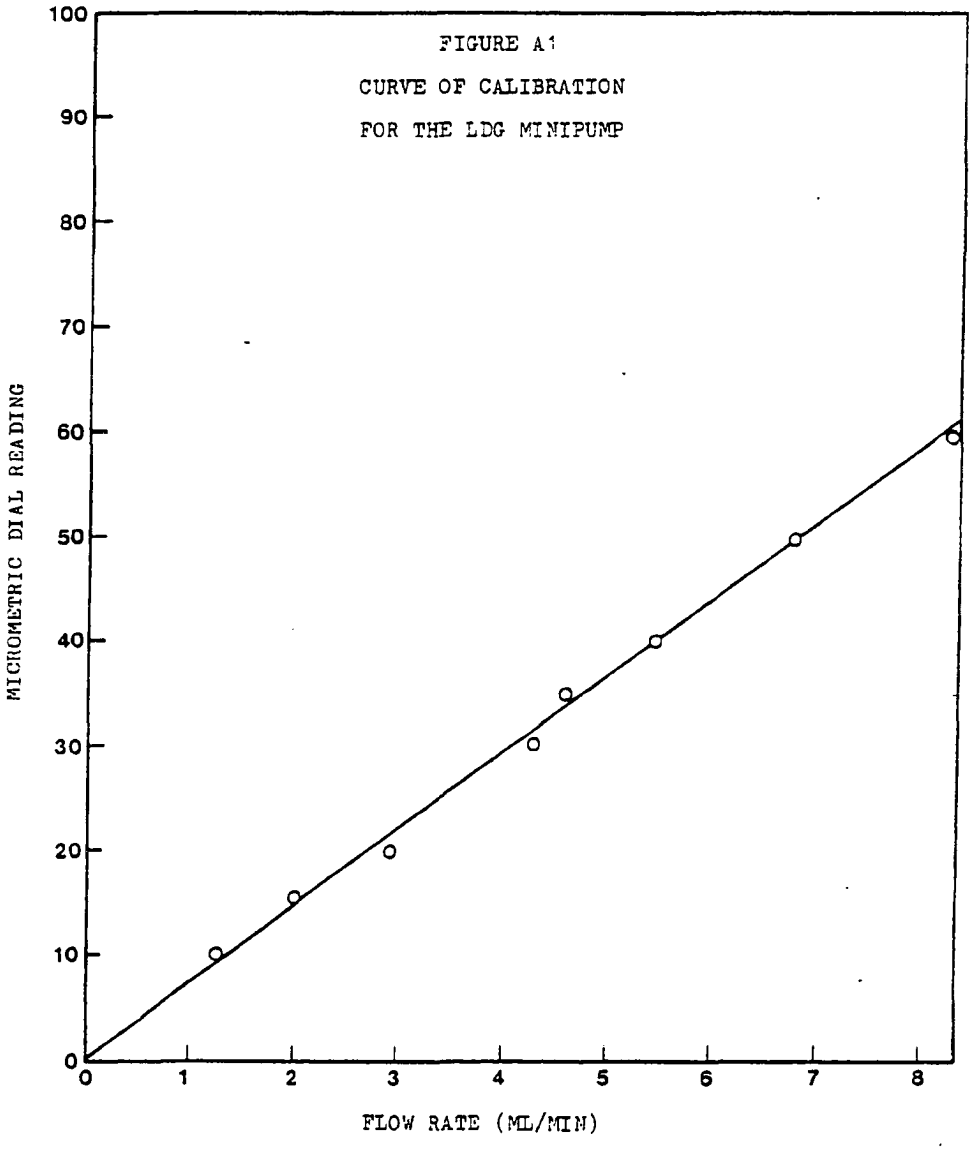
FIGURE A1
CURVE OF CALIBRATION
FOR THE LDG MINIPUMP
MICROMETRIC DIAL READING
FLOW RATE (ML/MIN)
0
10
20
30
40
50
60
70
80
90
100
0
1
2
3
4
5
6
7
8

APPENDIX B

CALIBRATION OF THE REFRACTOMETER

CALIBRATION OF THE REFRACTOMETER

In order to clean the model by using a miscible displacement it was necessary to prepare a refractometric curve with the purpose of obtaining the fraction composition from the mixture of naphtha - crude oil at different times in the displacement process.

From an optical point of view, two different types of naphtha were used in the cleaning process. For the first one, naphtha-1, 11 refractive indices were obtained. The results of the calibration are presented in figure B1.

For naphtha-2, a total of four samples were analyzed. The resultsof calibration are presented in figure B2.

An "ABBE" refractometer available at Oklahoma University was used in this experiment.

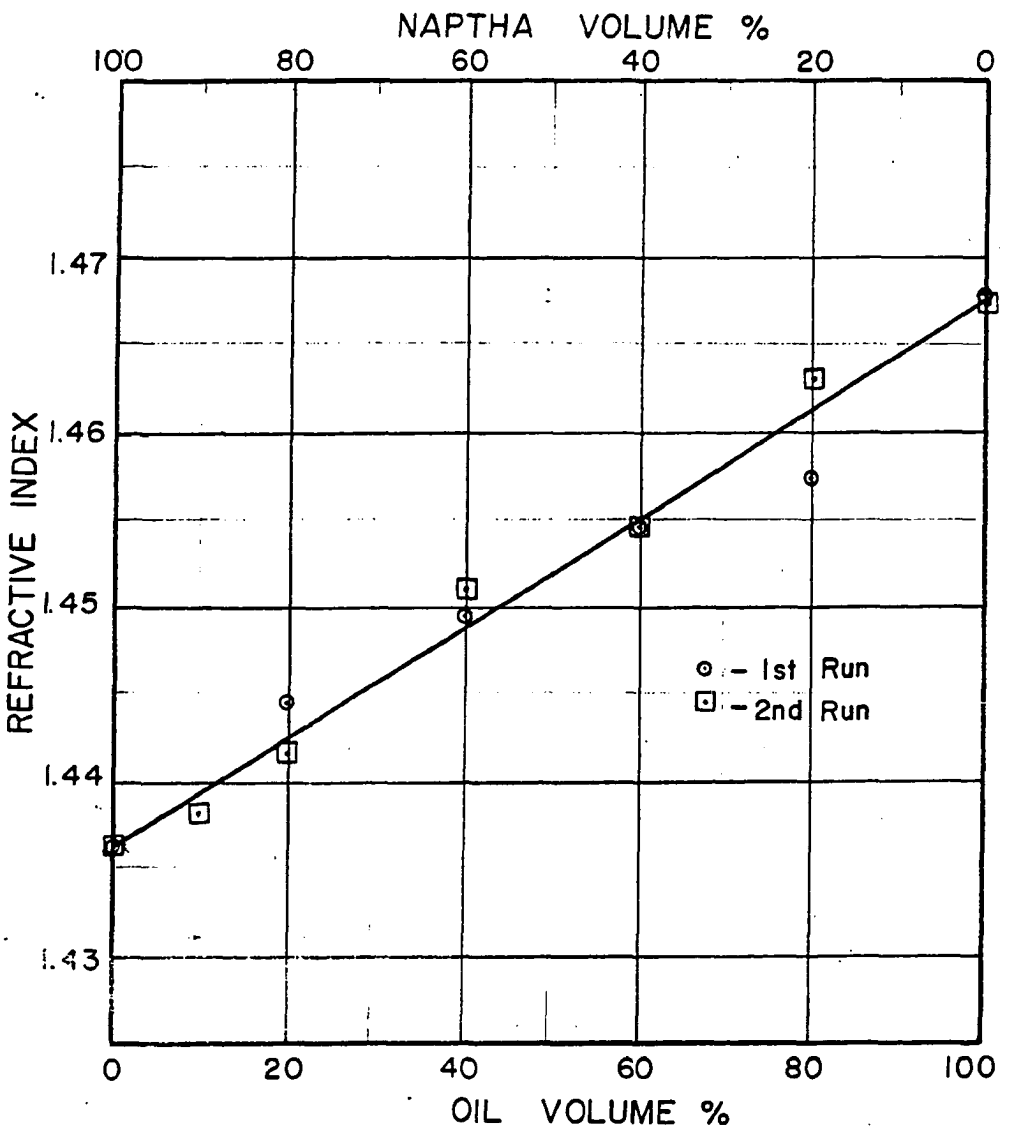

FIGURE B1 REFRACTOMETRIC CURVE FOR NAPTHA-1 — CRUDE OIL

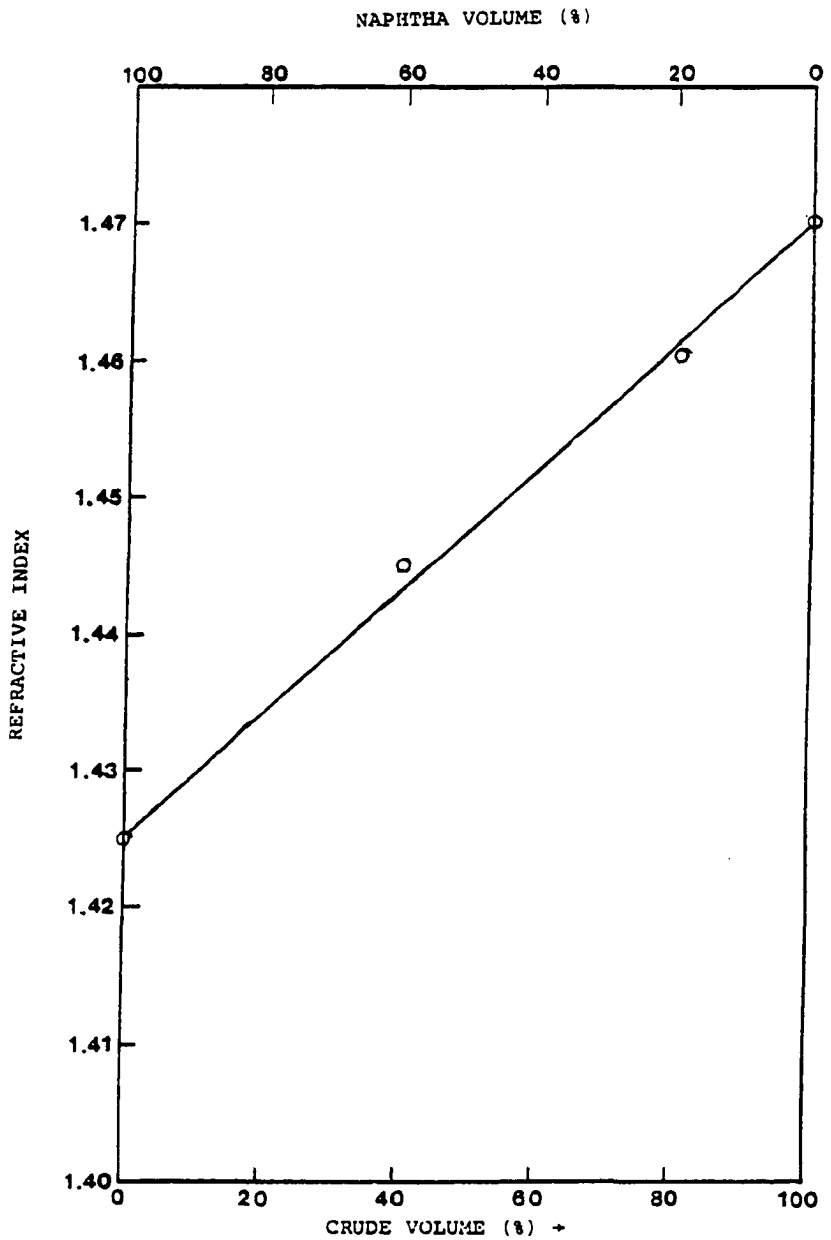

FIGURE B2 REFRACTOMETRIC CORVE FOR NAPTHA-2 - CRUDE

APPENDIX C

DETERMINATION OF ABSOLUTE PERMEABILITY OF THE RESERVOIR MODELS

DETERMINATION OF ABSOLUTE PERMEABILITY OF THE RESERVOIR MODELS FOR EXPERIMENTAL SETUP #1 & #2

PERMEABILITY MEASUREMENTS

The absolute permeability of the pore medium of the reservoir physical model was determined from flow test data. Nitrogen was displaced at different rates through the model. Each reading was taken after steady conditions were obtained for each pressure and flow. The average time for each reading was 24 hours. Table E1 shows the results obtained by displacing N_2. Permeability test for Setup #2 is detailed later.

N_2 was used as the flowing fluid for the following reasons:

a) Steady state flow is quickly obtained, which allows rapid determination in a long core;

b) Nitrogen does not alter the mineral constituents of the rock; and,

c) 100% saturation to the flowing fluid is easily obtained.

Specific instructions for permeability measurements may be found in the API Code no. 27. The pressure differential was measured by suitable manometer. The flow volume was obtained with a high precision gas meter.

Nitrogen permeability is calculated from a suitable form of Darcy's equation.

For linear fluid flow:

$$k = \frac{2q_2 \mu L P_2}{A(P_1^2 - P_2^2)} \quad \text{or} \quad k = \frac{q_m \mu L}{A \Delta P} \quad ....(1)$$

Where:

k = permeability, Darcy's

q_2 = flow rate at exit conditions, cc/sec

q_m = flow rate at mean conditions, $\frac{P_1 + P_2}{2}$, cc/sec

μ = gas viscosity at test temperature, cp.

L = sample length, cm

A = Core area, cm^2

P = pressure differential across sample, atm

P_1 = inlet pressure, atm (absolute)

P_2 = exit pressure, atm (absolute)

Based on this equation a computer program to calculate apparent absolute permeability was obtained. The listing of the program and result are given above in this appendix.

DISCUSSION

In order to obtain the absolute permeability of a rock from gas flow tests, it is necessary that an anomaly caused by the nature of a gas be accounted for. This was recognized by Klinkenberg and is known as the Klinkenberg effect or correction. This principle states that permea-

bility to gas is a function of the mean free path of the molecules, and therefore dependent on the mean pressure at which the test is performed. This is expressed by equation:

$$k_a = k_L \left(1 + \frac{b}{\bar{P}}\right) \quad \ldots\ldots\ldots\ldots\ldots\ldots (2)$$

Where:

k_a = apparent absolute permeability (measure at pressure P)

k_L = true absolute permeability of the core or equivalent liquid permeability.

b = a constant dependent on pore size which increases in value as pore size decreases.

$\bar{P}$ = mean pressure

In equation (2) when:

$$\bar{P} \rightarrow \infty \qquad \frac{k_L b}{P} \rightarrow 0$$

Then:

$$k_a \rightarrow k_L$$

Figure E1 shows the plotting of equation (2). The resultant absolute permeability was 910 md.

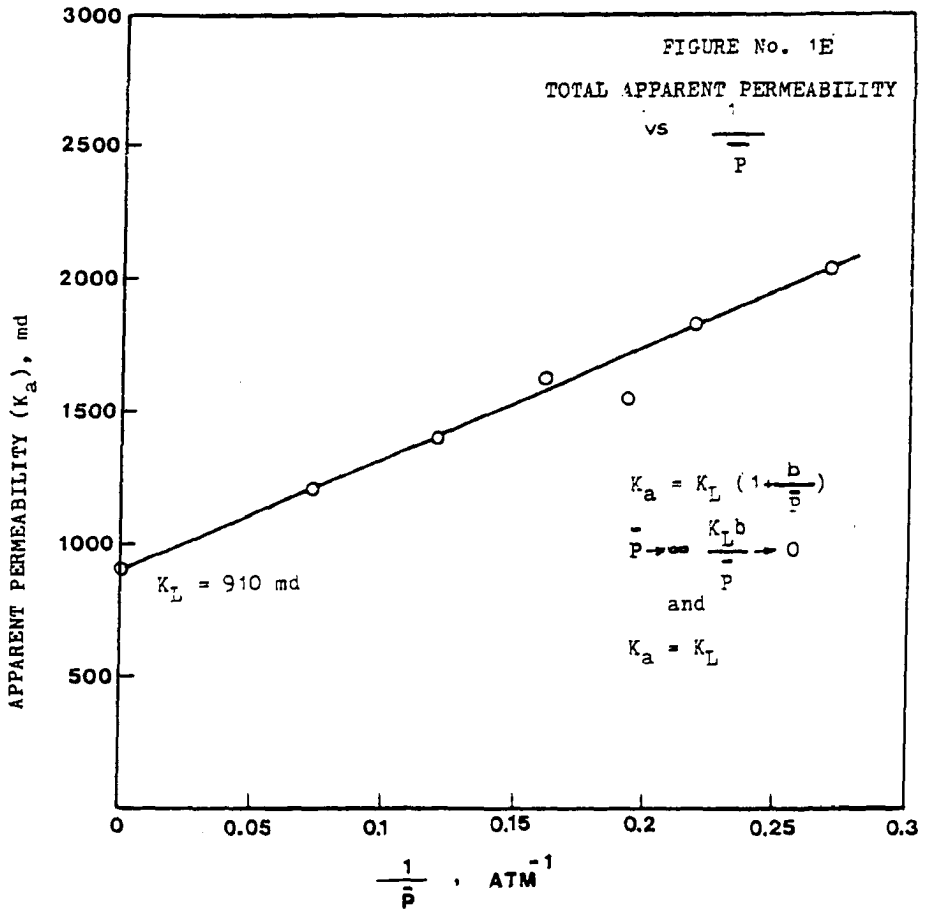
FIGURE No. 1E
TOTAL APPARENT PERMEABILITY
vs 1/P̄
APPARENT PERMEABILITY (Ka), md
3000
2500
2000
1500
1000
500
0
0.05
0.1
0.15
0.2
0.25
0.3
1/P̄ , ATM-1
KL = 910 md
Ka = KL (1 + b/P̄)
P̄ → ∞ KLb/P̄ → 0
and
Ka = KL

```
      $JOB
    1         REAL EP1,EP2,P3,EPBAR,EPPBAR,K,KK,C2
    2         DIMENSION EP1(100),EP2(100),Q2(100),EK(100),EKK(100),DELTP(100),
             1EPBAR(100),EPPBAR(100)
    3         READ(5,100) NJ,EL,ATUBE
    4  100    FORMAT(I4,7F8.0)
    5         DO 10 J=1,NJ
    6         READ(5,200) EP1(J),EP2(J),Q2(J)
    7  200    FORMAT(10F8.0)
    8  10     CONTINUE
    9         VISGAS = 0.0182
   10         DO 20 M=1,NJ
   11         EK(M)=2.*Q2(M)*VISGAS*EL*EP2(M)/(ATUBE*(EP1(M)**2.0-EP2(M)**2.0
             1))
   12         EKK(M)=EK(M)*1000.0
   13         DELTP(M) = EP1(M)-1.0
   14         EPBAR(M)  = EP2(M)+DELTP(M)/2.0
   15         EPPBAR(M) = 1/EPBAR(M)
   16  20     CONTINUE
   17         WRITE(6,500)
   18  500    FORMAT(1HI,6X,'PERMEABILITY',6X,'1/PBAR',6X,'FLOW RATE',6X,
             1'BAR. PRESSURE',4X,'INLET PRESSURE',/)
   19         WRITE(6,600)
   20  600    FORMAT(10X,'MIL. DARCY',7X,'1/ATM',10X,'CC/SEC',12X,'ATM',
             112X,'ATM',//)
   21         DO 30 JM=1,NJ
   22         WRITE(6,700) EKK(JM),EPPBAR(JM),Q2(JM),EP2(JM),EP1(JM)
   23  700    FORMAT(6X,F9.3,2X,F10.4,4X,F10.4,6X,F10.4,6X,F10.4,//)
   24  30     CONTINUE
   25         STOP
   26         END

      $EXEC
```

TABLE C1

Nitrogen Displacements to Obtain Absolute Permeability Data.

Nitrogen Viscosity = 0.0182 Cp.

Core Length = 3810 CM

Area = 1.0261 Cm^2

Standard pressure: 29.08" Hg.

Temperature: 70° F.

cc/sec	P_1 (PSIg)	P_2 (atm) Hg
363.65	382.77	29.08"
156.84	224.1	29.08"
97.02	164.6	29.08"
60.00	135.70	29.08"
47.50	111.42	29.08"
37.61	91.89	29.08"

DETERMINATION OF POROSITY AND PERMEABILITY OF SETUP #2

The porosity of the Berea core used in Experimental Setup #2 was first determined by the following procedure:

1. Weighed the clean dry core in a electronic balance Core Dia.=5.08cm; Length=19.69cm; W_1 = 1540.5 gms.
2. Weighed the clean dry core with four attachments and frame. W_2 = 2105.2 gms.
3. Saturated the core with oil (API 42.1°) SG = 0.815
4. Weighed the core without attachments after saturating with oil W_3 = 1585.8 gms.
5. Net weight of oil occupying the void volume is given by: $W_o = W_3 - W_1$ = 45.3 gms.
6. Volume of oil is given by: $V_o = W_o/SG$ = 45.3/0.815 = 55.58 cc
7. Porosity is therefore given by: $\phi = V_o/BV$
8. Bulk Volume (BV) of the core = $\frac{II \times (5.08)^2 \times 19.69}{4}$ = 399.083 cc

Hence, Porosity of the Berea core is = 55.58/399.083 = 13.92% ≃ 14%

Permeability of the Berea core was determined by using the following procedure:

1. Draw vacuum on clean dry core for four hours.
2. Flow water through the core and record the time, temperature, and effluent volume.
3. Table C2 shows the recorded values for the permeability test conducted on the Berea core.

TABLE C2 RECORD OF TIME AND EFFLUENT FLOW VOLUME FOR THE PERMEABILITY TEST OF THE BEREA CORE

Time (sec.)	Cumulative Flow (cc)	Temperature (^{o}F)
125	11.3	62
210	20.1	62
340	32.3	62
423	39.4	62
560	49.8	62

4. Viscosity of water at 62°F = 1.1 cp
5. Permeability of the core is determined by using the following equation:

$$K = q\mu l/A\,P \quad \ldots\ldots\ldots\ldots\ldots\ldots \quad (2)$$

Where:

q = flow rate
= 49.8/560 = 0.0889 cc/sec
μ = Viscosity of water @ 62°F
= 1.1 cp

l = Length of the core
= 19.69 cm
A = Flow cross sectional area
= 20.26 cm^2
P = Pressure differential, atm

Using equation (2) we get K = (0.889 x 1.1 x 19.69)/(20.26 x 1.19)

= 0.07986 Darcy
= 79.86 mD

APPENDIX D

LISTING OF COMPUTER PROGRAM 'DISCAL' USED FOR CALCULATION OF DISPERSIVITY

AND

OIL CONCENTRATION CURVES

```
c*****************************************************
c*
c*                    D I S C A L
c*
c*           CALCULATION OF DISPERSIVITY
c*
c*
c*             THIS PROGRAM IS DEVELOPED
c*
c*                        BY
c*
c*
c*                 SUBIJOY  DUTTA
c*
c*
c*
c*
c*               DEFINITION OF TERMS
c
c*
c*
c*
c*      exno    =  Experiment No.
c*
c*      efconc  =  Effluent Solvent Concentration
c*
c*      lamda   =  a ratio defined by equation (45)
c*
c*      fluin   =  Injected fluid volume
c*
c*      ri      =  refractive index
c*
c*      grad    =  gradient
c*
c*      sumoil  =  cumulative oil produced
c*
c*      oilin   =  Oil initially in place before
c*                 Tertiary flooding
c*
c*      lcore   =  Length of the core
c*
c*      perm    =  Permeability of the core
c*
c*      presnj  =  Injection pressure
c*
c*      grate   =  Flow rate
c*
c*      porvol  =  Pore volume
c*
c*      porsty  =  Porosity
c*
c*      ndata   =  Number of total data
c*
c*      disper  =  Dispersion coefficient
c*
c*      dispvt  =  Dispersivity
c*
c*
c*************************************************************
c
c
```

```
      implicit real (a-h,k,l,o-t,u-z)
      real*8 exno
      dimension efconc(100),lamda(100),fluin(100)
      dimension ri(100),time(100),grad(100),avgrad(100)
      pie = 3.1415927
      ncount = 0
      sumoil = 0.0
      read(5,100)exno,no,isetup,temp,perm,presaj
100   format(a8,i2,i2,2f6.1,f8.1)
      read(5,200)lcore,qrate,dia,porvol,porsty
200   format(f8.2,f8.4,f8.4,f8.2,f8.3)
      read(5,300)ndata,oilin
300   format(i3,f8.2)
      n = ndata
      read(5,400) (ri(i),fluin(i),time(i),efconc(i),i=1,n)
400   format(f8.4,f8.2,f8.0,f8.2)
      acore = pie*(dia**2)/4.0
      flovel = qrate/(acore*porsty)
      do 10 i=1,n
      ncount = ncount +1
c
c   Ratio of Volume injected to the pore volume, V/Vp is
c   defined as 'term1'
c
      term1     = fluin(i)/porvol
      den  = sqrt(term1)
      lamda(i)  = (term1 - 1.0)/den
10    continue
c
c  This Program uses arithmetic probability method
c  of linear interpolation and is DEVELOPED FOR THIS STUDY
c  to SUBSTITUTE CONVENTIONAL GRAPHICAL METHOD
c
      sumgrd = 0.0
      sumav  = 0.0
      ncont  = 0
      do 15 i = 1,n
      if(i .ge. n)go to 11
      diflam = lamda(i+1) - lamda(i)
      difcon  = efconc(i+1)-efconc(i)
      grad(i) = diflam/difcon
      ncont = ncont + 1
      sumgrd = sumgrd + grad(i)
      avgrad(i) = sumgrd/ncont
      sumav   = avgrad(i) + sumav
      avgrd   = sumav/ncont
11    continue
15    continue
25    continue
      do 40 jj=1,n
      if(efconc(jj) .gt. 85.0 .and. efconc(jj).le.90.0)jn=jj
40    continue
      lamd90  = lamda(jn) + avgrd*(90.0 - efconc(jn))
      do 50 ij=1,n
      if(efconc(ij) .gt. 2.0 .and. efconc(ij).le.10.0)in=ij
50    continue
      lamd10  = lamda(in) + avgrd*(10.0 - efconc(in))
      term2 = (lamd90 - lamd10)/3.625
      disper = flovel*lcore*(term2**2)
      dispvt = disper/flovel
      do 20 ii = 1,n
```

```
      rn1 = 234537856.0
      rn1 = 70036587.0
      iter = 100
      do 30 j = 1,iter
      random = rand(j*rn1)
      cfactr = rand(j*rn1)
30    continue
      if(ii .eq. n)go to 41
      fluvol = fluin(ii+1) - fluin(ii)
      if(no.eq.1)random=((efconc(ii)+efconc(ii+1))/200.0)
      if(no.eq.7)random=((efconc(ii)+efconc(ii+1))/200.0)
      oilvol = random*(1.0 - (efconc(ii)/100.0))*fluvol
      if(no.eq.1 .or. no.eq.7)oilvol=cfactr*(1.0-random)*fluvol
c  since oil volume is caluculated by measuring the area under
c  the curve as included in Appendix D, random variable is set
c  to 1.0 and is not used to correct any volumetric calculation
c
c
      random = 1.0
c
c
      sumoil = sumoil + oilvol
20    continue
41    continue
      if(no.eq.5)sumoil=0.50*sumoil
      if(no.eq.8)sumoil=53.4
      efflod = sumoil/oilin
      efflod = efflod*100.0
      porsty = porsty*100.0
c
c   read and write formats are written below and the write statements
c   are also written in the following lines
c
      write(6,101)exno,isetup
101   format(1h1,/////,37x,a8,//,30x,'EXPERIMENTAL SETUP # ',i2,////)
      write(6,201)lcore,flovel
201   format(16x,'Length of the Core        = ',f8.2,1x,'cm',
     1//,16x,'Average Interstitial ',/,16x,'Velocity',18x,'='
     1,f8.4,1x,'cm/sec',/)
      write(6,301)
301   format(16x,'Displacing Fluid          =  Naptha',//,16x,
     1'Displaced Fluid           = Crude Oil',/)
      write(6,401)temp,perm
401   format(16x,'Reservoir Model Temp.     = ',f6.1,1x,'F',
     1//,16x,'Permeability of the Core  = ',f8.0,1x,'mD',/)
      write(6,501)acore,porvol,porsty,presnj
501   format(16x,'Cross-sectional Area      = ',f8.4,1x,'sq. cm',
     1//,16x,'Pore Volume                = ',f8.2,1x,'cc',
     1//,16x,'Porosity                   = ',f6.3,1x,'%',
     1//,16x,'Injection Pressure         = ',f8.0,1x,'psi',/)
      write(6,601)random,sumoil,efflod
601   format(16x,'Random Correction Factor    = ',f6.4,
     1//,16x,'Cumulative Oil Recovered',/,16x,'By Tertiary Flooding
     1   = ',f8.2,1x,'cc',//,16x,'Efficiency of Tertiary
     1',/,16x,'Flooding',17x,'=',f8.2,1x,'%',//////////////)
      print *,'          LAMDA90 = ',lam490,'     LAMDA10 = ',lam410
      write(6,701)no
701   format(//////////////////,28x,'EXPERIMENTAL OBSERVATION # ',
     1i2,////,16x,'Refractive',5x,'Naptha',8x,'Time',5x,'Lamda',4x,
     1'Effluent',/,18x,'Index',7x,'Injected',26x,'Naptha Conc.',/,
     133x,'(cc)',7x,'(Sec.)',16x,'(%)',///)
```

```
      write(6,801)  (ri(i),fluin(i),time(i),lamda(i),effcnc(i),i=1,n)
801   format(18x,f8.4,3x,f8.2,4x,f6.0,2x,f8.4,3x,f8.2,/)
      write(6,901)disper,dispvt
901   format(16x,'Calculated Value of: ',//,16x,'DISPERSION
     1COEFFICIENT  = ',f8.4,1x,'sq cm/sec',//,16x,'DISPERSIVITY
     1  = ',f8.3,1x,'cm')
      stop
      end
```

INPUT DATA FOR 'DISCAL' COMPUTER MODEL:

```
RUN # 1 1 1  72.0 910.0  4000.0
2286.00    0.103  1.1049  614.47    0.280
10   86.10
 1.4663  525.00  3100.0    4.00
 1.4600  580.00  3193.0   21.50
 1.4580  596.00  3450.0   30.00
 1.4510  610.00  3693.0   57.40
 1.4470  622.00  3900.0   66.50
 1.4450  628.00  4000.0   72.00
 1.4440  646.00  4300.0   73.50
 1.4410  688.00  5000.0   84.10
 1.4395  724.00  5600.0   87.50
 1.4390  736.00  5800.0   90.00
 0
RUN # 2 2 1  69.5 910.0  4000.0
2286.00    0.063  1.1049  614.47    0.280
10   92.00
 1.4658  530.00  3250.0    7.00
 1.4650  540.00  4044.0    9.00
 1.4510  600.00  4680.0   57.10
 1.4460  610.00  4840.0   69.00
 1.4450  630.00  5157.0   71.50
 1.4430  645.00  5395.0   78.50
 1.4420  665.00  5712.0   81.00
 1.4410  705.00  6347.0   84.10
 1.4398  740.00  7061.0   88.00
 1.4390  760.00  7220.0   90.00
 0
RUN # 3 3 1  70.5 910.0  4000.0
3810.00    0.025  1.1049 1170.00    0.320
12   187.00
 1.4655  830.00 11380.0    8.50
 1.4618  900.00 14460.0   20.00
 1.4605  910.00 14640.00  22.00
 1.4525  945.00 14935.00  47.50
 1.4630  965.00 15580.00  18.50
 1.4625  970.00 15650.00  18.80
 1.4580  980.00 15860.00  29.80
 1.4620 1035.00 16455.00  19.00
 1.4600 1050.00 17000.00  21.50
 1.4520 1080.00 17300.00  55.00
 1.4500 1095.00 17550.00  58.00
 1.4390 1130.00 18190.00  90.00
```

```
 0
RUN # 4 4 1  69.5 910.0  4000.0
3810.00    0.028  1.1049 1170.00    0.320
11  279.00
 1.4665  750.00 11120.0     4.00
 1.4653  820.00 12548.0     5.80
 1.4639  875.00 14435.0    18.00
 1.4612  905.00 15120.0    21.00
 1.4563  945.00 15946.0    37.50
 1.4632  995.00 16435.0    17.50
 1.4645 1040.00 17576.0    11.00
 1.4573 1080.00 18680.0    32.00
 1.4538 1120.00 19710.0    48.00
 1.4392 1150.00 20530.0    89.20
 1.4370 1280.00 23430.0    97.50
 0
RUN # 5 5 1 120.0 910.0  4000.0
3810.00    0.036  1.1049 1170.00    0.320
```

```
11  104.00
 1.4650  700.00 10950.0     4.50
 1.4632  720.00 11780.0    11.20
 1.4610  780.00 13420.0    20.00
 1.4565  810.00 14180.0    38.00
 1.4555  840.00 14690.0    39.50
 1.4548  860.00 15200.0    41.00
 1.4534  920.00 16800.0    45.50
 1.4481 1010.00 18260.0    60.00
 1.4390 1070.00 18720.0    87.50
 1.4370 1150.00 19230.0    93.00
 1.4368 1210.00 20230.0    97.50
 0
```

```
RUN # 6 6 1 120.0 910.0  4000.0
3810.00    0.032  1.1049 1170.00    0.320
11  226.00
 1.4653  710.00 11100.0    4.00
 1.4630  730.00 11780.0   11.00
 1.4620  750.00 13420.0   21.50
 1.4570  770.00 14180.0   31.00
 1.4560  825.00 14690.0   40.00
 1.4550  900.00 15200.0   42.00
 1.4530  935.00 15350.0   47.00
 1.4470  980.00 16280.0   57.00
 1.4390 1110.00 16520.0   87.50
 1.4375 1210.00 17120.0   92.50
 1.4365 1365.00 19750.0   97.20
 0
RUN # 7 7 2  70.0  79.9    15.0
  19.69    0.019  5.0800   55.85    0.140
 7   54.40
 1.4800   50.00  1688.0    0.00
 1.4658   60.00  2120.0    3.50
 1.4625   70.00  2531.0   13.50
 1.4520   76.00  2869.0   44.50
 1.4410   90.00  3207.0   67.10
 1.4370  105.00  3545.0   72.00
 1.4290  135.00  4558.0   87.10
 1.4275  160.00  5402.0   91.10
RUN # 8 8 3  70.066800.     5.0
  28.89    0.625  4.4450  187.10    0.417
 7   66.00
 1.475    15.00    16.0    7.00
 1.444    44.00    45.3    51.0
 1.435    94.00   101.0    72.4
 1.427   144.00   147.00   79.2
 1.424   194.00   204.00   82.6
 1.420   244.00   250.00   88.6
 1.416   344.00   355.00   96.0
```

CRUDE OIL CONCENTRATION CURVES

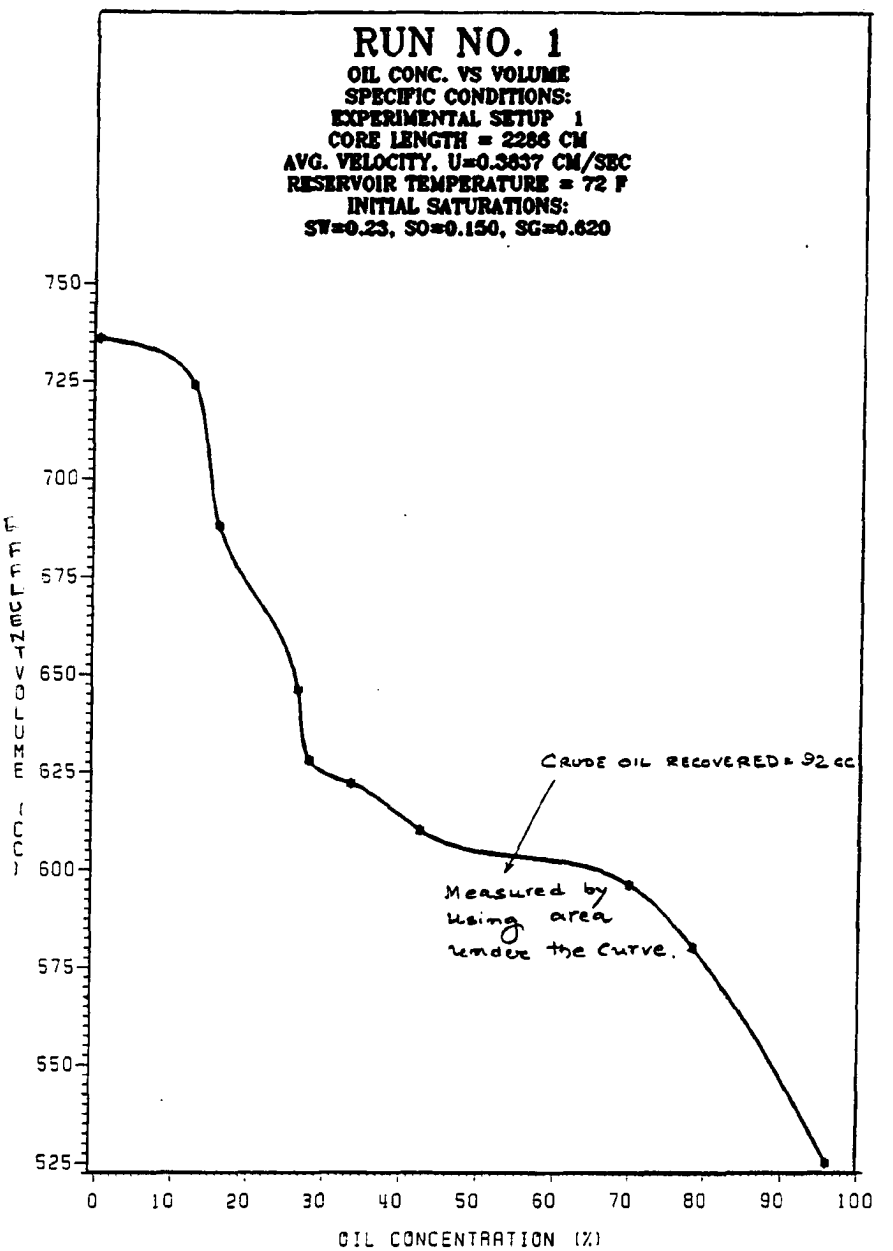

FIGURE D-1 OIL CONC. PROFILE WITH VOLUME

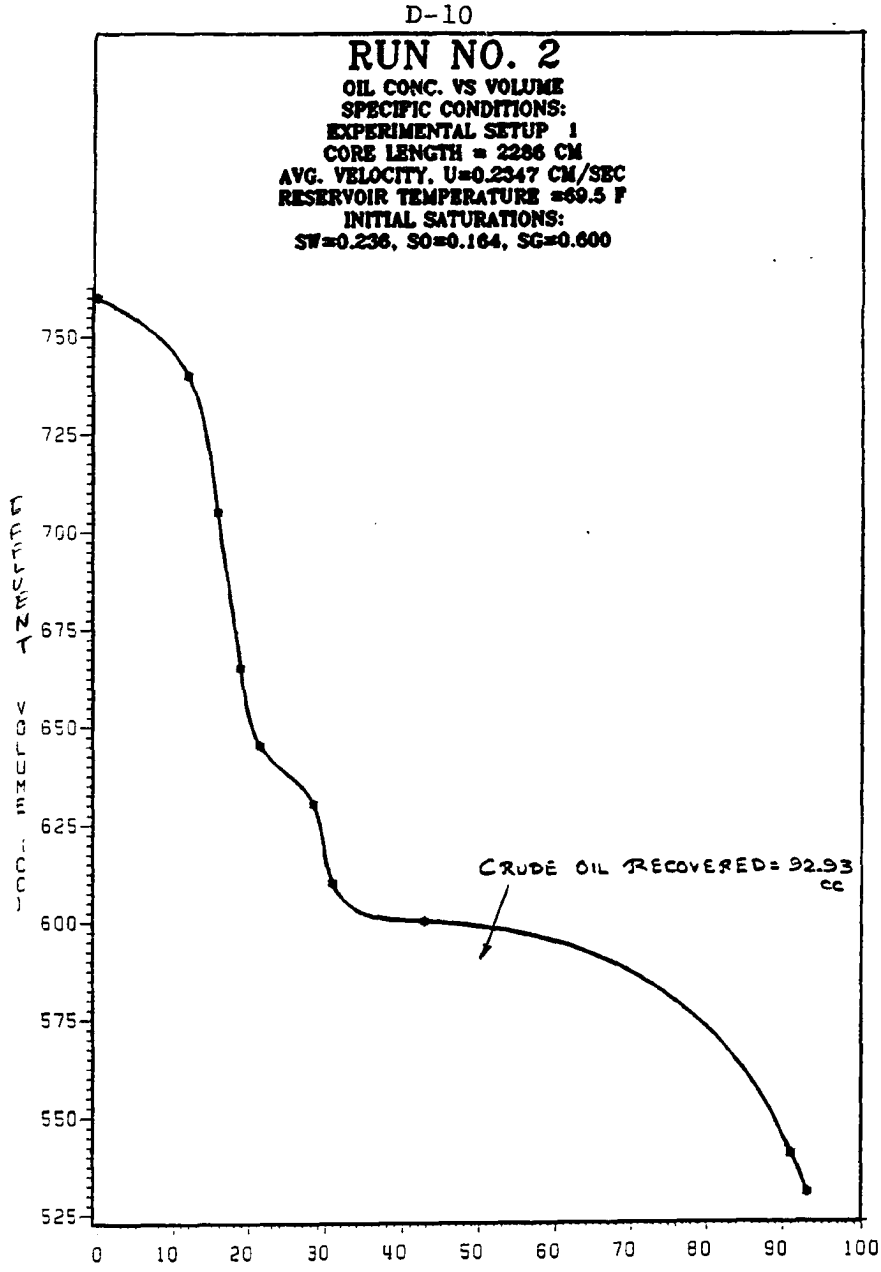

FIGURE D-2 OIL CONC. PROFILE VS VOLUME

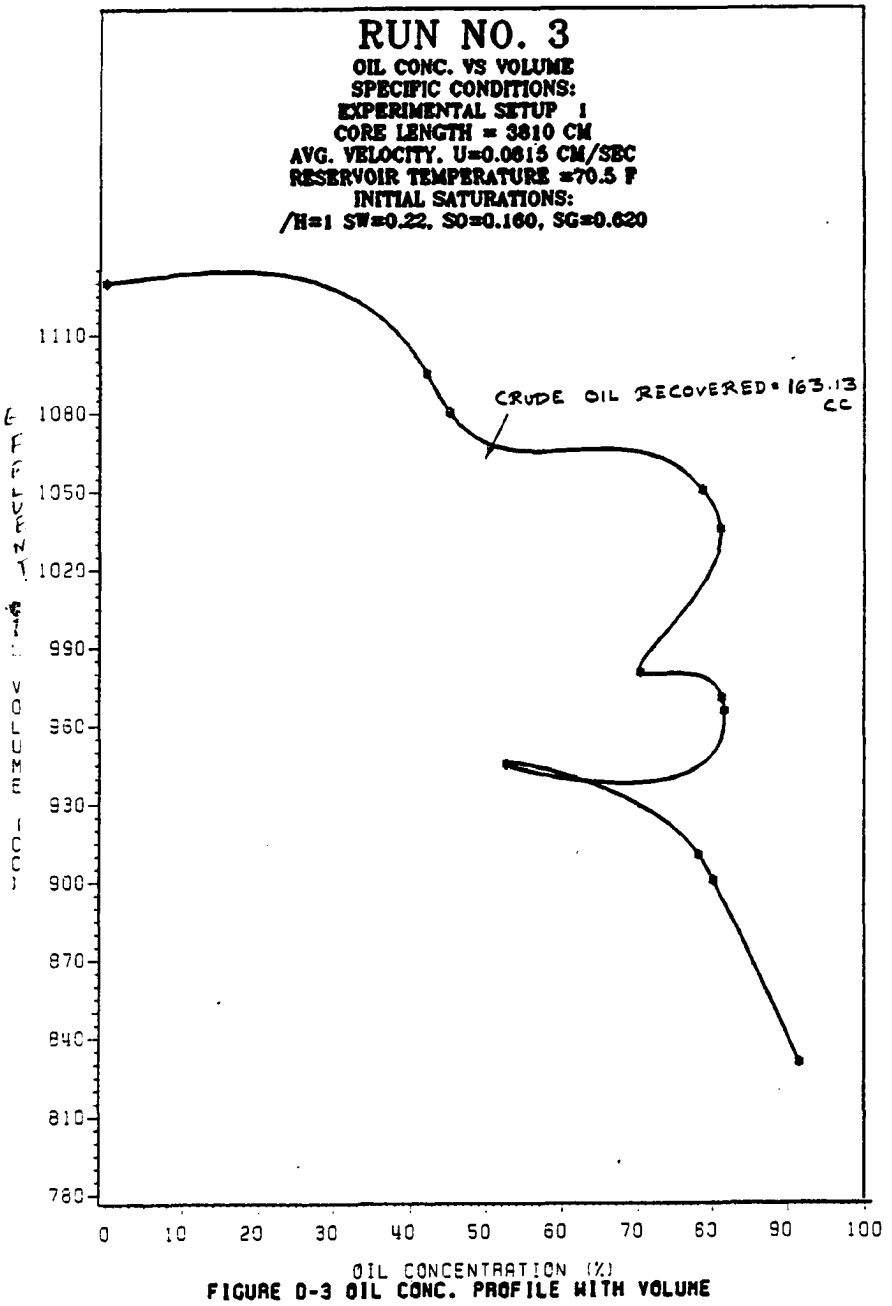

FIGURE D-3 OIL CONC. PROFILE WITH VOLUME

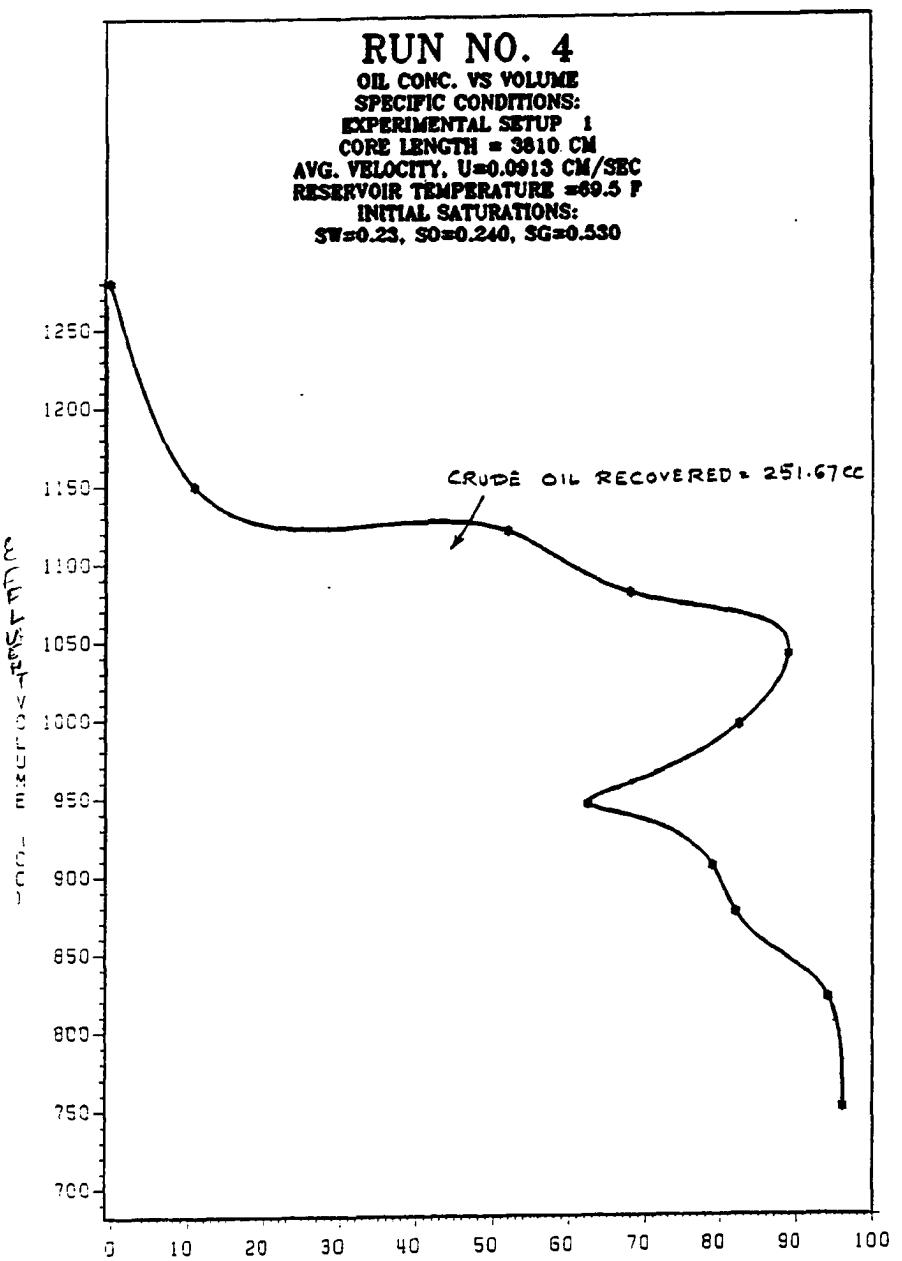

FIGURE D-4 OIL CONC. PROFILE WITH VOLUME

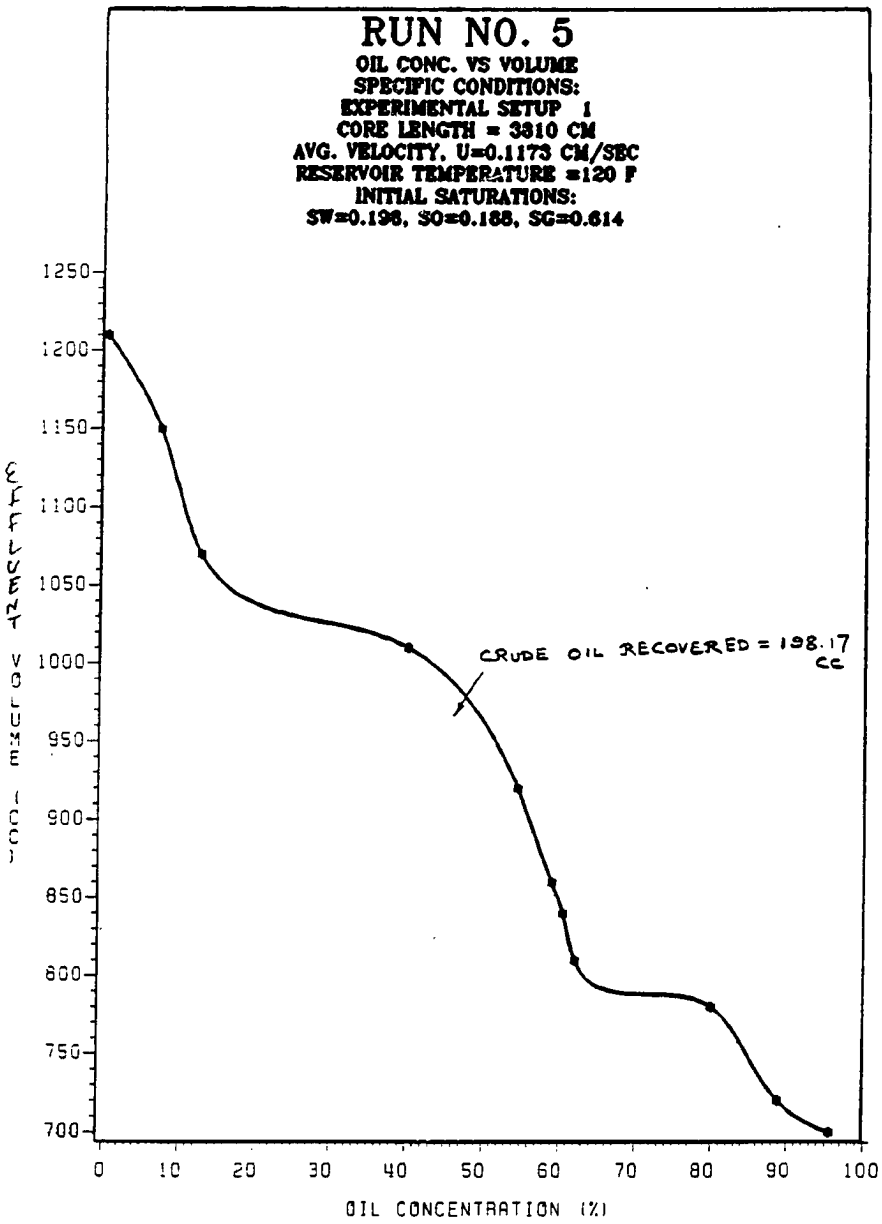

FIGURE D-5 VOLUME VS OIL CONC. PROFILE

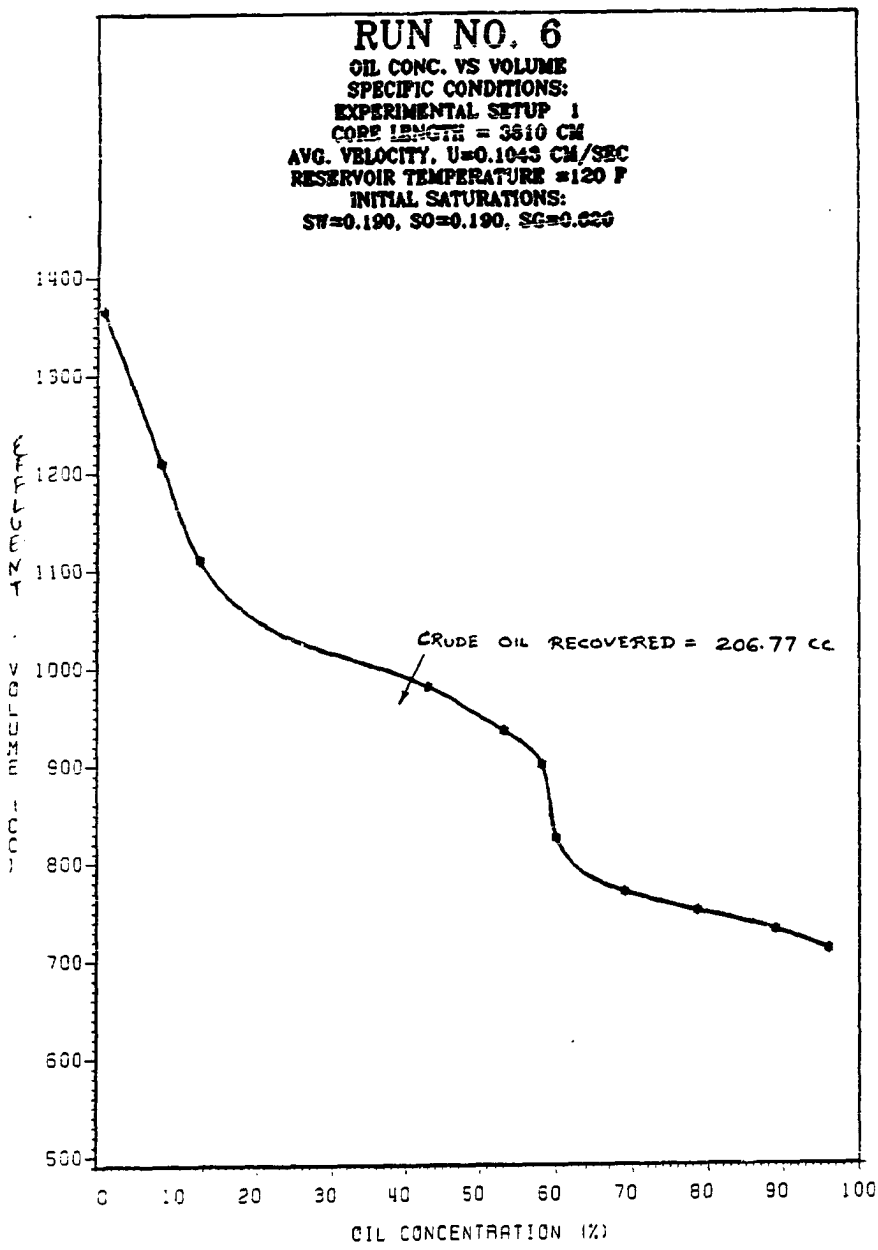

FIGURE D-6 OIL CONC. PROFILE WITH VOLUME

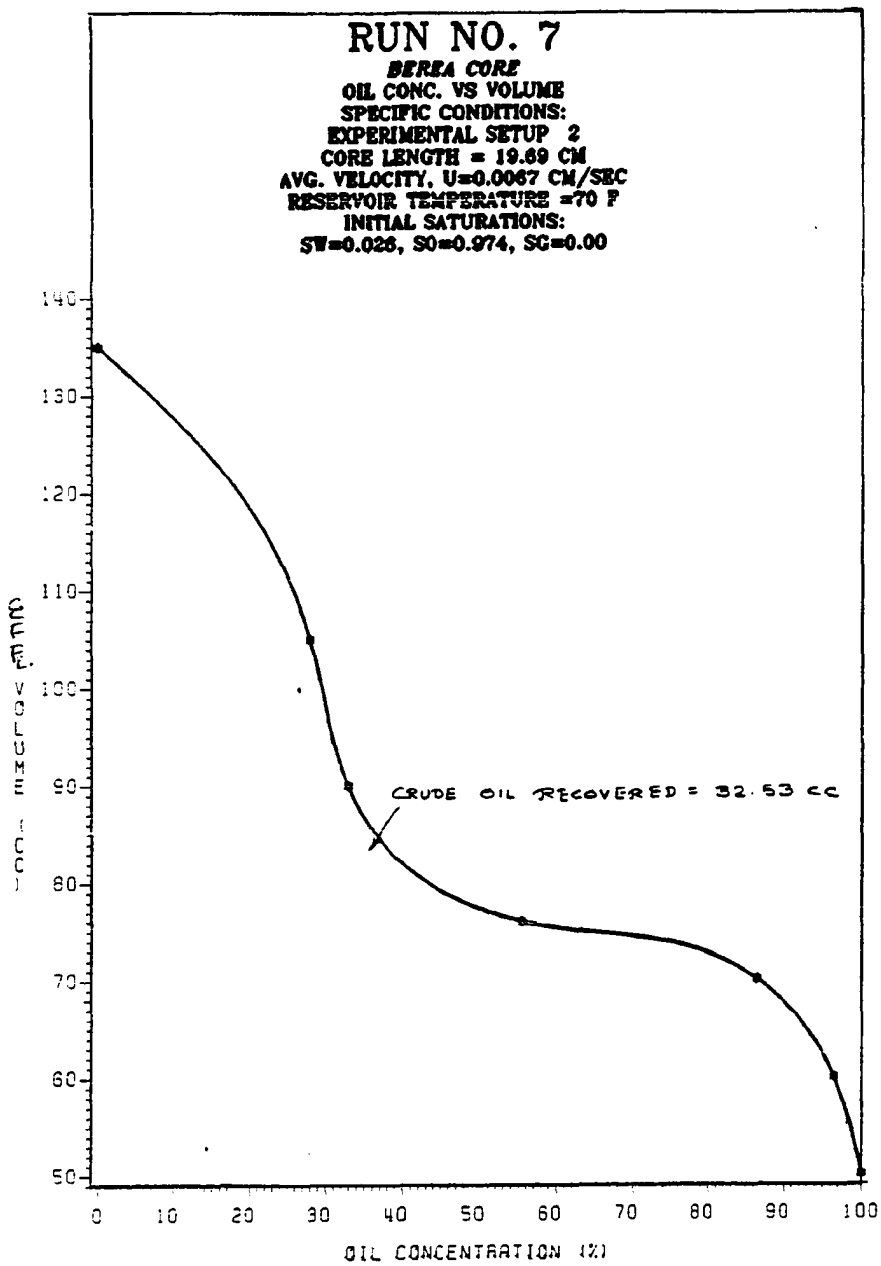

FIGURE D-7 OIL CONC. PROFILE WITH VOLUME

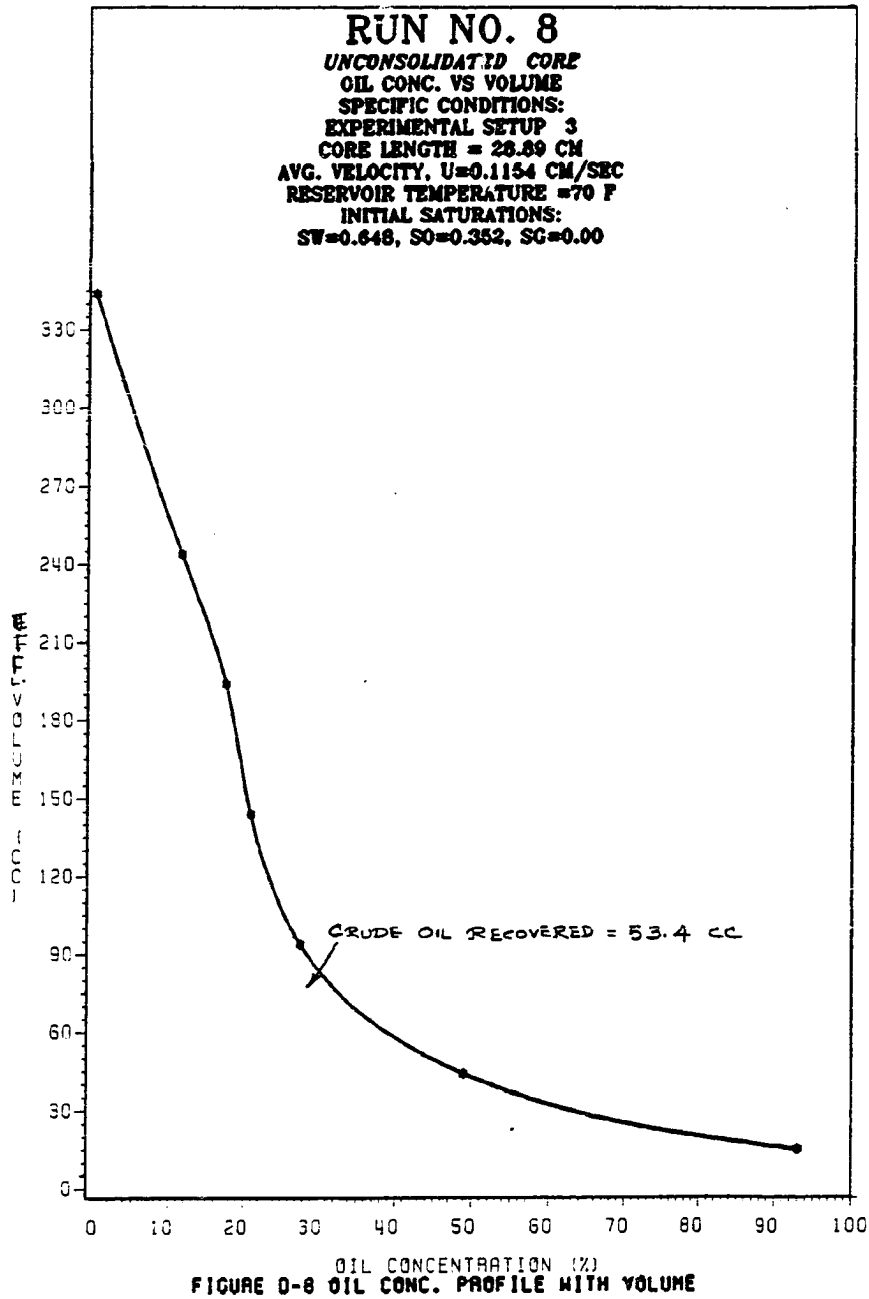

FIGURE D-8 OIL CONC. PROFILE WITH VOLUME